School of Doctoral Studies in Biological Sciences
University of South Bohemia in České Budějovice
Faculty of Science

Proteins involved in the tetrapyrrole pathway in *Synechocystis* sp. PCC 6803 and their localization in the proximity of PSII biogenesis

Ph.D. Thesis

Mgr. Petra Skotnicová

Supervisor: RNDr. Martin Tichý, Ph.D.
Institute of Microbiology, CAS, Centre Algatech
University of South Bohemia, Faculty of Science

České Budějovice 2019

This thesis should be cited as:
Skotnicová, P., 2019: Proteins involved in the tetrapyrrole pathway in *Synechocystis* sp. PCC 6803 and their localization in the proximity of PSII biogenesis, Ph.D. Thesis, in English. University of South Bohemia, Faculty of Science, School of Doctoral Studies in Biological Sciences, České Budějovice, Czech Republic, 118 pp.

Annotation

The goal of the thesis was to enhance our understanding of the tetrapyrrole pathway in cyanobacteria by a study of selected proteins involved in the pathway. During the project I have revealed functional connection between protoporphyrinogen IX oxidase HemJ and preceding enzyme in the pathway by complementation of protoporphyrinogen IX oxidase deletion mutant by its analog HemG from *Escherichia coli*. Heme *b* was identified as a cofactor of HemJ. Another protein deeply influencing tetrapyrrole accumulation, BtpA was found to form a complex with GluTR, the enzyme at the beginning of the tetrapyrrole pathway. Lastly, CurT protein, the component of the structures anticipated to function in PSII assembly and/or repair localized at plasma/thylakoid membrane interface, was co-isolated with the enzymes of the tetrapyrrole pathway suggesting that the specific CurT containing membranes could be a place of both photosystem II assembly/repair and chlorophyll delivery.

Declaration [in Czech]

Prohlašuji, že svoji disertační práci jsem vypracoval samostatně pouze s použitím pramenů a literatury uvedených v seznamu citované literatury.
Prohlašuji, že v souladu s § 47b zákona č. 111/1998 Sb. v platném znění souhlasím se zveřejněním své disertační práce, a to v úpravě vzniklé vypuštěním vyznačených částí archivovaných Přírodovědeckou fakultou elektronickou cestou ve veřejně přístupné části databáze STAG provozované Jihočeskou univerzitou v Českých Budějovicích na jejích internetových stránkách, a to se zachováním mého autorského práva k odevzdanému textu této kvalifikační práce. Souhlasím dále s tím, aby toutéž elektronickou cestou byly v souladu s uvedeným ustanovením zákona č. 111/1998 Sb. zveřejněny posudky školitele a oponentů práce i záznam o průběhu a výsledku obhajoby kvalifikační práce. Rovněž souhlasím s porovnáním textu mé kvalifikační práce s databází kvalifikačních prací Theses.cz provozovanou Národním registrem vysokoškolských kvalifikačních prací a systémem na odhalování plagiátů.

České Budějovice, 24.9.2019 .....
Petra Skotnicová

This thesis originated from a partnership of Faculty of Science, University of South Bohemia, and Institute of Microbiology, CAS, Centre Algatech, supporting doctoral studies in the Molecular and Cell Biology and Genetics study program

Přírodovědecká fakulta
Faculty of Science

Financial support

This work was financially supported by project Algatech Plus of the Czech Ministry of Education (LO1416). I was also supported by a Ph.D. student grant (GAJU 041/2013/P) of the Grant Agency of the University of South Bohemia.

Acknowledgements

First and foremost, my utmost gratitude belongs to my supervisor Martin Tichý for giving me the opportunity to work on such an interesting topic and to become a part of such a great and inspiring research team. I appreciate that he gave me guidance when needed, yet a lot of freedom in my scientific work as I believe that the possibility to make my own mistakes made me a better scientist. Also, I want to thank him for his patience in restraining my "originality" in writing.

Many thanks belong to Roman Sobotka for all the help, never-ending flow of theories and infectious scientific enthusiasm. I am thankful to Pepa Komenda for valuable advice and for making threatening gestures to hurry us up.

I would also like to thank all my colleagues from The Opatovický mlýn, which is an amazing working place with friendly people never hesitating to make fun. I am grateful to all my colleagues from our lab for all the help, advice, and discussions. My special thanks belong to my dearest friends hiding under the cover "Hloupé buchty", who supported me and cheered me up during my work. I am unbelievably happy that I met these clever, fabulous, loving, cheerful, generous, sometimes a bit crazy women.

I am indebted to Prof. Neil Hunter for a great opportunity to stay in his laboratory at The University of Sheffield. I am also grateful to the people from his lab, who took great care of me.

A v neposlední řadě bych chtěla poděkovat své rodině za jejich podporu a lásku.

List of papers and author's contribution

Skotnicová, P., Sobotka, R., Shepherd, M., Hájek, J., Hrouzek, P., and Tichý, M. (2018). The cyanobacterial protoporphyrinogen oxidase HemJ is a new *b*-type heme protein functionally coupled with coproporphyrinogen III oxidase. *Journal of Biological Chemistry* **293**, 12394-12404.

Petra Skotnicová carried all experiments except MS and precursor analyses; nevertheless, she was responsible for growing and harvesting the cells for those analyses. Petra Skotnicová also participated in data processing and their evaluation, and contributed equally to writing and reviewing the manuscript.

I hereby confirm that Petra Skotnicová contributed to the mentioned publication as described above.

.....

RNDr. Martin Tichý, Ph.D.

Content

List of abbreviations

Synechocystis 6803	*Synechocystis* sp. PCC 6803
PSI	photosystem I
PSII	photosystem II
Chl	chlorophyll
PBS	phycobilisome
LHC	light-harvesting complex
ROS	reactive oxygen species
Hli proteins	high light-inducible proteins
CAB	Chl *a*/*b*-binding
ALA	5-aminolevulinic acid
GluRS	glutamyl-tRNA synthetase
GluTR	glutamyl-tRNA reductase
GSA	glutamate-1-semialdehyde
GSAM	glutamate-1-semialdehyde-2,1-aminomutase
Coprogen	coproporphyrinogen III
Copro	coproporphyrin III
CPO	coproporphyrinogen III oxidase
Protogen	protoporphyrinogen IX
Proto	protoporphyrin IX
PPO	protoporphyrinogen IX oxidase
FeCH	ferrochelatase
MgCH	magnesium chelatase
MgP	Mg-protoporphyrin IX
MTF	Mg-protoporphyrin IX methyltransferase
MgPME	Mg-protoporphyrin IX monomethyl ester
Pchlide	3,8-divinyl protochlorophyllide
Cyclase	Mg-protoporphyrin IX monomethyl ester cyclase
POR	protochlorophyllide oxidoreductase
DV Chlide	3,8-divinyl chlorophyllide
MV Chlide	3-monovinyl chlorophyllide
GluBP	GluTR-binding protein
cpSRP43	chloroplast signal recognition particle 43
HO	heme oxygenase
R. sphaeroides	*Rhodobacter sphaeroides*
E. coli	*Escherichia coli*
GS-GOGAT cycle	glutamine synthetase-glutamate synthase cycle
NAGK	N-acetyl-L-glutamate kinase
CurT	curvature thylakoids
CAAD	aminoacyl-tRNA synthetases appended domain
SDS-PAGE	SDS- electrophoresis
CN-PAGE	clear native gel
TEM	transmission electron microscopy
HPLC	high-performance liquid chromatography

1. Introduction

1.1 Oxygenic photosynthesis

In the process of oxygenic photosynthesis, cyanobacteria, plants, and algae perform the conversion of the light energy from the sun into the chemical energy. It is a highly important process to sustain all the life on Earth providing food and oxygen. The oxygenic photosynthesis is performed via huge multi-subunit protein/pigment complexes: photosystem II (PSII), cytochrome b_6f complex, photosystem I (PSI), and ATP synthase, which are embedded in the thylakoid membrane. In cyanobacteria, thylakoid membranes are organized as sheets in the cytoplasm, while in photosynthetic eukaryotes, they are placed inside specialized organelles called chloroplast. Light energy is absorbed by proteins of photosynthetic reaction centers from PSII and PSI, containing chlorophyll (Chl). PSII optimally absorbs photons of the wavelength of 680 nm and PSI that of 700 nm. To improve the efficiency of light absorption, photosynthetic organisms contain peripheral antennae (etc. light-harvesting complex (LHC) and phycobilisome (PBS)) consisting of additional pigments increasing the range of wavelength absorbed.

PSII carries out the first step of photosynthetic electron transport, the light-catalyzed extraction of electrons from water. Excited electrons from PSII are shuttled through the cytochrome b_6f complex to PSI via an electron transport chain. The final stage of photosynthetic electron transport, the light-driven electron transfer from plastocyanin to ferredoxin, is catalyzed by PSI (Grotjohann and Fromme, 2005). Ferredoxin transfers the electron to the ferredoxin-NADP+ reductase, which then reduces NADP+ to NADPH (Grotjohann and Fromme, 2005). As the addition of the whole process, there is created a proton gradient across the membrane, which is finally used by an ATP synthase to synthesize ATP. NADPH and ATP generated by oxygenic photosynthesis are utilized for the synthesis of carbohydrates from carbon dioxide.

Cyanobacteria serve as exceptional model organisms for photosynthetic research. Cyanobacteria and chloroplasts have a common ancestor and they share many common features of oxygenic photosynthesis and pigment biosynthesis. However, cyanobacteria offer better tools for genetic manipulation and a shorter cell cycle. Also, structures of cyanobacterial PSI and II are well described by means of high-resolution techniques (Malavath et al., 2018; Umena et al., 2011).

1.2 *Synechocystis* sp. PCC 6803 as a model organism to study photosynthesis

One of the model cyanobacteria is *Synechocystis* sp. PCC 6803 (hereafter *Synechocystis* 6803). *Synechocystis* 6803 is a unicellular, freshwater, non-nitrogen fixing cyanobacterium. Its circular chromosome has ~3.6 Mbp and total genome size including its 7 plasmids is ~3.9 Mbp. This cyanobacterium is naturally transformable by exogenous DNA via homologous recombination. It enables routine gene inactivation, modification,

and regulated expression. *Synechocystis* 6803 is capable of mixotrophic growth without photosynthesis in the presence of glucose, which enables the generation and characterization of nonphotosynthetic mutants. All these factors make *Synechocystis* 6803 an extremely useful model organism.

An interesting feature of *Synechocystis* 6803 is its genome plasticity. The organism is known for frequent point mutations and tandem duplications on a small or large scale (Tichý et al., 2016). This leads, particularly in mutants with strongly impaired phenotype, to the generation of secondary mutants with improved phenotype. Such mutants called suppressor mutants contain suppressor mutation in another gene, which helps the suppressor mutant complement the effect of the original mutation. Identification of the secondary mutation(s) helps to identify new protein-protein interactions or intersection of biological pathways (Kufryk and Vermaas, 2001; Prosecka et al., 2009; Tichý and Vermaas, 2000).

1.3 Photosystem II

Photosystems perform absorption and transfer of light energy, which involves the transfer of electrons. In PSI and PSII both light collection and charge separation are predominantly performed by Chl embedded in transmembrane proteins (Komenda and Sobotka, 2019). PSII acts first, nevertheless, it is named PSII as it was discovered after the PSI.

Cyanobacterial PSII is an integral thylakoid membrane protein complex consisting of 20 subunits (17 intrinsic and three extrinsic) with a total molecular mass of 350 kDa. Photosystem II contains a number of cofactors, there are 35 Chls, 11 β-carotenes, two pheophytins, two hemes, a non-heme iron, two plastoquinones, four manganese atoms, three or four calcium ions, three chloride ions, one bicarbonate ion and more than 20 lipids (Umena et al., 2011).

The core of PSII is formed by D1 and D2 reaction center subunits, on either side are Chl binding proteins CP43 and CP47 (Figure 1). These proteins bind the majority of Chl molecules. 13 low molecular mass subunits (PsbI, H, J, Z, E, F, K, L, M, T, X, 30, Y) are bound at the periphery of the complex and three extrinsic sub-units (PsbO, PsbU and PsbV) on the lumenal side of the complex (reviewed by Nixon et al. (2010)). To the lumenal surface of PSII are bound different sets of extrinsic proteins depending on the species (reviewed by Enami et al. (2008)).

Recent results suggest that PSII assembly occurs in a step-wise fashion and is closely coupled to Chl biosynthesis (Figure 1; Komenda et al. (2012)). The entire process involves a number of proteins called assembly factors, which are assisting the assembly but they are not the component of functional PSII (see Komenda and Sobotka (2019)). The assembly of PSII proceeds in parallel with quality control by FtsH proteases and

photoprotection of the newly made modules and assembly intermediates (Komenda et al., 2006; Komenda and Sobotka, 2016).

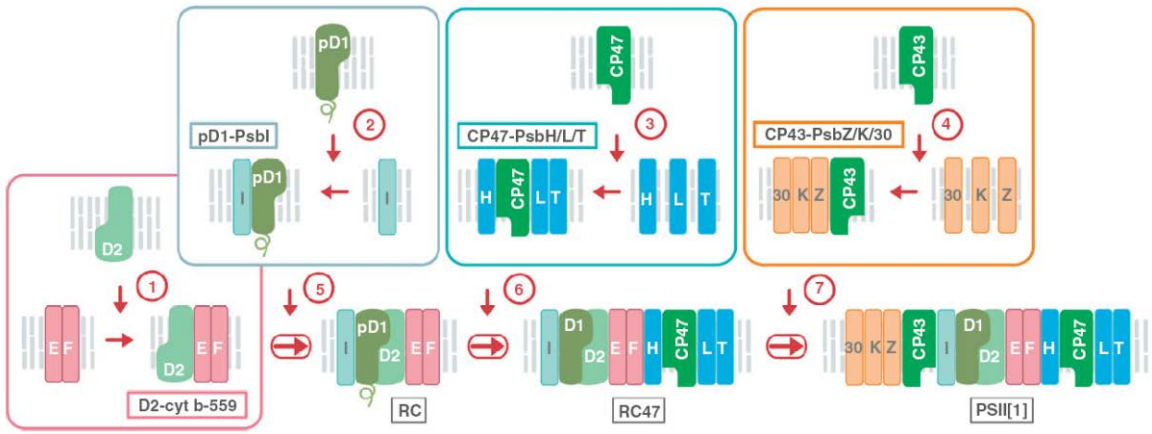

Figure 1

Model for modular assembly of Photosystem II (Komenda et al., 2012)

The assembly of PSII involves four basic subcomplexes. First, the D2-Cyt b-559 subcomplex containing PsbE and PsbF subunits binds the pD1-PsbI subcomplex resulting in the RC complex. The second step involves the attachment of the CP47 pre-complex with bound PsbH, PsbL and PsbT forming the RC47 complex. Then monomeric PSII is generated by binding the CP43-pre-complex comprising PsbK, PsbZ, and Psb30 subunits. Finally, the Mn_4CaO_5 cluster is assembled, PsbO, PsbV and PsbU extrinsic subunits are attached and PSII dimerizes.

PSII is prone to various types of irreversible photodamage. The repair of PSII involves partial disassembly of the damaged complex, selective replacement of the damaged subunit (predominantly the D1) by a newly synthesized copy, and reassembly (Nixon et al., 2010).

1.4 Photosystem I

PSI complex of cyanobacteria functions as a trimer with a molecular mass nearly 1 MDa with cofactors contributing to more than 30% of its total mass (Jordan et al., 2001). In *Synechocystis* 6803, PSI consists of 33 subunits, 285 Chls, 72 carotenoids, 51 lipids, 9 iron-sulfur clusters, 6 phylloquinone molecules, and 6 putative Ca^{2+} ions (Malavath et al., 2018).

The core of PSI is formed by PsaA and PsaB subunits. They harbor most of the Chls (86 of the 95) and carotenoids of the antenna system. A number of these Chls display a red shift in the absorption and emission spectra. The main contact between the monomers is provided by the three PsaL subunits. Other proteins (PsaD, PsaI, and PsaM) are supporting further contact between monomers, either directly or indirectly by interaction with cofactors or PsaL (Grotjohann and Fromme, 2005). PsaC interacts with the stromal sides of PsaA and PsaB and together with other two stromal subunits (PsaD, PsaE) provides the docking site for ferredoxin (Jordan et al., 2001).

Plant PSI functions as a monomer and contains additional light-harvesting complexes (LHC) located in the membrane. There are also some differences in the subunit composition of plant PSI (reviewed by Schöttler et al. (2011)).

There is significantly less information about the assembly process of PSI compared to PSII. Generally, PSI assembly is fast and its intermediates accumulate only in small amounts (Ozawa et al., 2010).

1.5 Tetrapyrroles

Tetrapyrroles are also called the pigments of life since they are involved in fundamental processes of living organisms like photosynthesis and respiration. Tetrapyrroles contain four pyrrole (pyrrole-like) rings bound together with direct covalent bonds or by one carbon bridge. Pyrroles are five atoms heterocyclic rings with a formula C_4H_4NH. They show different structural and functional properties defined by the structure of conjugated double bonds, the variety of substituted side chains and the chelation by different metal ions. A most common form of tetrapyrroles is metallated macrocycle (Figure 2).

The tetrapyrrole pathway in cyanobacteria, algae, and plants is responsible for the synthesis of three major end products: Chl, heme (Figure 2) and linear bilins via a common branched pathway.

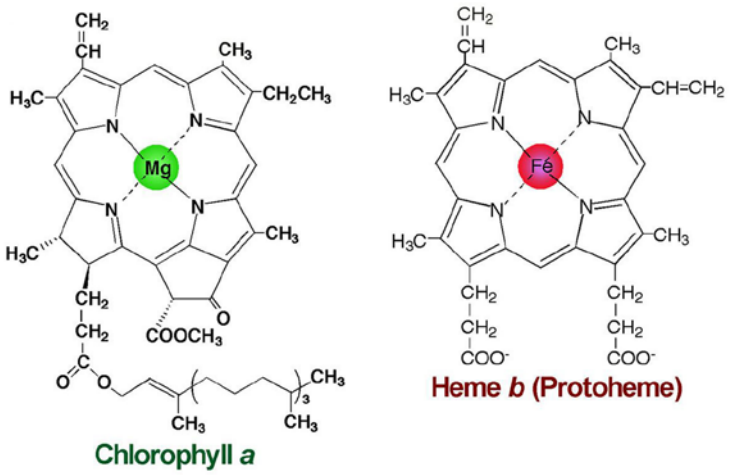

Figure 2

Structures of chlorophyll *a* and protoheme (adapted from Kobayashi and Masuda (2016))

Chlorophylls contain magnesium (Mg) as a central atom, whereas hemes contain iron (Fe).

Bilins, the open-chain tetrapyrroles, are usually derived by cleavage of cyclic metalloporphyrins (Warren and Smith, 2009). In cyanobacteria, phycobilins bound in phycobiliproteins serve to harvest visible light and transfer its energy to photosynthetic reaction centers. In plants, phytochromobilins are part of phytochromes serving as light sensors.

1.6 Phototoxicity

Organisms performing oxygenic photosynthesis have to synthesize tetrapyrroles under light illumination in the presence of oxygen. Under such conditions, tetrapyrroles, their precursors and breakdown products can be easily photo-oxidized and generate free radicals and reactive oxygen species (ROS) (Krieger-Liszkay, 2005). ROS are hurtful for key cellular components such as nucleic acids, lipids, proteins, and pigments. Respiration and photosynthetic electron transport are thought to be the main source of ROS production inside the photosynthetic cell (Latifi et al., 2009).

Especially Chl is potentially the most dangerous photodynamic agent in the photosynthetic cell since it is highly abundant, very efficient in absorbing light and its excited states are long-lived. If the excitation energy is not efficiently used or quenched, it can lead to the formation of the Chl triplet states, which can react with oxygen to yield singlet oxygen (Krieger-Liszkay et al., 2008). Since the lifetime of singlet oxygen in hydrocarbon solvents or micelles is significantly higher than in the water (20-25 μs compared to 3-4 μs), the singlet-oxygen-mediated photodamage will increase when Chl or other porphyrins and their targets are located in hydrophobic regions like membranes (Ricchelli, 1995).

As mechanisms for coping with oxidative stress are crucial for the viability of organisms, photosynthetic organisms developed numerous strategies to avoid ROS production or their scavenging. One of these mechanisms is nonphotochemical quenching of excited energy either by orange carotenoid protein interacting with PBS in cyanobacteria (Wilson et al., 2006) or by the LHC of PSII in plants and green algae. The other mechanism of energy dissipation involves high light-inducible proteins (Hli proteins).

Hli proteins are small proteins (~7 kDa) containing a single transmembrane helix similar to the first and third helix of LHC proteins present in plants and algae (Staleva et al., 2015). They have also the same Chl *a*/*b*-binding (CAB) motif, which is conserved in the whole LHC family. Apart from Chls, Hli proteins in *Synechocystis* 6803 were shown to bind carotenoid β-carotene (Figure 3, Shukla et al. (2018); Staleva et al. (2015)). Hli proteins can be found in all cyanobacteria nevertheless their number varies significantly among different species (Bhaya et al., 2002). Interestingly, also ferrochelatase (FeCH) in cyanobacteria and chloroplasts catalyzing the synthesis of protoheme, contains CAB domain.

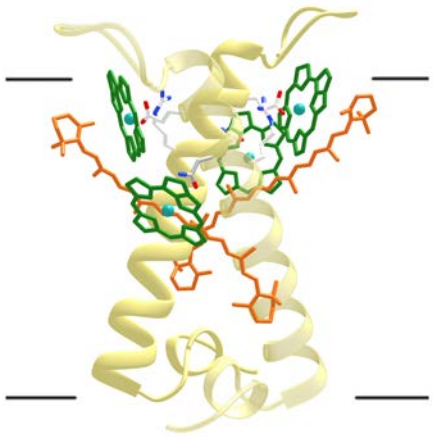

Figure 3

A structural model of the putative HliC dimer (Shukla et al., 2018).

HliC binds 2 chlorophylls and 1 β-carotene per monomer. For clarity, only porphyrin rings of chlorophyll molecules are shown

Hli proteins may have a photoprotective function as they perform energy dissipation via energy transfer from Chl *a* to carotenoid (Staleva et al., 2015). It was shown that all four Hli proteins present in *Synechocystis* 6803 (HliA-D) assist during biogenesis and repair of PSII (Knoppová et al., 2014; Yao et al., 2007). Moreover, HliD was also co-purified with Chl synthase together with YidC insertase (called also Alb3 or Oxa1), the protein involved in the synthesis of membrane proteins (Chidgey et al., 2014). This machinery is probably used for incorporation of newly synthesized Chl into Chl-binding protein during its translation. Hli proteins might protect components of Chl-binding proteins biosynthetic machinery against photodamage in case of accidental Chl release (Komenda and Sobotka, 2016).

1.7 Overview of the tetrapyrrole biosynthetic pathway

All tetrapyrroles are produced by a common biosynthetic pathway (reviewed by Tanaka and Tanaka (2007)). Their synthesis starts with the formation of 5-aminolevulinic acid (ALA), a common precursor for all naturally occurring tetrapyrroles. Among organisms, ALA is synthesized by two distinct biosynthetic routes. The first one found in metazoans, fungi and α-proteobacteria is called "C4" or "Shemin" and involves condensation of glycine and succinyl coenzyme A by ALA synthase (Figure 4A). The second one called "C5" is used in plants, archaea and most bacteria including cyanobacteria and starts from glutamate (Fig. 4B). In the first step, glutamyl-tRNA^{Glu} is made from glutamate by glutamyl-tRNA synthetase (GluRS). Glutamyl-tRNA reductase (GluTR) subsequently converts glutamyl-tRNA to a labile intermediate glutamate-1-semialdehyde (GSA) in an NADPH-dependent reaction. GSA is finally converted to ALA by glutamate-1-semialdehyde-2, 1-aminomutase (GSAM).

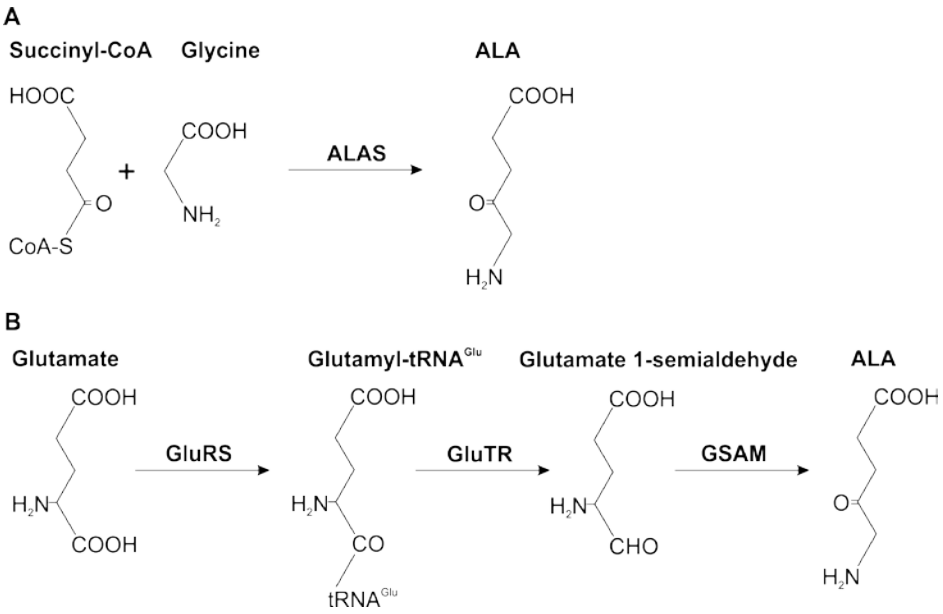

Figure 4

Two routes of ALA synthesis (adapted from Panek and O'Brian (2002))
A) by ALA synthetase (ALAS) B) by the C5 pathway. GluRS reaction of Glutamyl-tRNA^{Glu} synthesis participates in ALA as well as protein biosyntheses. Abbreviations: ALA, aminolevulinic acid; ALAS, ALA synthase; GluRS, glutamyl-tRNA synthetase; GluTR, glutamyl-tRNA reductase; GSAM, glutamate 1-semialdehyde-aminotransferase

Next three steps, catalyzed by porphobilinogen synthase, hydroxymethylbilane synthase, and uroporphyrinogen synthase, are highly conserved from archaea to eukaryotes (Dailey et al., 2017). They give rise to the first cyclic intermediate of tetrapyrrole biosynthesis, uroporphyrinogen III. Afterward, uroporphyrinogen III decarboxylase performs the stepwise decarboxylation of four acetic acid side chains of uroporphyrinogen III into methyl groups, yielding coproporphyrinogen III (Coprogen).

Coprogen is then oxidatively decarboxylated to protoporphyrinogen IX (Protogen) by coproporphyrinogen III oxidase (CPO). There are two distinct types of CPO (Figure 5), one oxygen dependent and the other working at anoxygenic conditions (Goto et al., 2010). Protogen is then oxidized into protoporphyrin IX (Proto), the last common precursor of heme and Chl pathway. The Protogen oxidation reaction is catalyzed by protoporphyrinogen IX oxidase (PPO). There are three PPOs without any homology (HemY, HemG, and HemJ).

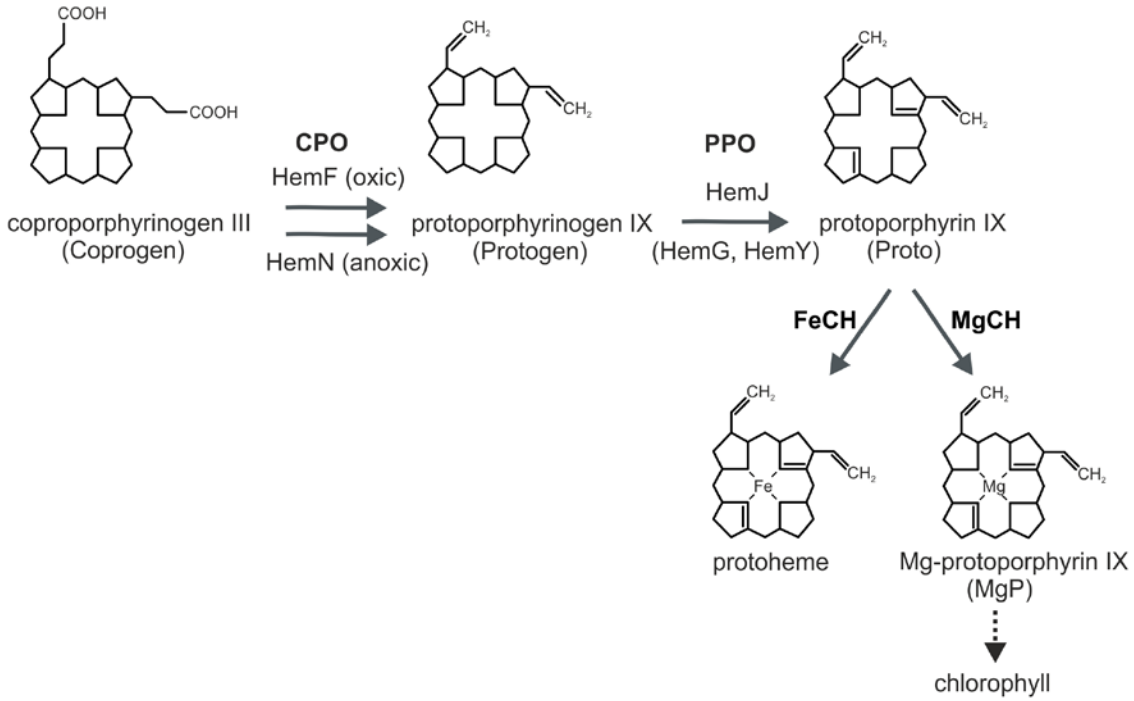

Figure 5

Late steps of common tetrapyrrole biosynthesis in cyanobacteria (*Synechocystis* 6803)

Conversion of Coprogen to Protogen is catalyzed by coproporphyrinogen III oxidase (CPO). In *Synechocystis* 6803 HemF works as the sole CPO under oxic conditions and HemN under anoxic conditions. The CPO product Protogen is oxidized to Proto by protoporphyrinogen IX oxidase (PPO). In most cyanobacteria, this reaction is performed by HemJ PPO isoform, in others by HemG or HemY. Proto is than channeled to ferrochelatase (FeCH) leading to protoheme or to Mg-chelatase (MgCH), the first enzyme of the dedicated chlorophyll pathway. For clarity, the structure of the tetrapyrrole ring is shown in a simplified way and only side chains important for displayed reactions are presented.

At the Proto branch point, insertion of iron ion (Fe^{2+}) by FeCH leads to the formation of protoheme, while insertion of magnesium ion (Mg^{2+}) by magnesium chelatase (MgCH) leads to Mg-protoporphyrin IX (MgP), the first intermediate of the Chl branch (Figure 6, reviewed by Tanaka and Tanaka (2007)). Although reactions catalyzed by these chelatases are similar, the two chelatase enzymes have a remarkably different structure and properties (Cornah et al., 2003). FeCH creates homodimer (Grzybowska et al., 2002; Sobotka et al., 2011) and does not need ATP for its activity (Al-Karadaghi et

al., 2006). In contrast, MgCH, which consists of three different subunits (ChlH, ChlI, ChlD), is ATP dependent (Adams et al., 2016).

In cyanobacteria, protoheme is the source of the major photosynthetic pigments bilins. Here, protoheme is further processed by heme oxygenase to yield biliverdin IXα, which serves as a precursor for all functional bilins found in photosynthetic organisms, particularly phytochromobilin, phycocyanobilin, and phycoerythrobilin (Frankenberg-Dinkel and Terry, 2009). In cyanobacteria, bilins are attached to apoproteins forming phycobiliproteins and assembled to PBS performing light harvesting.

At the Chl branch, the addition of methyl group to MgP by Mg-protoporphyrin IX methyltransferase (MTF) leads to Mg-protoporphyrin IX monomethyl ester (Mg PME), which is subsequently converted to 3,8-divinyl protochlorophyllide (Pchlide) by Mg-protoporphyrin IX monomethyl ester cyclase (hereafter cyclase). Pchlide is reduced by protochlorophyllide oxidoreductase (POR) to form 3,8-divinyl chlorophyllide (DV Chlide). Majority of plants, algae, and cyanobacteria contain two POR enzymes. The main one is operating only in the presence of light because its reaction is driven by the absorption of two photons by Pchlide (Heyes et al., 2003). In the dark, Chl can be synthesized due to the dark-operative POR. On the contrary, angiosperms possess only light-dependent POR and Pchlide reduction is blocked in the dark. Next reduction step performed by divinylchlorophyllide reductase leads to 3-monovinyl chlorophyllide (MV Chlide). In the last step catalyzed by Chl-synthase, esterification of MV Chlide with phytyl pyrophosphate (provided by isoprenoid pathway) gives rise to the Chl *a*. This esterification increases significantly hydrophobicity of the Chl molecule, which is important for specific interaction with Chl-binding proteins. In most cyanobacteria, Chl *a* is the only Chl species whereas plants and some algae also possess Chl *b*, which is mostly found in the antennae. Chl *b* is made by conversion of a portion of Chl *a* by Chlide *a* oxygenase.

Most of the Chl in the cyanobacterial cell can be recycled. Chl is de-esterified yielding MV Chlide and free phytol, and up to 80% of MV Chlide (at high light intensities) can be reused in Chl biosynthesis (Vavilin and Vermaas, 2007).

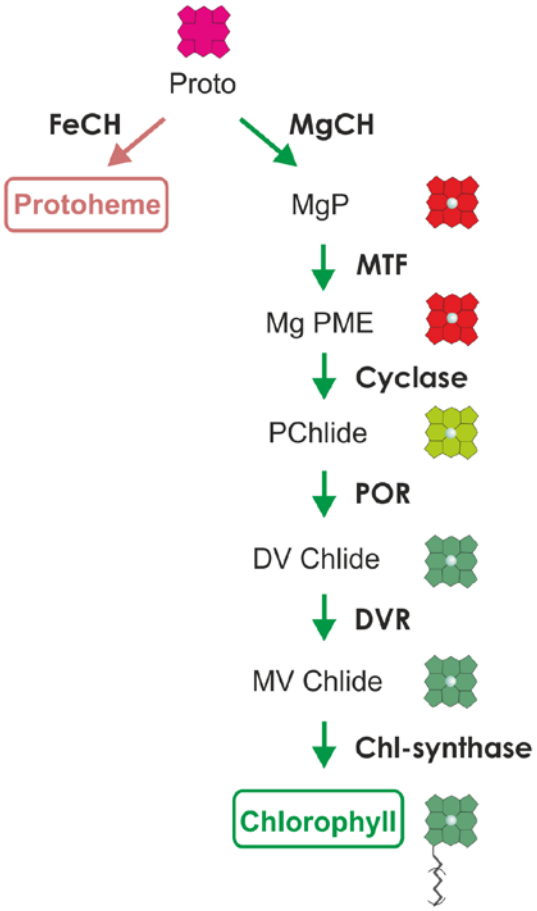

Figure 6

A schema of the chlorophyll biosynthesis pathway started from the protoheme/chlorophyll branchpoint (adapted from Sobotka (2014))

Abbreviations of enzymes: FeCH, ferrochelatase; MgCH, Mg-chelatase; MTF, Mg protoporphyrin IX methyltransferase; Cyclase, Mg-protoporphyrin IX monomethyl ester oxidative cyclase; POR, light-dependent protochlorophyllide oxidoreductase; DVR, divinyl-chlorophyllide reductase

Abbreviations of intermediates: Proto, Protoporphyrin IX; MgP, Mg-protoporphyrin IX; Mg PME, Mg protoporphyrin IX monomethyl ester; PChlide, divinyl-protochlorophyllide; DV Chlide, divinyl chlorophyllide; MV Chlide, monovinyl chlorophyllide

1.8 Overview of the regulatory mechanisms

As enzymes involved in tetrapyrrole pathway are mostly known and biochemically characterized, the research moves towards their 3D structure, exploration of their integration into multi-enzyme complexes and elucidation of the complex network of metabolic and regulatory interactions (Brzezowski et al., 2015).

Tight regulation of the tetrapyrrole pathway is necessary because of tetrapyrrole phototoxicity and different demand for individual end products within the cell. It is apparent that the synthesis of tetrapyrroles must be coordinated with an expression of cognate apoproteins so neither free tetrapyrroles nor apoproteins do accumulate (Sobotka, 2014). Although the tetrapyrrole biosynthesis in cyanobacteria closely resembles that in plants, there are some significant differences. In plants, the amount of heme is about 50 times lower than the amount of Chl (Papenbrock et al., 1999), which means that most porphyrins are channeled through the Chl branch. Nevertheless, cyanobacteria use both Chl and phycobilins in light energy transfer. Therefore, phycobilins accumulate in larger quantities in the cell in comparison to plant linear tetrapyrrole phytochromobilin. In our laboratory, we estimate that in *Synechocystis* 6803 the molar ratio between Chl and phycobilins is around 2:1 (unpublished data) under normal conditions.

Moreover, requirements for various tetrapyrroles especially for Chl can change quickly, for example with a change of light intensity (Kopečná et al., 2012) or nutrient availability (Klotz et al., 2016). Circadian oscillations direct expression of many enzymes of the tetrapyrrole pathway (Papenbrock et al., 1999). Nevertheless, in general, the transcriptional levels do not always correspond with that of the proteins (Griffin et al., 2002) and tetrapyrrole pathway seems to be highly regulated also post-translationally to facilitate rapid response to varying environmental conditions (Czarnecki and Grimm, 2012).

1.8.1 ALA formation

ALA synthesis is the major control point of the plant and cyanobacterial tetrapyrrole pathway, determining the total flux through the pathway. As glutamyl-tRNA serves as a building block for both the tetrapyrrole and protein biosyntheses, the formation of ALA is a possible target for the control of coordinated biosynthesis of Chl and its apoproteins (Sobotka, 2014). The importance of the study of ALA synthesis and regulation has been further strengthened by ALA approval for photodynamic therapy (Mahmoudi et al., 2019).

GluTR, the first enzyme of ALA synthesis, is an important regulatory point of the tetrapyrrole pathway. Heme was shown to act as a feedback regulator by inhibiting the GluTR activity (Pontoppidan and Kannangara, 1994; Rieble and Beale, 1991). In agreement with that, mutants with affected degradation of heme have reduced level of Pchlide due to the inhibition of ALA synthesis (Terry and Kendrick, 1999). Later, the

GluTR-binding protein (GluBP) was found (Czarnecki et al., 2011) and identified as a heme-binding protein (Zhao et al., 2014). Recently, it has been shown that GluBP binds to GluTR in heme-dependent mode (Richter et al., 2019). Binding of heme inhibits its interaction with GluTR and as GluBP protects GluTR against Clp protease degradation (Apitz et al., 2016), its release makes GluTR accessible for degradation.

N-terminus of GluTR is essential for GluBP binding (Apitz et al., 2016) and thus mediates GluTR inhibition by heme in plants (Vothknecht et al., 1998). However, the N-terminal sequence responsible for heme regulation in plants is not present in bacterial enzymes. Nevertheless, GluTR is inhibited by heme in cell extracts from several bacterial species (Dailey et al., 2017) and in *Salmonella typhimurium*, the stability of GluTR is increased in heme-limited cells (Wang et al., 1999). Thus in bacteria, there might be a different way of heme feedback inhibition.

Recently, also chloroplast signal recognition particle 43 (cpSRP43) was shown to stabilize GluTR independently of GluBP (Wang et al., 2018). CpSRP pathway is responsible for the transport of nucleus encoded light-harvesting Chl binding proteins into the stroma and their following integration to the membrane (Richter et al., 2010). For the integration also YidC translocase is required, which has been co-purified with plant Chl synthase in *Synechocystis* 6803 (Proctor et al., 2018) implying co-ordination of Chl biosynthesis with its insertion into nascent polypeptide. Interaction of cpSRP43 with GluTR suggests another posttranslational mechanism for coordination of Chl binding proteins insertion to the membrane with Chl biosynthesis (Wang et al., 2018).

In plants, another mechanism balancing GluTR activity and Chl biosynthesis is the FLU protein, a posttranslational negative regulator of GluTR. Lack of FLU resulted in an increase of Pchlide in the darkness (Meskauskiene et al., 2001). It was proposed that FLU protein regulates GluTR activity independently from regulation by heme (Goslings et al., 2004). C-terminus coiled-coil domain of GluTR and tetratricopeptide repeat domain of FLU are involved in the interaction (Goslings et al., 2004; Meskauskiene and Apel, 2002). The FLU protein was co-immunoprecipitated with enzymes of Chl pathway: cyclase, POR and geranylgeranyl reductase (Kauss et al., 2012), the latter is the enzyme providing phytol for Chl and tocopherol synthesis. It is presumed that FLU is involved in feedback regulation of ALA synthesis as a response to the increased level of Pchlide.

It seems that GluTR is mostly regulated by feedback or another kind of allosteric regulation, which might either affect activity or stability/accessibility for protease. For example, GluBP was shown to stimulate GluTR (Zhao et al., 2014), nevertheless, GluBP null mutants exhibited reduced levels of GluTR and consequently ALA synthesis and Chl level (Wang et al., 2018).

Cyanobacteria do not possess any homologs of proteins regulating stability or activity of GluTR in plants (FLU, GluBP, cpSRP43) and it is probable that other proteins are performing this role.

1.8.2 The branchpoint of Chl and heme biosynthesis

Highly important in the regulation of the tetrapyrrole pathway is the branchpoint of heme and Chl biosynthesis, where MgCH and FeCH compete for Proto (Figure 6). One of the proteins controlling the flow of the substrate at this step is Gun4. This protein interacts with ChlH subunit of MgCH (Sobotka et al., 2008a). Even though Gun4 has an affinity to both Proto and MgP (Larkin et al., 2003), it exhibits a preference for MgP (Peter and Grimm, 2009). It was suggested that Gun4 with bound porphyrin might stabilize membrane-associated MgCH/MTF complex (Kopečná et al., 2015a) and stimulate MgCH activity by assisting with the release of MgP (Verdecia et al., 2005), therefore control the diversion of tetrapyrroles into Chl synthesis. Other mechanisms affecting MgCH are redox control and the concentration of Mg^{2+} and ATP (Ikegami et al., 2007; Jensen et al., 1999). Interestingly, most of the proposed regulatory mechanisms at the branchpoint primarily concern MgCH and not FeCH (reviewed by Czarnecki and Grimm, 2012).

Nevertheless, FeCH itself might possess a regulatory role. Decrease of its activity by inhibitor or mutation can rescue some mutant strains displaying Chl deficiency (Bučinská et al., 2018; Sobotka et al., 2005). The CAB domain fused to the C-terminal end of FeCH occurring in oxygenic phototrophs might be involved in regulation. The CAB domain is essential for protein dimerization (Sobotka et al., 2008b; Sobotka et al., 2011) and when dimerized, it is able to bind Chl and carotenoids (Pazderník et al., 2019). Moreover, the strain missing the CAB domain retains more Chl under high-light conditions, which suggests the possible role of the domain in the regulation of Chl biosynthesis or its distribution to Chl-binding proteins (Sobotka et al., 2011).

1.8.3 Effect of oxygen level on tetrapyrrole biosynthesis

Cyanobacteria have adapted to a wide variety of environments on the Earth. Increased level of oxygen in the atmosphere led to changes in metabolism and incorporation of oxygen-dependent enzymes instead of some oxygen-sensitive ones (Aoki et al., 2011). For several enzymatic steps, cyanobacteria possess both oxygenic and anoxygenic variant of the enzymes (Aoki et al., 2012; Fujita et al., 2015), possibly because they are exposed to fluctuating oxygen levels. The oxygenic variant functions under oxic conditions and the anoxygenic under anoxic or microoxic conditions. Three such enzyme pairs operate within the Chl and bilin biosynthetic pathway (Figure 7).

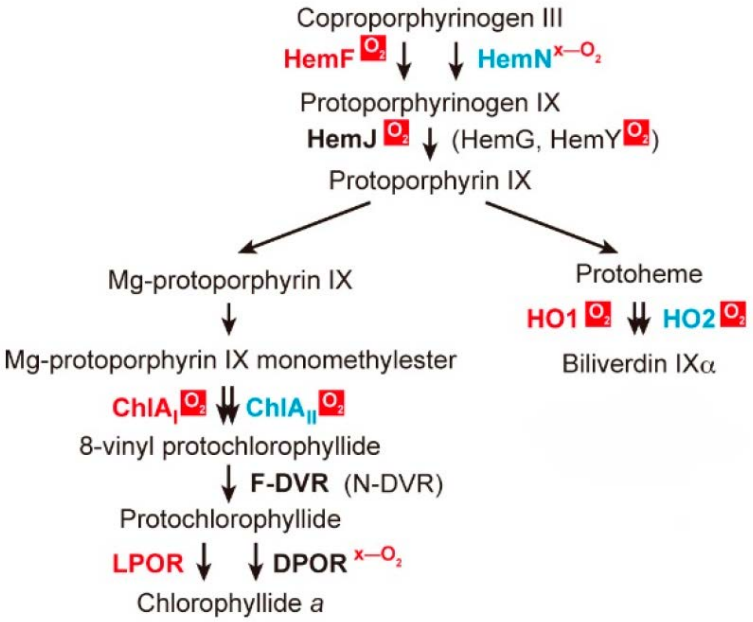

Figure 7

Tetrapyrrole (Chl, heme, and bilins) biosynthesis in cyanobacteria affected by oxygen (adapted from Fujita et al. (2015))

Steps involving more than two enzymes are shown by two arrows. Two separated arrows indicate that two enzymes are evolutionarily distinct, and two overlapped arrows indicate that two enzymes are isoforms. Enzymes that have an essential role under oxic conditions are shown in red. Enzymes that operate mainly under microoxic conditions are shown in blue. Enzymes that require oxygen for catalysis are shown by "O_2" in the red background, and enzymes that are inactivated by oxygen are shown by red "x-O_2" symbols.

CPO reaction is performed by either HemF or HemN, which are evolutionary unrelated enzymes (Goto et al., 2010). Whereas HemF uses oxygen as an electron acceptor (Breckau et al., 2003), HemN (as SAM family member) uses [4Fe-4S] cluster as a cofactor (Layer et al., 2002). This iron-sulfur cluster is inactivated in the presence of oxygen, thus HemN is functional at the anoxic or microoxic condition. HemF as an oxygen-dependent enzyme is also able to operate under microoxic conditions probably because of its high affinity for oxygen (Goto et al., 2010).

There are also two isoforms of heme oxygenase in *Synechocystis* 6803 (HO1 and HO2). HO1 is essential for growth under oxic conditions and dispensable under micro-oxic conditions (Aoki et al., 2011), whereas HO2 seems to be dominant at high light and micro-oxic conditions and accessory HO under low-light conditions. As both HO requires oxygen for their reaction, it is expected that HO2 has a higher affinity for oxygen compared to HO1 (Aoki et al., 2011).

Also, the reaction performed by cyclase is catalyzed by two enzymes according to the oxygen level (Minamizaki et al., 2008). In *Synechocystis* 6803, these two condition-dependent variants of cyclase (named $ChlA_I$ and $ChlA_{II}$) display significant similarity to each other (Fujita et al., 2015). In *Synechocystis* 6803, *hemN* and $chlA_{II}$ genes together with *HO2* form an operon transcribed at low oxygen condition. In some other cyanobacteria oxygen-independent cyclase BchE containing [4Fe-4S] cluster performs cyclase reaction at low-oxygen conditions (Ouchane et al., 2004).

Furthermore, DV Chlide biosynthetic step is influenced by oxygen as dark-operative POR contains oxygen sensitive iron-sulfur cluster.

1.8.4 Tetrapyrroles and nitrogen utilization

Cyanobacteria need to tune their photosynthetic apparatus according to nutrient availability, as the growth under nutrient depletion is retarded and excess of light may cause severe damage to the cell (Forchhammer and Schwarz, 2019). Nitrogen is a macronutrient present in proteins, and nucleic acids and also tetrapyrroles. As a source of nitrogen, cyanobacteria can use a number of compounds including ammonium, nitrate, nitrite, and urea (Flores and Herrero, 2005). Moreover, many cyanobacteria also assimilate atmospheric N_2.

Uptaken nitrogen compounds are converted to ammonium, which is incorporated through the glutamine synthetase (GS) – glutamate synthase (GOGAT) cycle (Figure 8). GS-GOGAT cycle uses 2-oxoglutarate, the intermediate of the Krebs cycle as a carbon skeleton, which makes 2-oxoglutarate the cell sensor for nitrogen/carbon balance (Figure 8, Zhang et al. (2018)).

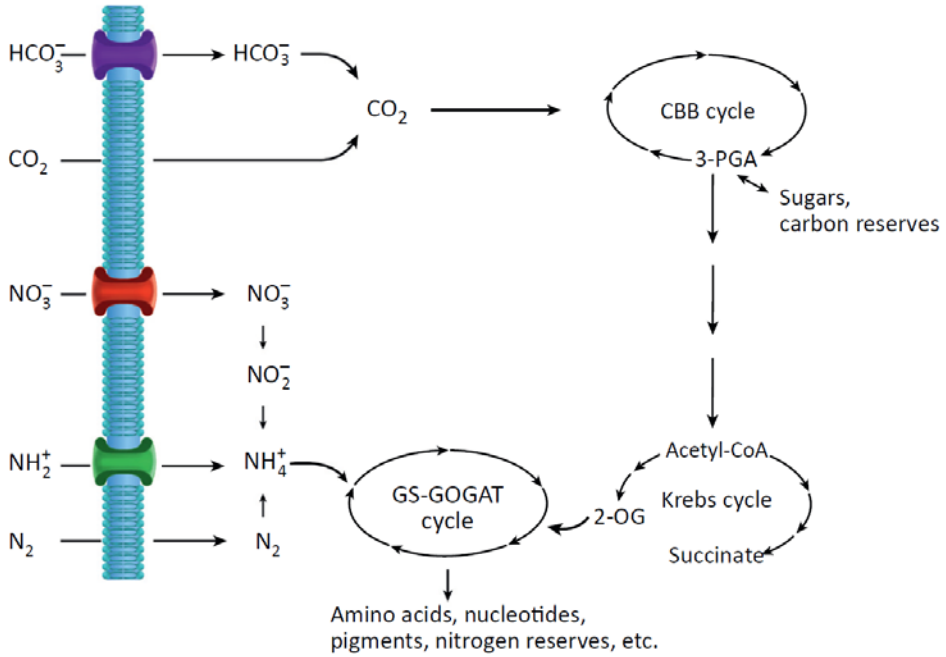

Figure 8

Coupling between carbon and nitrogen metabolism (Zhang et al., 2018)

Inorganic carbon, as CO2 or HCO_3^-, enters the cells, and it is in the form of CO_2 that is assimilated into organic carbons through the Calvin-Benson-Bassham (CBB) cycle. Fixed carbon through the CBB cycle is further used for biosynthesis or to feed the Krebs cycle (incomplete in cyanobacteria due to the lack of the 2-oxoglutarate (2-OG) dehydrogenase). Different forms of inorganic nitrogen converted to NH4+ are assimilated through the glutamine synthetase-glutamate synthase (GS-GOGAT) cycle using 2-OG as a carbon skeleton. Glu and Gln, the two amino acids produced from the GS-GOGAT cycle are also important nitrogen donors for the synthesis of a variety of nitrogen-containing compounds.

Cyanobacteria have evolved mechanisms to adapt to environmental stress and nutrient availability. This involves accumulation of storage compounds in the form of inclusions and granules. Cyanobacteria use PBSs and cyanophycin as storage of nitrogen (Zhang and Yang, 2019). Cyanophycin is a non-ribosomally synthesized polyamide consisting of aspartate and arginine (Watzer and Forchhammer, 2018). As arginine is a key building block of cyanophycin, its metabolism plays a key role in cyanobacterial nitrogen storage and remobilization. The nitrogen status is sensed by the PII protein. PII binds 2-oxoglutarate and also ADP/ATP (Forcada-Nadal et al., 2018), thus it can react to the energy status of the cell. At nitrogen excess, the level of 2-oxoglutarate level is low and PII forms a complex with N-acetyl-L-glutamate kinase (NAGK) catalyzing the step of arginine biosynthesis (Burillo et al., 2004). PII binding to NAGK increases arginine biosynthesis and finally leads to accumulation of cyanophycin (Maheswaran et al., 2006). If the level of 2-oxoglutarate is high, which signals nitrogen limitation, PII-NAGK complex is disassembled. Moreover, the PII-interacting protein releases from PII and binds to transcription activator NtcA (reviewed in Forcada-Nadal et al. (2018)), which leads to enhanced expression of NtcA dependent genes causing upregulation of nitrogen uptake systems and mobilization of nitrogen reserves stored as cyanophycin (Muro-Pastor et al., 2001; Tolonen et al., 2006). If these actions do not lead to improvement of nitrogen status, the cell starts to degrade PBSs (Collier and Grossman, 1992). In the case of ongoing nitrogen starvation, the cell gradually degrades the cellular content including photosystems, which leads to a radical decrease of Chl content. After several weeks cells persist in a state of highly reduced metabolic activity and contain only residual amounts of PBSs and PSII but substantial level of PSI (Spät et al., 2018). Interestingly, the transcription levels of FeCH and Chl-synthase increase during nitrogen starvation, probably to avoid accumulation of toxic Proto and MV Chlide (Klotz et al., 2016). During recovery from nitrogen starvation, the first photosynthetic activity can be detected 12 hours after nitrate addition (Forchhammer and Schwarz, 2019). The re-appearance of photosynthetic activity has to be linked with re-start of pigment synthesis. The question is how turning on/off the tetrapyrrole pathway is achieved as a response to nitrogen availability.

1.8.5 Complex formation

As the intermediates of the tetrapyrrole biosynthetic pathway are highly photoreactive, it has been proposed, that direct channeling of potentially toxic intermediates from one enzyme to the next one would be beneficial for the cell. The existence of such a multienzyme system has been discussed for decades (Shlyk, 1971; Wang and Grimm, 2015). However, some evidence exists only for the formation of partial subcomplexes (discussed further below). This may be due to low stability of many protein complexes involved in the synthesis of tetrapyrroles reflecting their transient and highly dynamic nature to achieve rapid change when metabolic requirements alter (Wang and Grimm, 2015). Further, I discuss enzymes of the tetrapyrrole pathway indicated to form complexes.

At the ALA synthesis step, the product of reaction performed by GluTR is highly reactive GSA, which has a lifetime less than 4 minutes at physiological conditions (Hoober et al., 1988). It has been confirmed and that GluTR forms a complex with GSAM (Figure 9), which ensures channeling of GSA without exposure to the aqueous environment (Luer et al., 2005; Nogaj and Beale, 2005).

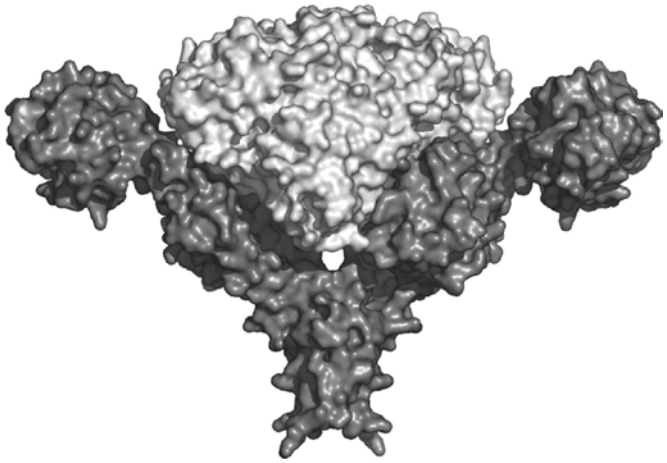

Figure 9
The model complex of glutamyl-tRNA reductase (*dark gray*) and glutamate-1-semialdehyde 1,2-aminomutase (*light gray*) from *Escherichia coli* (Luer et al., 2005).

Complex formation is also assumed for the last three enzymes of the heme biosynthetic pathway (CPO, PPO, and FeCH). Proto, containing 13 conjugated double bonds, is the first photoactive intermediate of the tetrapyrrole pathway. Even though CPO and PPO substrates itself (Coprogen and Protogen, respectively) are not photoactive, their oxidized products are. Therefore their production and channeling have to be carefully regulated. Ferreira et al. (1988) proposed the complex formation of PPO with CPO and FeCH. According to the results of co-immunoprecipitation and double-immunogold labeling/electron microscope experiments in *Thermosynechococcus elongatus*, complex formation between FeCH and HemY variant of PPO seems very likely (Masoumi et al., 2008). In these experiments stable complex formation with CPO was ruled out,

nevertheless, the transient interaction cannot be fully excluded. Formation of PPO and FeCH complex was also supported by data from co-immunoprecipitation of tagged heme biosynthesis enzymes purified from developing erythroid cell cultures (Medlock et al., 2015).

Also, enzymes involved in Chl biosynthesis are speculated to form a multienzyme complex, since Chls and their intermediates are considered to be one of the most dangerous photodynamic agents. Gorchein (1972) measured the activity of Mg-chelatase in whole cells of *Rhodobacter sphaeroides* (*R. sphaeroides*) and detected Mg PME as a product, suggesting that Mg-chelatase reaction and following methylation step are closely coupled. Shepherd et al. (2005) demonstrated that ChlH subunit of Mg-chelatase has a dramatic stimulatory effect on MTF. Also, cyclase and POR are expected to form a complex as they were both co-immunoprecipitated with FLU (Kauss et al., 2012).

Since the majority of Chl is associated with photosystems, it is hypothesized that Chl biosynthetic machinery might be directly integrated with the process of photosystem assembly (Komenda et al., 2012). This is supported by decrease of photosystems and antennae as a reaction to disruption of the Chl pathway (Kopečná et al., 2013; Papenbrock et al., 2000; Sobotka et al., 2008a), since any decline of Chl synthesis affects also the synthesis of Chl binding proteins (e.g. CP43; CP47). It appears that Chl incorporation occurs during protein synthesis and it is probably vital for proper protein folding and stability (Eichacker et al., 1996; Sobotka, 2014). On the other hand, there is probably also reverse regulation to avoid free Chl accumulation, as genetic deletion of some of the PSI and PSII subunits leads to reduced Chl content in *Synechocystis* 6803 (Bečková et al., 2017; Shen et al., 1993; Sobotka et al., 2005).

1.9 Proteins characterized in the thesis

1.9.1 BtpA

BtpA (biogenesis of thylakoid proteins A) is a 30 kDa peripheral membrane protein exposed to the cytoplasm (Zak et al., 1999). Structurally BtpA forms a TIM-barrel consisting of 8 βα units. TIM barrel is one of the most common protein folds and TIM-barrel proteins display a variety of enzymatic functions (Wierenga, 2001). TIM-barrel proteins possess the central protein core created by eight parallel β-strands that are covered by eight α-helices on the outside. In BtpA there is an additional C-terminal hydrophobic region. BtpA from *Synechocystis* 6803 overexpressed in *Escherichia coli* (*E.coli*) formed oligomers, although it was not clear if that was not an artifact of isolation (Schwabe et al., 2003).

BtpA was identified during genetic complementation of *Synechocystis* 6803 mutant strain with reduced PSI content but normal level of PSII (Bartsevich and Pakrasi, 1997). This strain also displayed a significantly lower level of Chl (15 to 20% of WT strain). It was shown that a point missense mutation in the *btpA* gene (*sll0634*), resulting in the replacement of Val51 for Gly51, is responsible for the phenotype. The Δ*btpA* strain had higher degradation rate of the PSI reaction center protein PsaA (Zak and Pakrasi, 2000). It was suggested that BtpA might function as a chaperone interacting with PsaA and/or PsaB, stabilizing reaction center proteins indirectly or it is involved in the insertion/assembly of cofactors in PSI.

Proteins homologous to BtpA are present in archaebacteria, eubacteria, and animalia suggesting that the role of BtpA may be more general (Bartsevich and Pakrasi, 1997). However, it is not clear if the function of the protein is the same in these organisms, considering the conserved structure of the TIM barrel. BtpA is present in most cyanobacteria with the exception of *Prochlorococcus* (Mareš et al., 2019), which underwent loss of many genes in its early evolutionary stage (Sun and Blanchard, 2014). Among cyanobacteria, BtpA displays peculiar phylogeny (Mareš et al., 2019), when BtpA from *Chloroflexus* is basal to marine *Synechococcus*, followed by *Gloeobacter*. Otherwise, its phylogeny follows the phylogenic tree.

1.9.2 PPO

PPO is the last enzyme common for heme and Chl pathway. Although the six electron oxidation of Protogen occurs also spontaneously, its enzymatic conversion is apparently necessary for the correct channeling of Proto to chelatases for metal insertion. Until now, three different enzymes without any homology are known to serve as a protoporphyrinogen oxidase (HemY, HemG, and HemJ) (Figure 10). Such variability in the middle of the tetrapyrrole pathway is surprising considering the foreseen need for strict regulation of Proto production and Proto channeling within enzymatic complexes.

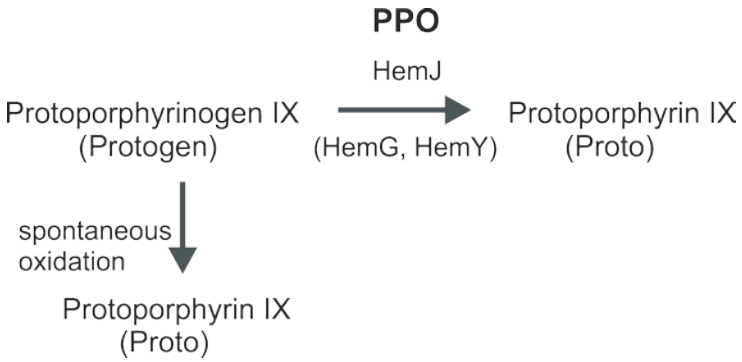

Figure 10

Enzymatic and non-enzymatic oxidation of Protogen

Protoporphyrinogen IX is enzymatically converted into Protoporphyrin IX by protoporphyrinogen oxidase (PPO). Protoporphyrin IX can be also created nonenzymatically by spontaneous reaction of Protoporphyrinogen IX with molecular oxygen.

The HemY is an oxygen-dependent enzyme with approximately 55 kDa, creating membrane-bound dimers and using flavin-adenine dinucleotide as a cofactor. Recent data suggest that HemY in *Chlamydomonas reinhardtii* uses oxidized plastoquinone as an electron acceptor (Brzezowski et al., 2019). HemY occurs among most of the bacterium phyla and almost all the eukaryotes. It may imply that HemY is the ancestral type of PPO (Kobayashi et al., 2014). The only known exception of HemY distribution among eukaryotes is *Leishmania major*, which contains HemG (Zwerschke et al., 2014).

HemG (21 kDa) is mostly found in γ-proteobacteria (Kobayashi et al., 2014). The protein forms membrane-associated oligomers (Boynton et al., 2009; Möbius et al., 2010), uses flavin mononucleotide as a cofactor and is functional in aerobic as well as anaerobic condition (Boynton et al., 2009). Electrons from the Proto oxidation catalyzed by HemG are withdrawn via ubiquinone, cytochrome *bo*' and cytochrome *bd* oxidases to oxygen, or under anoxic conditions to the terminal electron acceptors fumarate and nitrate by corresponding reductases (Möbius et al., 2010).

Lastly, *slr1790* gene of the cyanobacterium *Synechocystis* 6803 was found to encode the third PPO (22 kDa) named HemJ (Kato et al., 2010). HemJ probably evolved within α-proteobacteria and spread to cyanobacteria and various proteobacteria through multiple horizontal gene transfer. This is apparently common also for distribution of other PPO variants as different PPOs frequently co-occur in the same phylum (Kobayashi et al., 2014). *HemJ* appears to be essential and could not be inactivated in *Synechocystis* 6803 (Kato et al., 2010). A partially segregated *Synechocystis* 6803 strain contained less than half of the Chl compared to wild type (WT) and although it accumulated Proto, that probably originated from the non-enzymatic oxidation of Protogen (Figure 9). Accordingly, the *hemJ* deletion strain from *Acinetobacter baylyi* (*A. baylyi*) exhibited auxotrophy for hemin and accumulated porphyrins when supplemented with ALA (Boynton et al., 2011). Interestingly, cyanobacterium *Gloeobacter violaceus* and some

green photosynthetic bacteria possess homologs of 2 different PPOs. However, it is not clear, whether both of them are functional protoporphyrinogen oxidases (Kobayashi et al., 2014).

Several organisms do not contain any of three known PPOs. They can be divided into two groups. The first group represents parasitic or symbiotic organisms, in which most of the heme biosynthesis genes are missing probably as a result of secondary gene losses (Dailey et al., 2017). The second group of organisms contains alternative heme biosynthetic pathway for instance through precorrin-2 and siroheme (Kühler et al., 2014).

1.9.3 Sll1106

Sll1106 is a membrane protein with an unknown function containing an extended glycine zipper motif (Figure 11), which can be found in a number of channel-forming proteins (Kim et al., 2005). Expression of *sll1106* is induced in response to short-term salt stress (Pandhal et al., 2009) and hyperosmotic stress (Vidal et al., 2009). The similar expression pattern share also surrounding genes *sll1107* (a type IV pilus biogenesis protein) and *slr1192* (a member of alcohol dehydrogenase/reductase family) (Vidal et al., 2009), nevertheless, there was not found any functional relationship of Sll1106 with these proteins.

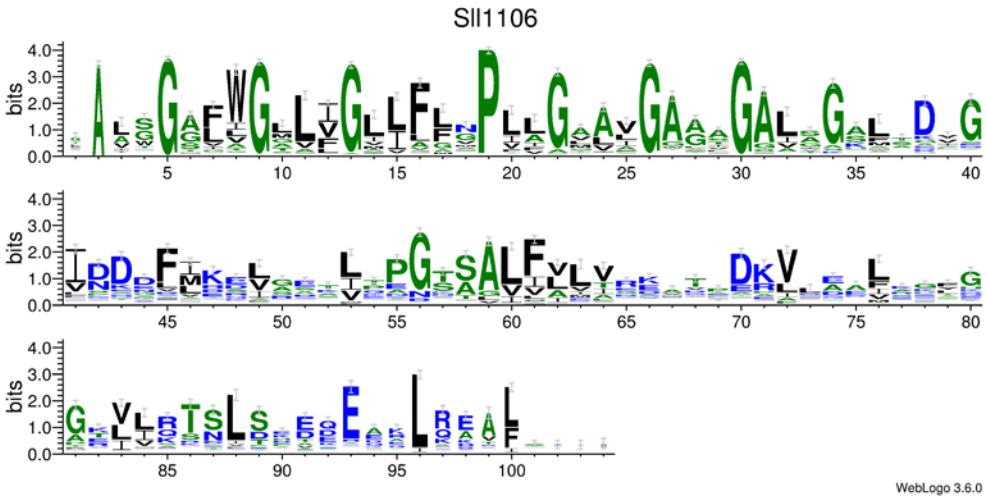

Figure 11

Sequence conservation of the proteins from a Duf1269 family

The consensus sequence of the Pfam family of proteins containing Sll1106 (Duf1269), was generated with Weblogo 3.6.0. (Crooks et al., 2004). The height of the letters correlates with their conservation. Black, blue and green letters indicate hydrophobic, hydrophilic and other residues, respectively. Data for this logo consist of 468 sequences from the PF06897 Pfam family.

1.9.4 CurT (Slr0483)

Curvature thylakoids (CurT) proteins have been described in *Arabidopsis thaliana* as proteins modifying the thylakoid architecture by inducing the curvature of the membrane (Armbruster et al., 2013). Plants genomes usually carry several genes with homology to CurT. In *Arabidopsis thaliana,* the CurT family contains 4 proteins (CurT1A-D). These proteins from *Arabidopsis thaliana* creates oligomers and are highly enriched in grana margins (Figure 12, Pribil et al. (2014)). CurT homologs are found in plants, algae, and cyanobacteria (Armbruster et al., 2013). However, CurT is missing in several basal cyanobacterial lineages (Mareš et al., 2019).

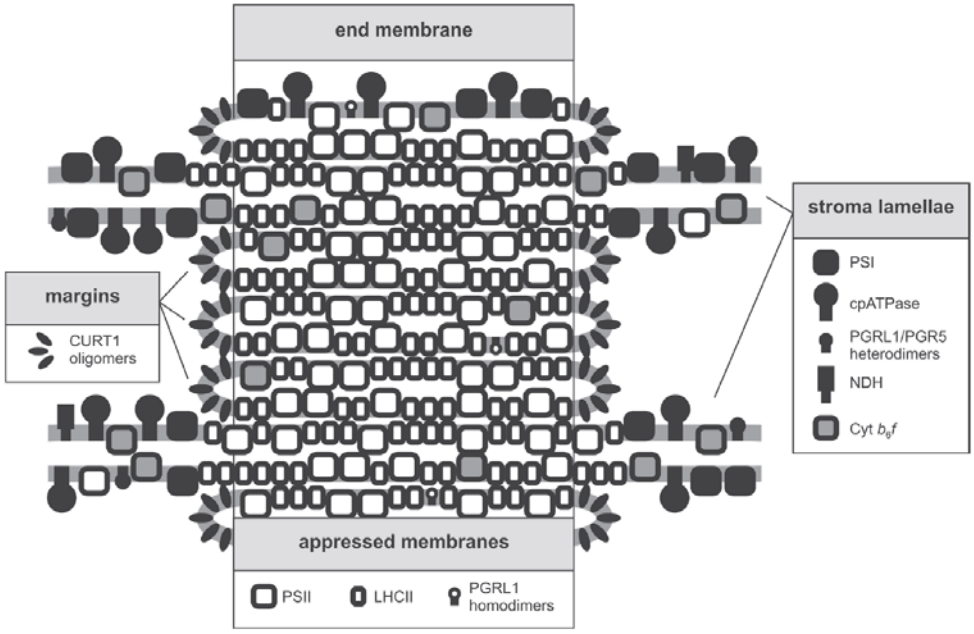

Figure 12

Lateral heterogeneity in plant thylakoids (Pribil et al., 2014)

Protein complexes predominantly located in the stroma lamellae [PSI, cpATPase, NAD(P)H dehydrogenase (NDH), and PGRL1–PGR5 heterodimers] are shaded in black, whereas complexes found in the appressed membranes of the grana (PSII dimers and LHCII trimers) are shown in white. The dimeric Cyt *b6f* complex (grey shading) is thought to be present in both stroma lamellae and appressed regions (Dekker and Boekema, 2005), whereas CURT1 oligomers (black ellipses) are found in the highly curved regions of thylakoids, in particular in the grana margins (Armbruster et al., 2013).

In *Synechocystis* 6803, the single CurT protein is encoded by *slr0483* gene and it is predicted to have 149 amino acids (Figure 13). Its domain composition is similar to that of *Arabidopsis thaliana* (Armbruster et al., 2013). It contains 2 transmembrane helices, and its C- and N-terminal are exposed to the cytoplasm. The N-terminal part contains a conserved amphipathic helix implicated in membrane bending. C-terminal domain of all CurT proteins is homologous to cyanobacterial aminoacyl-tRNA synthetases appended domain (CAAD) present in around one-third of cyanobacterial species as a part of one or

two aminoacyl-tRNA synthetases (Luque and Ochoa de Alda, 2014). This CAAD domain is responsible for the localization of associated aminoacyl-tRNA synthetases to thylakoids and may also mediate channeling of other members of the gene translation machinery to this location (Olmedo-Verd et al., 2011).

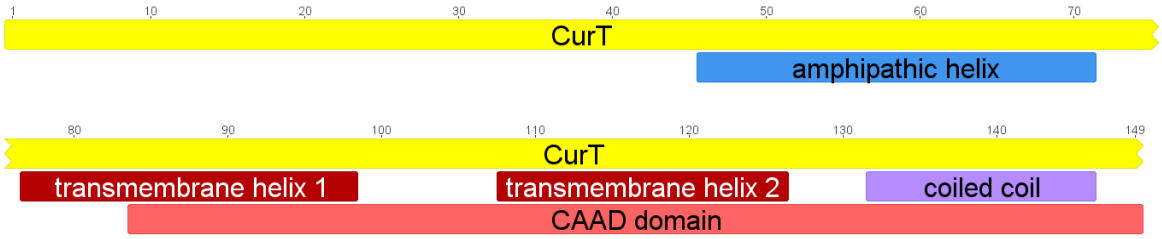

Figure 13

Scheme of domains in the CurT protein

Position of amphipathic helix and CAAD domain consisting of 2 transmembrane helices and coiled coil are marked in the scheme created by Geneious 8.1 (https://www.geneious.com).

CurT is an abundant protein in *Synechocystis* 6803 as its molar amount is similar or higher than the amount of PSII (Krynická and Jackson, unpublished results). The functional complementation of *Synechocystis* 6803 CurT by its counterpart from *Arabidopsis thaliana* confirmed that the function of CurT proteins is evolutionary conserved. The Δ*curT* strain of *Synechocystis* 6803 obtained by Heinz et al. (2016) showed massive disorganization of the thylakoid membrane system and the cells contained only half of the PSII. CurT was localized to the regions with low Chl autofluorescence to the thylakoid convergence zones (Rast et al., 2019), and was also detected to extend to the cytoplasm. Loss of CurT also led to the loss of competence for DNA uptake (Heinz et al., 2016).

2. Objectives of the thesis

The tetrapyrrole pathway has to be regulated based on nutrient and light availability, to fulfill the changing cell demands for its end products heme and Chl. Moreover, the accumulation of individual intermediates has to be avoided as the majority of them is phototoxic. To accomplish this, the tetrapyrrole pathway must be interconnected with the assembly of photosystems as heme and Chl are vital components of photosystems. This creates highly sophisticated regulatory machinery, which is only partially understood.

The goal of this thesis is to enhance our understanding of the regulation of the tetrapyrrole pathway by a study of selected proteins with the connection to the tetrapyrrole pathway. The main goals were to uncover nature of the low tetrapyrrole phenotype of Δ*btpA* mutant prepared in our lab and closer characterization of the last discovered PPO variant, HemJ. To reveal or clarify their role in the tetrapyrrole pathway, I have used particular deletion mutants and extensively also their suppressor mutants. To uncover potential binding partners, the FLAG-tagged version of the proteins were prepared and purified by affinity chromatography under native conditions. Two additional proteins (Sll1106 and CurT) were characterized on the basis of their co-purification with HemJ and the following enzyme in the pathway, FeCH, which has been studied in our lab for a long time.

3. Materials and methods

3.1 Construction of *Synechocystis* 6803 strains

The strains used in this thesis (Table 1, Table 2) were derived from non-motile, glucose-tolerant *Synechocystis* 6803 strain obtained from the laboratory of Peter J. Nixon (Imperial College, London, UK). To prepare a strain expressing proteins with a 3xFLAG tag at the N- or C-terminus, the respective gene was cloned into the pPD-FLAG or pPD-*C*FLAG plasmid, respectively. These plasmids contain the *Synechocystis* 6803 *psbAII* promoter, a sequence encoding the tag, kanamycin resistance cassette and flanking sequences for homologous recombination. The flanking regions allow the insertion of a gene with the tag into the *Synechocystis* 6803 genome in place of the *psbAII* gene (Chidgey et al., 2014). *Synechocystis* 6803 cells were transformed with 1-2 µl of the respective plasmid. As for most of the studied genes were impossible to fully segregate their deletion mutants or they tend to create the suppressor mutants, insertion of modified gene preceded the deletion of the native gene (with the exception of sll1106).

As pPD-*C*FLAG plasmid containing *hemJ.f* (pPD-*hemJ.f*) isolated from *E. coli* frequently contained frameshift mutations within *hemJ,* the fragment for this transformation was obtained by PCR using pPD-*hemJ.f* ligation mixture as a template. The resultant PCR fragment was used for transformation of WT and ΔPSI strains (Shen et al., 1993).

To prepare *Synechocystis* 6803 strain expressing HemG from *E. coli* under the *Synechocystis* 6803 *psbAII* promoter, the *hemG* gene (Sasarman et al., 1993) was again cloned into the pPD-*C*FLAG plasmid, leaving out the 3xFLAG tag. The WT strain was transformed with the resultant plasmid, and the WT copy was subsequently deleted.

To construct the P(*petJ*)::*hemJ* strain expressing HemJ under the control of copper-repressed promoter, pPsbAIpetJ-FLAG plasmid (Knoppová et al., 2014) was used with the *hemJ* gene inserted into specific restriction sites, leaving out the 3xFLAG tag. The resulting plasmid was used for WT transformation, and the WT copy of *hemJ* was deleted afterward.

ΔbtpA and Δ*curT* R1-R5 in our background (Table 1) were obtained by transformation of WT with chromosomal DNA isolated from the Δ*btpA* strain (Zak et al., 1999), Δ*curT* bearing zeocin resistance (Hollingshead, unpublished), respectively.

The vectors used for the disruption of other genes by a resistance cassette were constructed using the megaprimer PCR method (Lee et al., 2004). Firstly, upstream and downstream regions of the respective gene were amplified from WT genomic DNA with flanking sequences of resistance cassette. Then the upstream and downstream regions with overhangs for resistance cassette were used as primers to amplify the construct for deletion. 5µl of the resulting PCR reaction mixture was used for transformation of *Synechocystis* 6803 strains.

As *Synechocystis* 6803 contains multiple copies of the genomic DNA, transformants were selected on BG11 agar plates with increasing levels of the corresponding antibiotic to achieve homozygosity of the mutated locus. Full segregation was confirmed by PCR.

Table 1

List of strains with gene deletion

Strain name	Deleted gene	Type of deletion	Localization of deletion	Resistance	Source of the construct/other notes
Δ*btpA*	*sll0634*	insertion	207	kanamycin	Zak et al. (1999)
btpA.f*/Δ*btpA	*sll0634*	deletion	57-808 of 867	erythromycin	
Δ*hemJ*	*slr1790*	deletion	43-534 of 582	chloramphenicol	unsegregated
hemJ.f*/Δ*hemJ	*slr1790*	deletion	43-534 of 582	chloramphenicol	
hemG*/Δ*hemJ	*slr1790*	deletion	43-534 of 582	chloramphenicol	
P(*petJ*)::*hemJ*	*slr1790*	deletion	43-534 of 582	chloramphenicol	derived from *hemJpetJ* (Table 2)
Δ*sll1106*	*sll1106*	deletion	71-496 of 516	erythromycin	
hemJ.f*/Δ*sll1106	*sll1106*	deletion	71-496 of 516	erythromycin	
Δ*curT* R1-R5	*slr0483*	deletion	50-339 of 450	zeocin	S. Hollingshead (lab of N. Hunter)
curT.f*/Δ*curT	*slr0483*	deletion	24-422 of 450	erythromycin	
Δ*curT*	*slr0483*	deletion	24-422 of 450	erythromycin	unsegregated
Δ*curT*/Δ*psbE*	*slr0483*	deletion	24-422 of 450	erythromycin	
Δ*curT*/ΔCP47	*slr0483*	deletion	24-422 of 450	erythromycin	

Table 2

List of other strains

Strain name	Gene	Protein	Tag	Protein end	Promoter	Resistance	Source of the strain
btpA.f	*sll0634*	BtpA	3xFLAG	N	*psbAII*	kanamycin	
gluTR.f	*slr1808*	GluTR	3xFLAG	N	*psbAII*	kanamycin	J.Kopečná
hemJ.f	*slr1790*	HemJ	3xFLAG	C	*psbAII*	kanamycin	
***hemJ.f*/ΔPSI**	*slr1790*	HemJ	3xFLAG	C	*psbAII*	kanamycin	
hemJpetJ	*slr1790*	HemJ	-	-	*petJ*	kanamycin	
hemG	*xxx*	HemG	-	-	*psbAI*	kanamycin	
sll1106.f	*sll1106*	Sll1106	3xFLAG	C	*psbAII*	kanamycin	
f.sll1106	*sll1106*	Sll1106	3xFLAG	N	*psbAII*	kanamycin	
His-*C-tn*/ΔH324	*slr0839*	FeCH	6xHis	-	*psbAII*	zeocin	Pazderník et al. (2019)
FLAG-*hemH*/ Δ*hemH*	*slr0839*	FeCH	3xFLAG	N	*petJ*	kanamycin	Sobotka et al. (2011)

3.2 Growth conditions

Synechocystis 6803 strains were grown photoautotrophically in the BG11 medium in shaken conical flasks at 29 °C and irradiance of 40 μmol photons m^{-2} s^{-1}. Δ*btpA* and Δ*hemJ*/*hemG* and Δ*curT* R1-R5 strains were grown in the medium supplemented with 5 mM glucose. P(*petJ*)::*hemJ* strain was grown in the medium without copper and addition of 1 μM $CuSO_4$ was used for repression of *hemJ* expression. For the purification of FLAG-tagged proteins, 4 liters of cells were grown photoautotrophically or mixotrophically (supplemented with 5 mM glucose) to OD_{730} of 0.5 to 0.7 in the BG11 medium.

3.3 Analysis of cellular tetrapyrroles

Whole-cell absorption spectra were measured with Shimadzu UV-3000 spectrophotometer. Heme/Chl precursors were measured from 2 ml of culture OD_{730} ~ 0.4 using high-performance liquid chromatography (HPLC) according to the procedure described in Pilný et al. (2015). For the detection of porphyrins accumulated in the Δ*hemJ/hemG* strain, 50 ml of cells were grown without glucose for three days and harvested at OD_{730} ~ 0.4. Pigments were extracted by an excess of 70% methanol, separated by an HPLC method described in Pilný et al. (2015) and their absorbance was detected by a diode array detector.

Heme content was measured from 2 ml of culture OD_{730} ~ 0.4 using HPLC according to the procedure described in Horáková et al. (2017).

Chl fluorescence emission spectra (77 K) were measured using an Aminco Bowman Series 2 luminescence spectrometer (Spectronic Unicam). The spectra were normalized according to added rhodamin standard.

3.4 Preparation of thylakoid membranes and protein complexes purification

Harvested cells of and strains were mostly washed and resuspended in buffer A containing 25 mM MES/NaOH, pH 6.5, 25% glycerol, 10 mM $MgCl_2$, 10 mM $CaCl_2$. For BtpA strains was used buffer B containing 50 mM HEPES, pH 8, 0.5 M sucrose and 15 mM NaCl and for GluTR purification was used buffer C containing 20 mM HEPES, pH 8, 20% glycerol, 150 mM NaCl and 1 mM EDTA. The cells were broken by a Mini-Beadbeater-16 (Biospec, USA). For protein purification, EDTA-free Protease Inhibitor (Roche) was added into the buffer prior to breaking the cells for the majority of purifications. Only for purification of GluTR.f, Complete protease inhibitor (Roche) was used. Membranes were pelleted by centrifugation (55,000 x *g*, 20 min., 4 °C), resuspended in excess of the respective buffer and the centrifugation step was repeated.

Anti-FLAG-M2 agarose resin (Sigma-Aldrich) was used for the isolation of FLAG-tagged proteins. The soluble fraction was loaded directly onto the column. For the

isolation of tagged protein from a membrane fraction, the membranes were resuspended in the respective buffer and solubilized for 1 hour at 10 °C with 1.5% n-Dodecyl-β-D-maltoside (DDM - Enzo Life Sciences). After centrifugation (55,000 x *g*, 20 min., 4 °C), the solubilized proteins were loaded on the column with the resin. The resin was intensively washed with 20 resin volumes of the respective buffer. For membrane fractions, the buffer contained 0.04% DDM. FLAG-tagged proteins were finally eluted with two resin volumes of the buffer with the addition of 300 μg/ml of 3xFLAG peptide (Sigma-Aldrich).

3.5 Electrophoresis and size-exclusion chromatography

The protein composition of purified complexes was analyzed by SDS-electrophoresis (SDS-PAGE) either in a denaturing 12% polyacrylamide gel or 12-20% polyacrylamide gel containing 7 M urea (Dobáková et al., 2009). For native electrophoresis, solubilized membrane proteins or isolated complexes were separated by 4 to 14% clear native gel (CN-PAGE, Komenda et al. (2019)). To resolve individual components of protein complexes, the gel strip from the CN-PAGE was first incubated in 2% SDS and 1% dithiothreitol for 30 minutes at room temperature, and then proteins were separated along the second dimension by SDS-PAGE in a denaturing 12 to 20% polyacrylamide gel containing 7 M urea (Dobáková et al., 2009). Proteins separated by SDS-PAGE were stained with Coomassie Brilliant Blue (CBB) or SYPRO Orange afterward. Mass spectrometry analysis of CBB stained protein bands/spots from the SDS-PAGE gels was accomplished essentially as described by Bučinská et al. (2018).

For detection by a specific antibody, proteins were transferred from the SDS gel to a PVDF membrane (Immobilon-P from Merck Millipore). This membrane was incubated with a respective primary antibody and then with secondary antibody conjugated with horseradish peroxidase (Sigma-Aldrich). The BtpA antibody was obtained from H.B. Pakrasi. FeCH antibody was received from A. Wilde.

3.6 Isolation of GluTR-His for antibody preparation

The GluTR gene (M84218) was cloned into NotI, Cfr9I restriction sites of the pET49 plasmid. The sequence of the ligated plasmid was checked by sequencing. The plasmid was transformed into BL21 cells. 1.5 liter of cells were grown at 37 °C in AIM medium with 30 μg/ml of kanamycin. Cells were pelleted by centrifugation and resuspended in 25 mM phosphate buffer, pH 7.5 containing 10 mM $MgCl_2$ and 50 mM NaCl, then mixed with lysis buffer containing EDTA, lysozyme, and benzonase and incubated for 40 minutes at 30 °C. The cells were broken by 4 rounds of sonication (Bandelin Sonopuls). Cell fractions were separated by centrifugation at 55,000 x g for 10 minutes. GluTR-His was purified from the soluble fraction by anti-His agarose resin (Machinery-Nagel). 10 and 20 mM imidazole was used for washing out unspecifically

bound proteins and GluTR-His was eluted by 150 mM imidazole. Eluate was concentrated by 30 kDa cut-off microconcentrator (Millipore). The concentrated eluate was dialyzed against phosphate buffer with 10% glycerol and diluted to final concentration 1 mg/ml.

3.7 Transmission electron microscopy

Various strains of *Synechocystis* and WT cells were harvested in the logarithmic growth phase by centrifugation (5,000 x g, 10 minutes). Pelleted cells were processed by Leica EM PACT2 high-pressure freezer. Samples were processed similarly as described elsewhere (Klotz et al., 2016; van de Meene et al., 2006) with some modifications. Samples were freeze-substituted in an automatic substitution unit (Leica EM AFS) starting at -85 °C in a solution of 1% tannic acid dissolved in acetone for 24 h. Then the samples were 3 times rinsed in pure acetone for 1 h and the substitution medium was replaced with 1% osmium in acetone; the temperature was kept at -85 °C. After 4 h, the temperature started to be gradually increased to -20 °C (5 °C per hour) with a 4-6 h stop at temperature -60 °C and -40 °C, when the glutaraldehyde was added (0,5% v/v). At -20 °C samples were 3 times rinsed in pure acetone and infiltrated with increasing mixtures of Spurr resin (10%, 30%) at -20 °C and further steps (50%, 75%, 100% and 100%) at the room temperature, each step for a minimum of 4 h. Samples embedded in Spurr resin (EMS, Hatfield, USA) was polymerized at 60 °C oven for 48 h. Ultra-thin sections (50-70 nm) were cut using Leica UCT ultramicrotome, collected on meshed copper grids (EMS, Hatfield, USA) with the formvar coating. Sections were stained with 1% aqueous uranyl acetate for 10 minutes and with Sato's lead citrate for 3 minutes (Hanaichi et al., 1986). Images were acquired using a transmission electron microscope Jeol 1010 operated at 80 kV equipped with a Mega View III camera (SIS) at Laboratory of electron microscopy (Biology Centre, CAS, České Budějovice).

3.8 Sequencing of the suppressor mutants

The DNA for genomic sequencing of the suppressor mutants was isolated as described by Ermakova-Gerdes and Vermaas (1999), with slight modifications. Briefly, the cells were washed by saturated NaI solution, lysed by lysozyme and SDS. The lysate was treated with proteinase K, extracted with phenol, phenol/chloroform, and chloroform and treated with RNase. The DNA was precipitated by sodium acetate and ethanol, briefly air-dried and resuspended in water. The sequencing was performed commercially. One hundred base paired-end sequencing was performed on an Illumina HiSeq 2000 system (12 samples per lane). Raw paired reads were mapped to the GT-Kazusa sequence using CLC Genomics Workbench software (https://www.qiagenbioinformatics.com). Only variants with a higher than 60% frequency were considered.

4. Results

4.1 BtpA

To characterize the phenotype of the BtpA deletion mutant (Δ*btpA*) in our background we used the same construct which was used for the creation of the original Δ*btpA* (Zak and Pakrasi, 2000). However, our Δ*btpA* deletion mutant displayed much stronger phenotype than the original one. The strain was pale grayish containing only about 2.5% of the WT Chl levels (680 nm peak) and also significantly low level of phycobiliproteins (625 nm peak) and carotenoids (region at 450 to 520 nm) (Figure 14A). As a result, the strain was deficient not only in the accumulation of PSI but also in the accumulation of PSII and PBS (Figure 14B). Most of the proteins in the thylakoids of the Δ*btpA* were reduced or missing as documented by 2D electrophoresis (Figure 14C). Indeed, the strain did not grow photoautotrophically and it was also necessary to keep it at low irradiance. When analyzed by transmission electron microscopy (made by Lenka Bučinská), the Δ*btpA* strain contained almost no membranes at most short disorganized fragments (Figure 15).

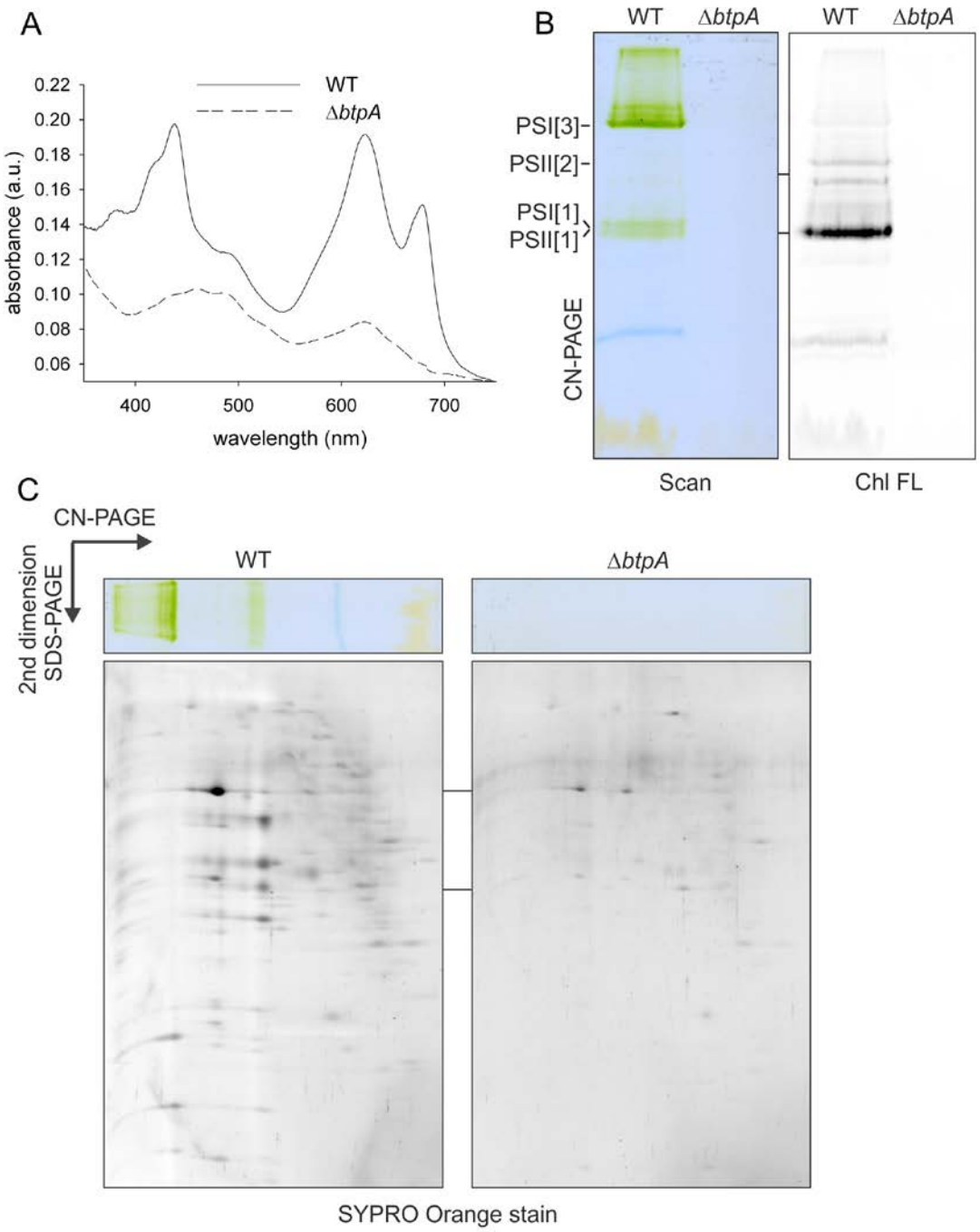

Figure 14

Characterization of the Δ*btpA* strain

(A) WT and mutant strains were grown at 5 µmol of photons $m^{-2}s^{-1}$ in the medium supplemented with 5 mM glucose and characterized by measuring the whole-cell absorption spectra. Chlorophyll is represented by 680 nm peak and phycobiliproteins by the 625 nm peak. Spectra were normalized to light scattering at 750 nm. Further determination of PSI and PSII content was done by separation of membrane complexes by 4-14% clear native gel (CN-PAGE) (B). For WT, membranes containing 5 µg of chlorophyll (Chl) were loaded; for Δ*btpA*, the amount was recalculated based on the Chl/OD ratio in both strains. The gel was scanned (Scan). Chl fluorescence (Chl FL) emitted by PSII was detected by LAS 4000 Imager (Fuji). (C) The gel strip from CN-PAGE was further separated in a second dimension by 12 to 20% SDS-PAGE and stained with SYPRO Orange.

Designation of complexes: PSI[3] and PSI[1], trimeric and monomeric PSI; PSII[2] and PSII[1], dimeric and monomeric PSII

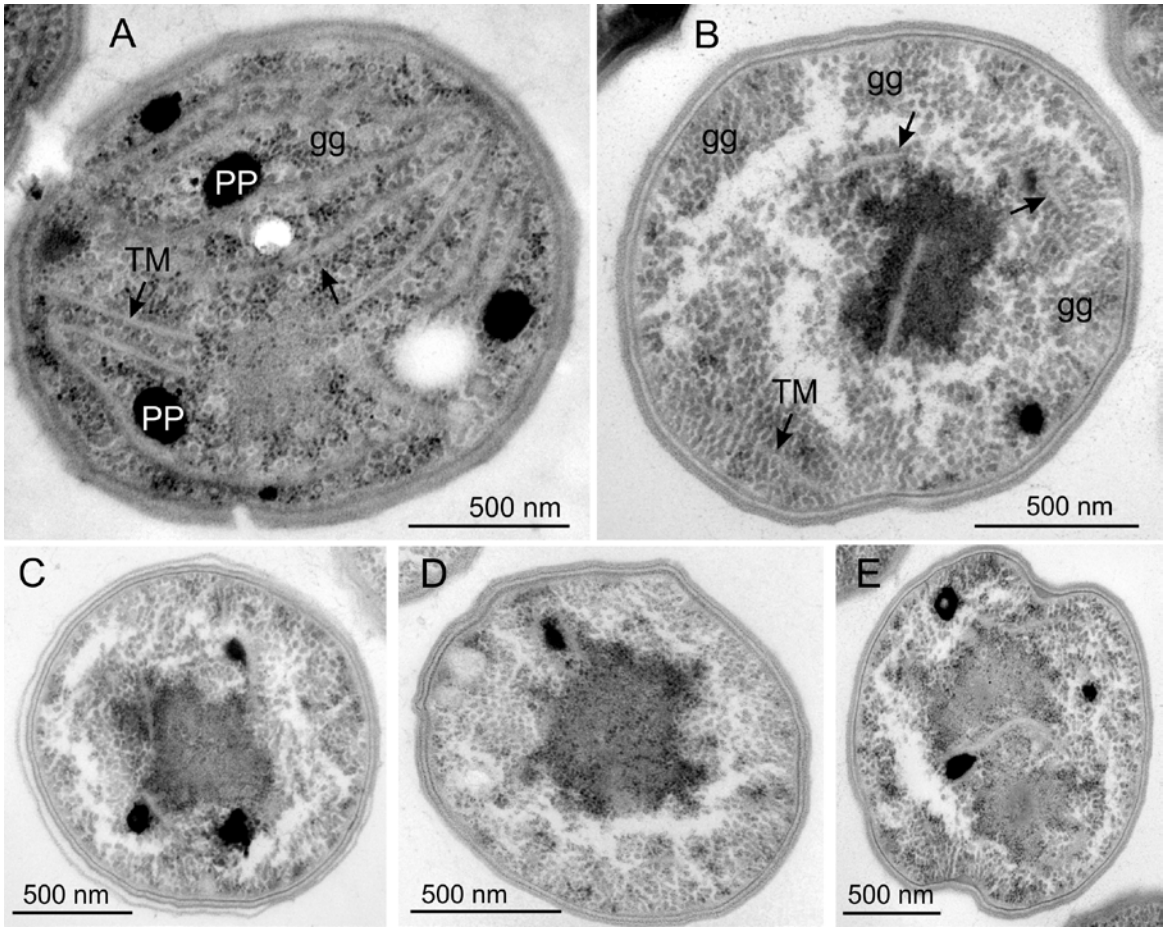

Figure 15

The Δ*btpA* ultrastructure

Ultrastructure of WT (A) and Δ*btpA* (B-D) were analyzed by transmission electron microscopy (made by Lenka Bučinská). Both strains were grown at 5 µmol of photons $m^{-2}s^{-1}$ in the medium supplemented with 5 mM glucose.

Abbreviations: TM – thylakoid membrane, gg – glycogen granules, PP – polyphosphate granules

The phenotype of the Δ*btpA* mutant was very unstable as it spontaneously formed fully photoautotrophic suppressor mutants with high frequency. Three suppressor mutants (Δ*btpA* P1-P3) were further characterized. These suppressor mutants were growing photoautotrophically and contained a normal level of pigments (data not shown) and photosynthetic complexes (Figure 16). Only suppressor mutants P1 and P2 contained lower level of PSII dimer. Additionally, 2 suppressor mutants (P2 and P3) exhibited highly increased amount of carotenoids.

To explore the genetic basis for the observed phenotype improvements, we performed whole-genome re-sequencing of the suppressor mutants using the Illumina HiSeq platform followed by genome assembly and by localization of the complementary mutations using CLC Genomics workbench. Interestingly, two of the complementary mutations were mapped into the locus containing *gluTR* gene (*slr1808*). The mutation of

P1 suppressor mutant was found in the -10 element from the transcription initiation site (Kopf et al., 2014). The P2 suppressor mutant had a missense mutation in the coding sequence for GluTR (G to C; resulting in a change of Val352 to Leu352). The last point mutation was localized in the gene for FtsH3 protease (*slr1604*) (T to C; leading to a change from Ser502 to Pro502).

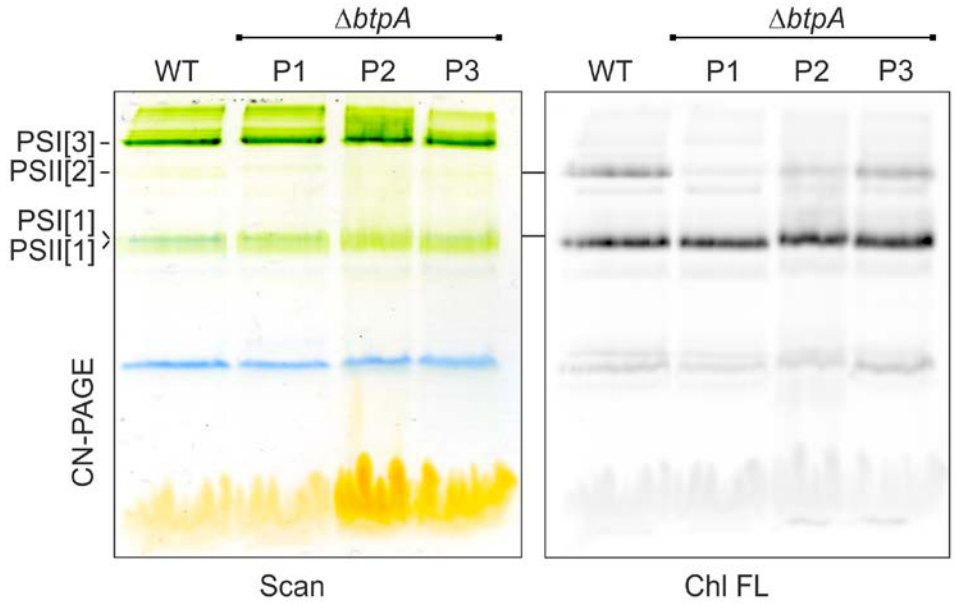

Figure 16

Separation of thylakoids from the Δ*btpA* suppressor mutants by clear native electrophoresis

Solubilized thylakoids from WT and 3 suppressor mutants of Δ*btpA* strain were separated by 4-14% clear native gel electrophoresis (CN-PAGE). The gel was scanned (Scan) and chlorophyll fluorescence (Chl FL) emitted by PSII was excited by blue light and detected by LAS 4000 Imager (Fuji). For each sample, membranes containing 5 μg of Chl were loaded.

Designation of complexes: PSI[3] and PSI[1], trimeric and monomeric PSI; PSII[2] and PSII[1], dimeric and monomeric PSII

To identify proteins interacting with BtpA, I prepared strain expressing BtpA with 3x FLAG tag under *psbAII* promoter (BtpA.f), in which I was able to delete the native BtpA. The complemented strain had a similar level of pigments as WT, showing that BtpA.f is functional (Figure 17A). Only the level of Chl was slightly higher, which is in agreement with a slightly increased level of PSI (Figure 17B).

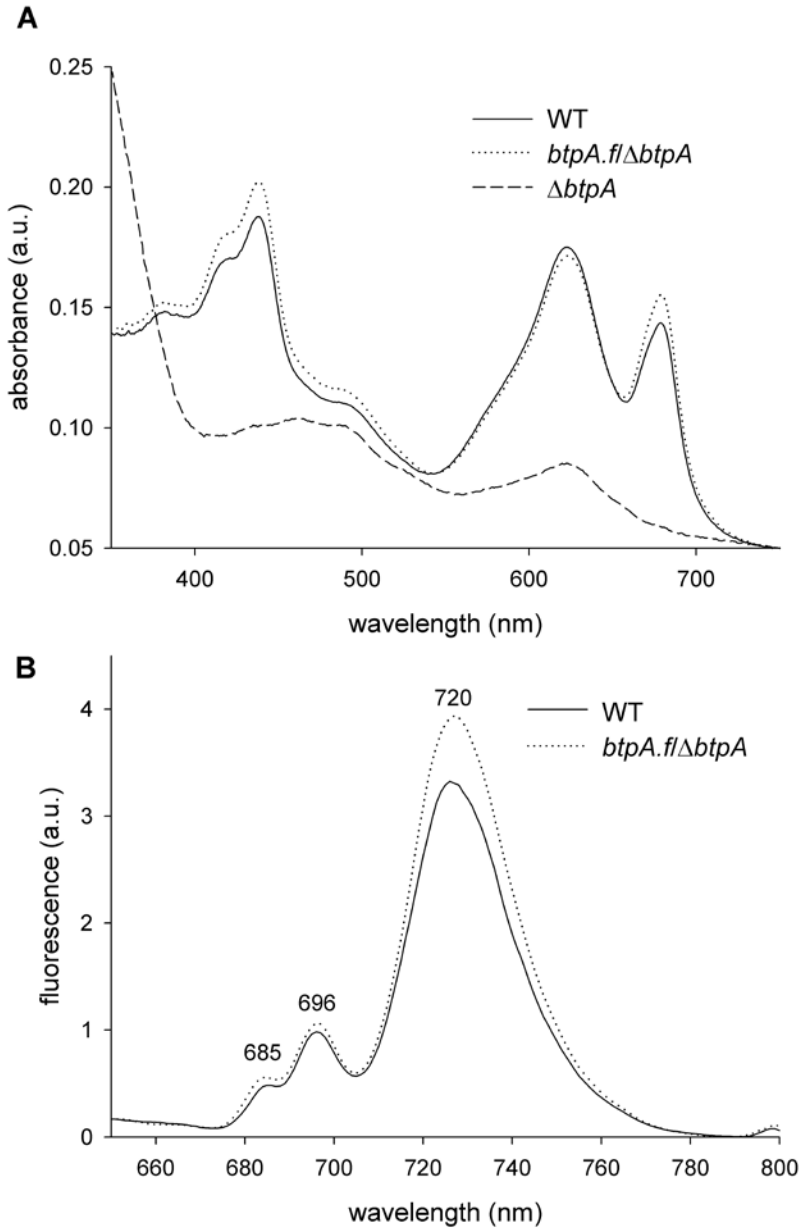

Figure 17

Complementation of Δ*btpA* by *btpA.f*

(A) Whole-cell absorption spectrum of the Δ*btpA* grown on glucose is compared with that of WT and of complemented strain *btpA.f*/Δ*btpA*. Peaks at 620 and 682 nm of the whole-cell absorption spectra represent linear bilins in phycobilisomes and chlorophyll, respectively. (B) The low-temperature (77K) chlorophyll fluorescence spectrum was measured using an Aminco Bowman Series 2 luminescence spectrometer. Equal amounts of cells were frozen in liquid nitrogen and excited at 435 nm. Spectra were normalized to the emission peak of the internal standard rhodamine at 570 nm. Peaks at 685, 696 represent PSII-related fluorescence and peak at 720 nm reflects the amount of PSI.

BtpA protein was found in a soluble as well as thylakoid fraction with more protein present in the membrane fraction (Figure 18A), consistent with its description as peripheral membrane protein (Zak et al., 1999). For this reason, the native purification using antiFLAG resin was performed from both soluble and membrane fractions of the BtpA.f strain in the WT and Δ*btpA* backgrounds. Native purification from WT was used as a negative control to exclude possible unspecific binding to the resin (Figure 18B).

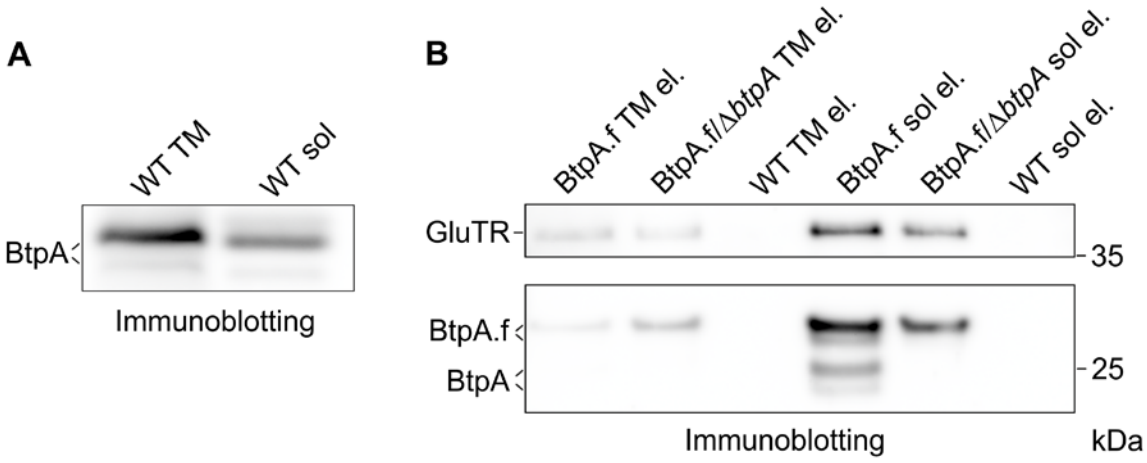

Figure 18

BtpA localization and BtpA, GluTR detection in the eluates

(A) BtpA distribution among membrane (TM) and soluble (sol) fraction in WT cells. (B) BtpA and GluTR were detected in eluates (el.) from BtpA.f, BtpA.f/Δ*btpA* and WT strains. Purification of WT expressing no BtpA.f was used as a negative control. Samples were separated by 12% SDS-PAGE and transferred to the PVDF membrane. The presence of GluTR and BtpA variants was detected by a specific antibody.

Even though the protein is present in membrane fraction in a higher amount, the membrane fractions provided lower yield of purified BtpA.f than the soluble ones (Figure 18B). This could be caused by incomplete solubilization as part of the protein from the membrane fraction could remain in the pellet after solubilization or more BtpA.f could be detached from the membrane during breaking the cells. Interestingly, BtpA.f from the soluble fraction of the BtpA.f mutant in the WT background was co-purified with the native BtpA protein (Figure 18B). This implicates that BtpA protein forms at least dimer. As two of the suppressor mutants contained mutation connected to GluTR, I tried to detect GluTR in the eluates by specific antibody prepared against His/GST-tagged GluTR from *Synechocystis* 6803 expressed in *E.coli* (for details see Material and methods). GluTR was present in all BtpA.f eluates and there seemed to be a correlation between the amount of BtpA and that of GluTR in the BtpA.f eluates. Neither GluTR nor BtpA was detectable in the eluate from WT control. To find if BtpA.f and GluTR create stable complex, the eluate from soluble fraction was also separated by 2D electrophoresis (CN/2D SDS-PAGE). After Coomassie staining, individual spots were identified by mass

spectrometry (made by Peter Koník). GluTR (band 1, Figure 19) clearly co-migrate with BtpA.f (band 2, Figure 19) indicating formation of BtpA.f complex with GluTR. Size of the native complex corresponding to the smeared lines of BtpA and GluTR is at the range from ca. 500 kDa to more than 1000 kDa. The rest of the spots from the 2D gel were identified as a protein with unknown function Slr1102 and different urease subunits or accessory proteins. As 50S ribosomal protein L11 and ferripyochelin binding protein are represented only by 1 peptide, their specificity would have to be further verified. PBS subunits are common contaminants in the eluates from a soluble fraction (band 10 and corresponding band in WT control).

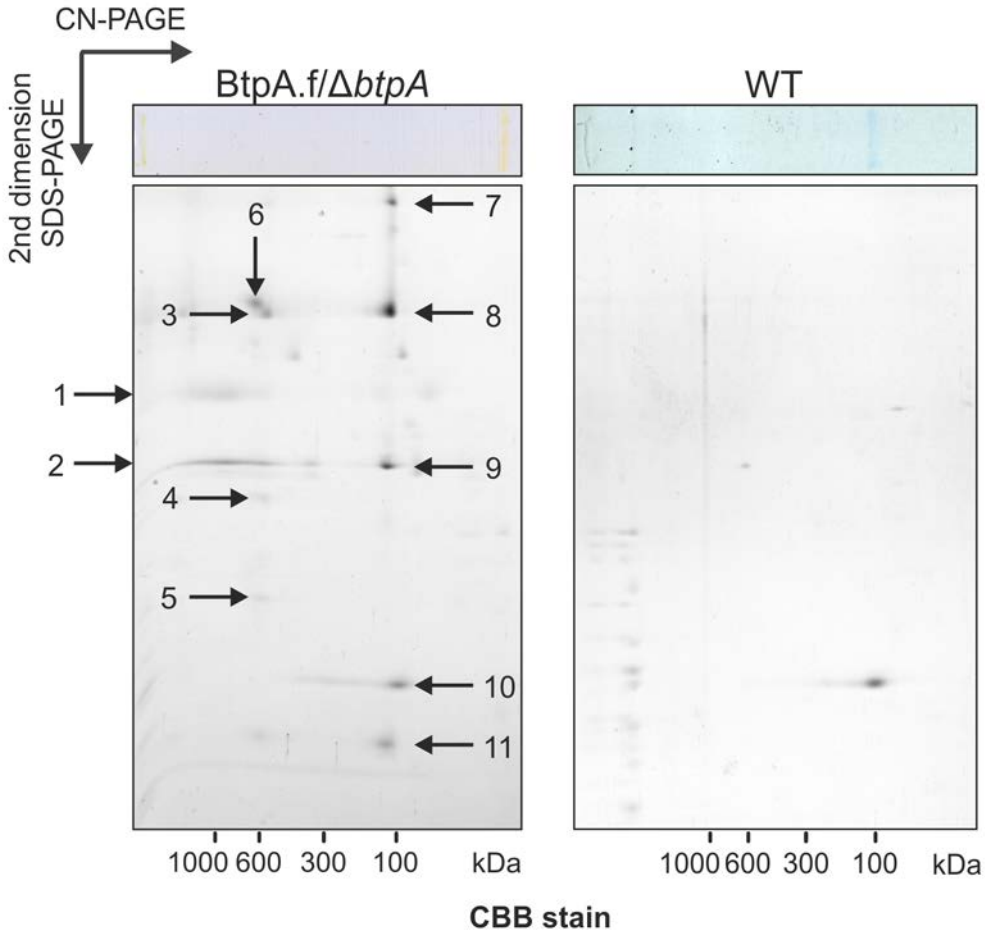

Figure 19

Two-dimensional CN/SDS-PAGE separation of BtpA.f and control (WT) eluate

Proteins isolated by affinity chromatography from the soluble fraction of BtpA.f/Δ*btpA* and WT strain were first separated by 4-14% CN-PAGE. Gel strip from CN-PAGE was further separated in a second dimension by 12 to 20% SDS-PAGE, stained with Coomassie brilliant blue (CBB) and the individual protein bands (1-11) were identified by mass spectrometry (Table 3).

Table 3

Proteins identified in the bands of BtpA.f/Δ*btpA* eluate separated by 2D SDS-PAGE
In the table are presented proteins with the coverage up to 10%.

	Gene	Protein description	mW (Da)	Peptides	Theoretical Peptides	Coverage (%)
1	*slr1808*	GluTR	51437	22	38	47.30
2	*sll0634*	BtpA	30023	15	17	73.17
3	*sll1750*	urease alpha subunit	60999	12	24	34.62
4	*sll1639*	urease accessory protein D	27141	5	15	29.46
5	*slr1899*	urease accessory protein F	20220	3	15	19.44
6	*slr1102*	hypothetical protein	96579	16	64	24.03
7	*sll1750*	urease alpha subunit	60999	11	24	39.72
	sll0420	urease beta subunit	11374	3	9	53.33
8	*sll1750*	urease alpha subunit	60999	17	24	40.77
9	*slr1884*	tryptophanyl tRNA synthetase	37739	17	23	35.01
10	*sll1578*	phycocyanin alpha subunit	17575	9	12	72.84
	sll1577	phycocyanin beta subunit	18115	7	15	59.88
	sll1743	50S ribosomal protein L11	14968	1	13	16.31
	sll1636	ferripyochelin binding protein	19535	1	13	10.00
11	*slr1256*	urease gamma subunit	11048	4	12	83.00
	sll0420	urease beta subunit	11374	4	9	60.00
	sll1577	phycocyanin beta subunit	18115	3	15	33.14

Previously, BtpA has been co-isolated with the FLAG-tagged GluTR protein (GluTR.f). by Kopečná (2012). To reproduce the result, it was necessary to perform the GluTR.f purification with protease inhibitor effective against metalloproteases. To achieve the proper function of the inhibitor, divalent salts were excluded from the buffer (see Material and methods – buffer C). The presence of BtpA in reverse purification of GluTR.f was proved by immunoblotting with a specific antibody (Figure 20A). To reveal other possible binding partners of GluTR, eluates from both fractions of the GluTR.f strain were separated by SDS-PAGE and bands were identified by mass spectrometry (Figure 20B). Two bands were identified as GluTR (Figure 20). Given that the native copy of GluTR was still present in the GluTR.f strain, there is no signal in WT

membranes equivalent to the upper band (Figure 20A), and GluTR is known to create a dimer (Moser et al., 2001), the upper one is described as GluTR.f and lower one the native GluTR. BtpA was found in both membrane and soluble fractions confirming the result from BtpA.f pull-downs. In addition, Slr1098 was found in both eluates and ArgJ (arginine biosynthesis protein) in the soluble fraction. Phycocyanin subunits are contamination as they are present in WT control eluate from the soluble fraction (Figure 19).

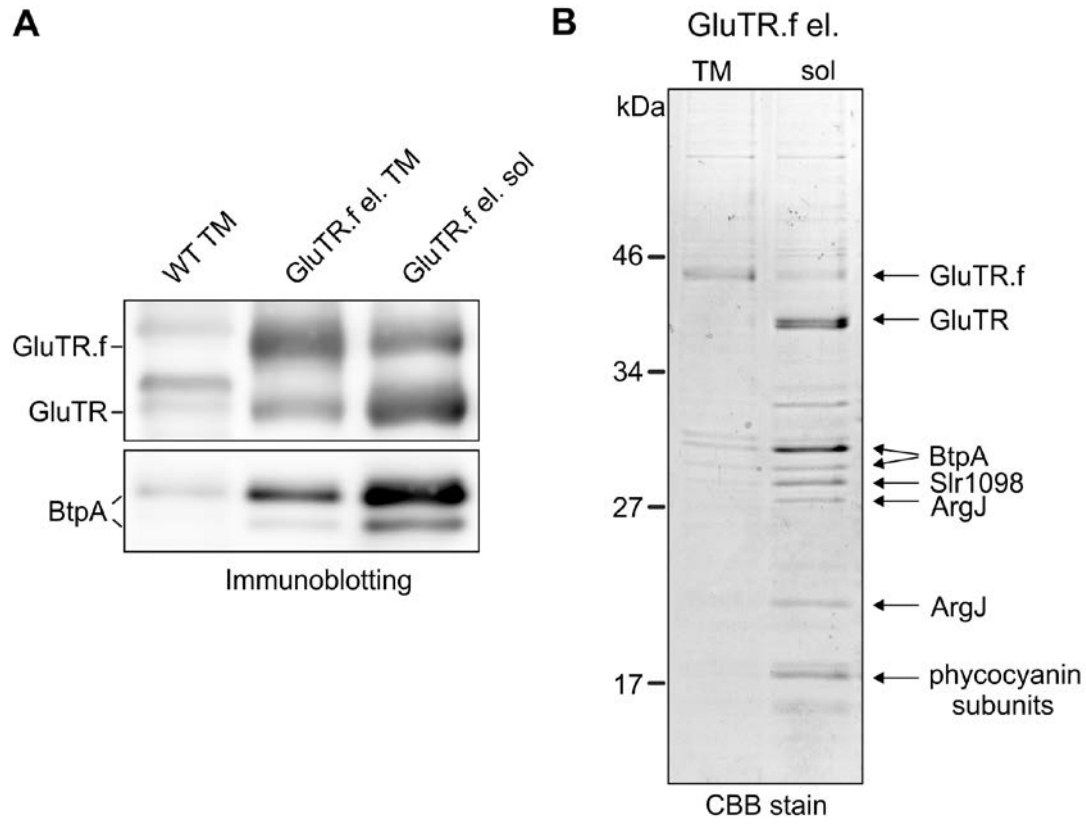

Figure 20

Identification of proteins in GluTR.f eluates separated by 1D SDS-PAGE

(A) WT membranes and eluates from soluble and membrane fraction of GluTR.f were separated by 12 to 20% SDS-PAGE and transferred to the PVDF membrane. The presence of GluTR variants and BtpA was detected by a specific antibody. (B) Proteins isolated by affinity chromatography from thylakoid membrane and soluble fraction of *gluTR.f* strain were separated by 12 to 20% SDS-PAGE and stained with Coomassie brilliant blue (CBB). The individual proteins bands were identified by mass spectrometry. The described proteins were the only one identified in the bands.

Abbreviations: el. – eluate, TM – thylakoid membrane fraction, sol – soluble fraction

4.2 HemJ

HemJ was the last discovered form of PPO and as such also the least characterized one. As a heterologous expression of HemJ proteins from various organisms frequently resulted in no or poor expression (Boynton et al., 2011; Kato et al., 2010), I expressed the HemJ enzyme fused on its C-terminus with 3xFLAG-tag (HemJ.f) homologously in *Synechocystis* 6803 under *psbAII* promoter. After full segregation of the *hemJ.f* strain, it was possible to delete the WT copy of the *hemJ* gene, demonstrating that the HemJ.f protein is functional (Figure 21).

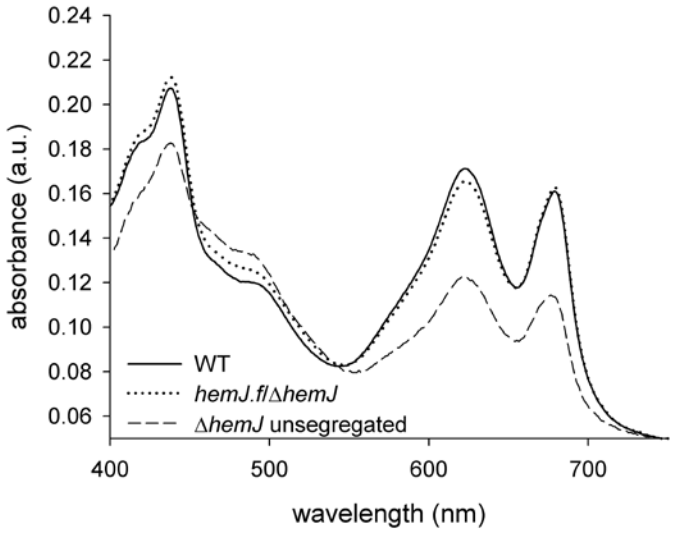

Figure 21

Whole-cell absorption spectra suggesting complementation of Δ*hemJ* by FLAG-tagged *hemJ*

A whole-cell absorption spectra of the *Synechocystis* 6803 WT, *hemJ.f/*Δ*hemJ* and unsegregated Δ*hemJ* (supplemented with 20 μg/ml of chloramphenicol) grown at 40 μmol of photons $m^{-2}s^{-1}$. Chlorophyll is represented by 680 nm peak and phycobiliproteins by the 625 nm peak. Spectra were normalized to light scattering at 750 nm.

However, for the HemJ isolation, a strain containing both WT and tagged variants of HemJ was used as in case of BtpA and GluTR. After affinity chromatography of *hemJ.f* membrane fraction solubilized by non-ionic detergent, the purified HemJ.f eluate was markedly reddish. Native separation of the eluate on the CN-PAGE resulted in two reddish bands - CN1, and only slightly visible CN2 (Figure 22). Photosystem I (PSI), also present in the eluate, was shown to bind nonspecifically to the anti-FLAG affinity resin (Bučinská et al., 2018). Hence, HemJ.f was also isolated from a strain lacking PSI (ΔPSI) to achieve maximum purity (Figure 22A).

To identify the proteins forming the reddish band, CN1 band (Figure 22A) was cut out and characterized by mass spectrometry (made by Peter Koník). Together with HemJ, the band contained also a protein with unknown function Sll1106. As the same reddish bands were present when HemJ.f was purified also from the Δ*sll1106* background

(Figure 22B), it was clear that the reddish color is associated with HemJ.f. The Δ*sll1106* is further characterized in chapter 4.3.

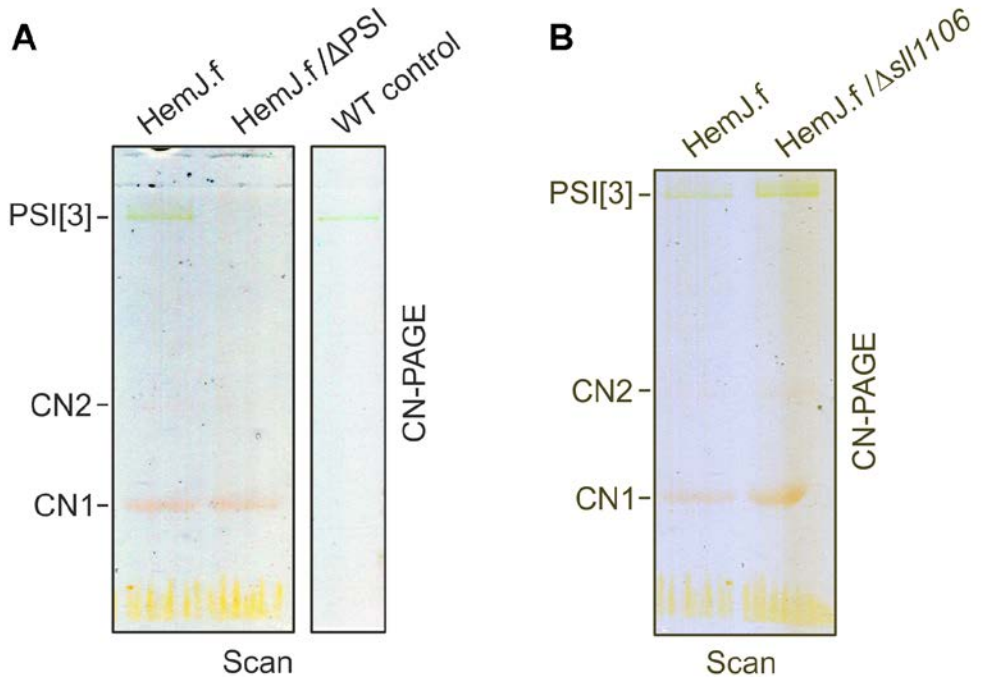

Figure 22

Separation of the purified HemJ.f by clear native gel electrophoresis

(A) Native isolations of HemJ.f from WT and ΔPSI backgrounds that resulted in reddish eluates were further separated by 4-14% clear native gel electrophoresis (CN-PAGE). Reddish bands CN1 and CN2 (poorly visible) were identified as HemJ.f. As already reported (Bučinská et al., 2018), a small amount of trimeric PSI (PSI[3]) is typical contamination of FLAG eluates obtained from *Synechocystis* 6803. (B) The HemJ pull-down obtained from Δ*sll1106* mutant of *Synechocystis* 6803 was separated by 4-14% CN-PAGE. The gels were scanned (Scan).

Absorption spectra of the eluted HemJ.f protein showed an absorption maximum at 412 nm (Figure 23A), which was presumed to be the Soret band of a bound tetrapyrrole. After deletion of PSI, only a small amount of Chl (absorbing at 671 nm) and a variable amount of carotenoids (absorbance 450 - 520 nm) co-eluted with HemJ.f (Figure 23A). The bound tetrapyrrole was extracted by acetone and was identified as protoheme by HPLC (Skotnicová et al., 2018). To spectroscopically characterize this bound heme further, absorption spectra of the HemJ.f eluate from the ΔPSI strain was measured after oxidation by air or after reduction by dithionite (Figure 23B). The eluate with the lowest carotenoid content was used for the measurement to ensure the proper visibility of heme *b* Soret peaks. The oxidized spectrum indicated a high spin heme *b* (λ_{max} = 411 nm), and the reduced spectrum (λ_{max} = 424 nm) was typical for a ferrous six-coordinate *b*-type heme.

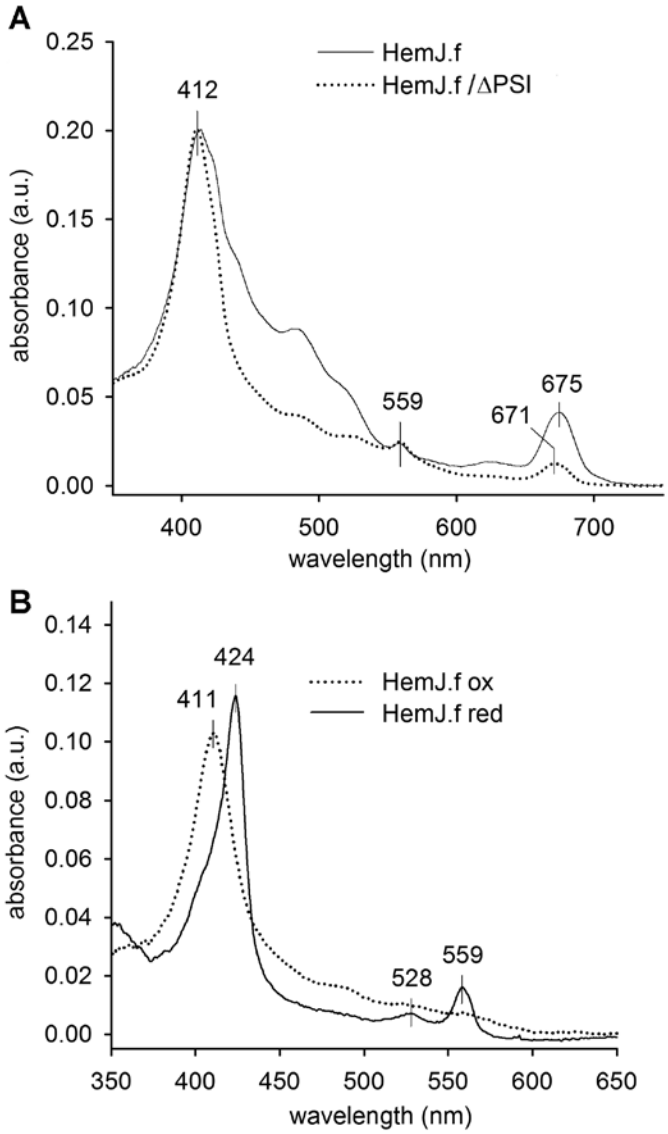

Figure 23

Spectroscopy analysis of the purified HemJ.f

(A) Absorption spectra of HemJ.f eluate. The peak at 675 nm derives from chlorophyll, while the peaks at 412 and 559 nm are characteristic for heme. The eluate with lower carotenoid content (absorption at 450 to 520 nm) was used for spectroscopy analysis. (B) Absorption spectra of oxidized and reduced HemJ.f eluate obtained from the ΔPSI genetic background.

a.u. – absorbance units

Proteins co-purified with HemJ.f were separated by SDS-PAGE (Figure 24A) and identified by mass-spectrometry (Table 4) as Sll1106 (band 6) and all four *Synechocystis* 6803 FtsH proteases (bands 1 and 2). There were three bands containing HemJ. The upper (band 3) represents HemJ dimer, which seems to withstand SDS treatment (see also Figure 25). The lower ones are expected to be HemJ.f (band 4) and native HemJ or partially degraded HemJ.f (band 5).

FeCH is known to create a complex with other PPO types (Kim et al., 2018; Masoumi et al., 2008). Even though it was not identified by mass-spectrometry, it was detected by specific FeCH antibody in HemJ.f eluate from WT and ΔPSI backgrounds.

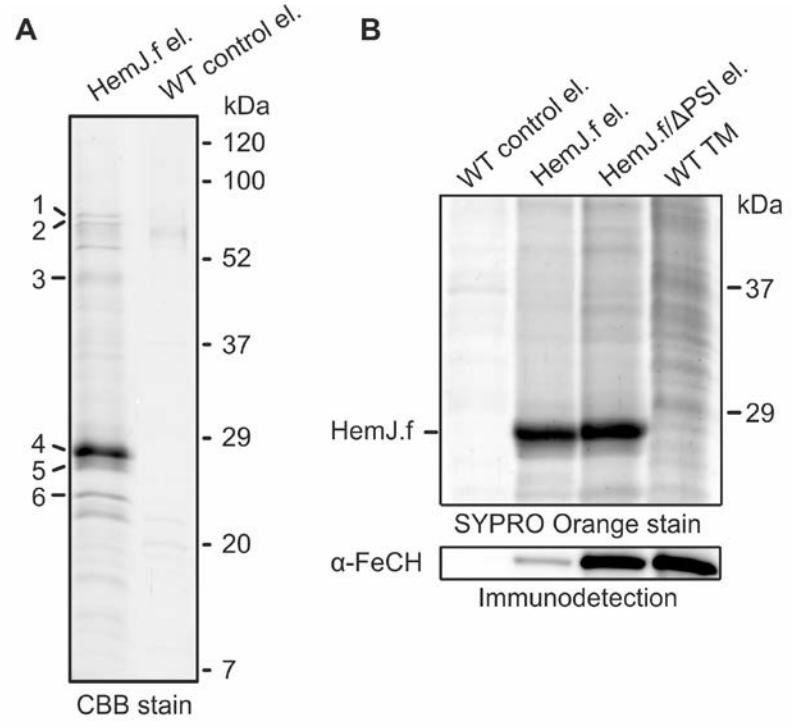

Figure 24

One-dimensional SDS-PAGE separation of HemJ.f eluate

(A) Proteins isolated by affinity chromatography from HemJ.f strain and from WT control cells were separated by 12 to 20% SDS-PAGE, stained with Coomassie brilliant blue (CBB) and the individual proteins bands (1-6) were identified by mass spectrometry (Table **4**). (B) FeCH was detected by a specific antibody in the HemJ.f eluates and WT control eluate. WT membranes (WT TM) were used as a control of the antibody signal. SYPRO Orange stain served as a control of the loading.

Table 4

Proteins identified in the bands of HemJ.f eluate separated by SDS-PAGE

In the table are presented proteins with the coverage up to 10%.

	Gene	Protein description	mW (Da)	Peptides	Theoretical Peptides	Coverage (%)
1	*slr0228*	FtsH2 protease	68453	18	48	37.16
	sll1463	FtsH4 protease	68157	14	60	32.01
	slr1390	FtsH1 protease	69261	11	49	26.48
2	*slr1604*	FtsH3 protease	67209	22	45	46.10
3	*slr1790*	HemJ	22049	3	14	20.73
4	*slr1790*	HemJ	22049	7	14	29.02
5	*slr1790*	HemJ	22049	4	14	21.24
6	*sll1106*	hypothetical protein	18019	8	10	46.78

To further characterize the nature of CN1 and CN2 bands, the gel strip from CN-PAGE (Figure 22A) was separated in a second dimension by SDS-PAGE (Figure 25), colored CN1 and CN2 bands dissociated into two spots, apparently representing monomer and dimer of the HemJ.f (27 kDa). The upper CN2 band contains the HemJ.f oligomer, most probably a tetramer, which agrees with the size of the complex (~150 kDa) determined by the size-exclusion chromatography (Skotnicová et al., 2018).

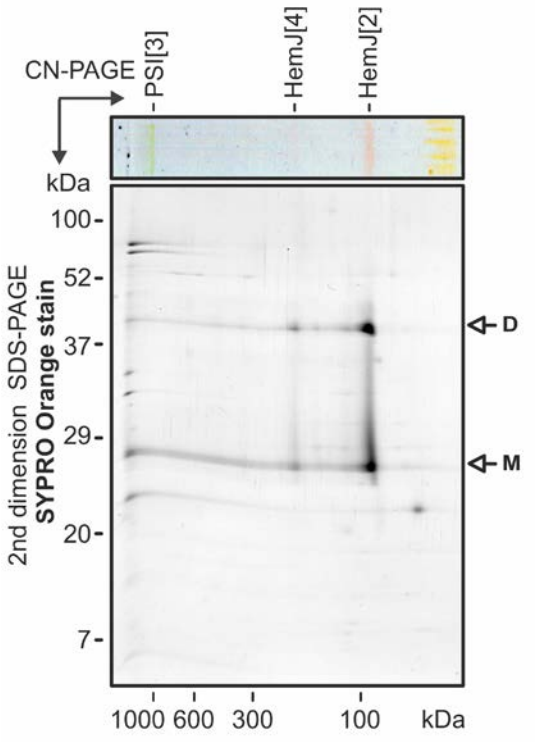

Figure 25

Two-dimensional CN/SDS-PAGE separation of HemJ.f eluate

The gel strip from CN-PAGE (see Figure 22) was further separated in a second dimension by 12 to 20% SDS-PAGE and stained with SYPRO Orange. HemJ.f bands (marked as CN1 and CN2 in Figure 22B) were tentatively assigned as dimeric (HemJ[2]) and tetrameric (HemJ[4]) HemJ.f oligomers, respectively.

No PPO activity of the HemJ.f eluate was detected when measured with or without artificial electron acceptors (Skotnicová et al., 2018). Hence, I decided to confirm the function of HemJ by silencing the *hemJ* gene and via complementation with the PPO analog HemG. Two strains were engineered, one with the *Synechocystis* 6803 *hemJ* gene placed under a copper-regulated promoter (*petJ*) and the second expressing *hemG* from *E. coli* under the *psbAII* promoter. In both strains it was possible to delete the WT *hemJ* gene, indicating that both constructs were functional. In the P(*petJ*)::*hemJ*/Δ*hemJ* strain (latter only as P(*petJ*)::*hemJ*), it was possible to decrease the amount of *hemJ* by adding copper to the growth medium. This led to lower amounts of enzymatically produced Proto, followed by decreases in the levels of phycobilins and Chl (Figure 26A) and lower levels of major Chl-binding photosynthetic complexes, especially trimeric PSI (Figure 26B).

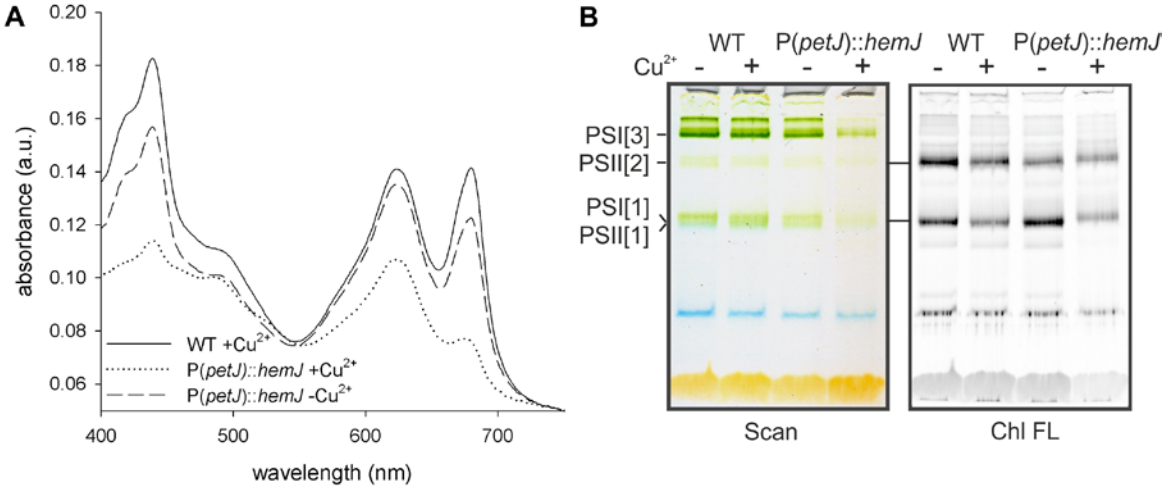

Figure 26

Whole-cell absorption spectra of P(*petJ*)::*hemJ* and Δ*hemJ*/*hemG* strains and CN-PAGE of solubilized membrane complexes

Synechocystis 6803 strains grown at 40 µmol of photons $m^{-2}s^{-1}$ were used for whole-cell absorption spectra (A) and CN-PAGE (B). Chlorophyll is represented by 680 nm peak and phycobiliproteins by the 625 nm peak. Spectra were normalized to light scattering at 750 nm. P(*petJ*)::*hemJ* strain was grown in the medium without copper; $+Cu^{2+}$ refers to the cells to which medium was added 1 µM $CuSO_4$ for 2 days. The CN gel (B) was scanned (Scan); chlorophyll fluorescence (Chl FL) emitted by PSII was excited by blue light and detected by LAS 4000 Imager (Fuji).

Designation of complexes: PSI[3] and PSI[1], trimeric and monomeric PSI; PSII[2] and PSII[1], dimeric and monomeric PSII

To identify how the repression of *hemJ* expression affects tetrapyrrole biosynthesis, the accumulation of Chl/heme intermediates was analyzed in the P(*petJ*)::*hemJ* strain suppressed by copper (Figure 27). The suppressed strain exhibited significantly decreased levels of the Chl precursors MgP and Pchlide along with an accumulation of Copro and Proto; the latter tetrapyrrole was also visibly excreted into the medium. Detection of both Copro and Proto was likely to result from the accumulation and non-enzymatic oxidation of their reduced precursors in the cell (Kato et al., 2010; Lermontova and Grimm, 2006).

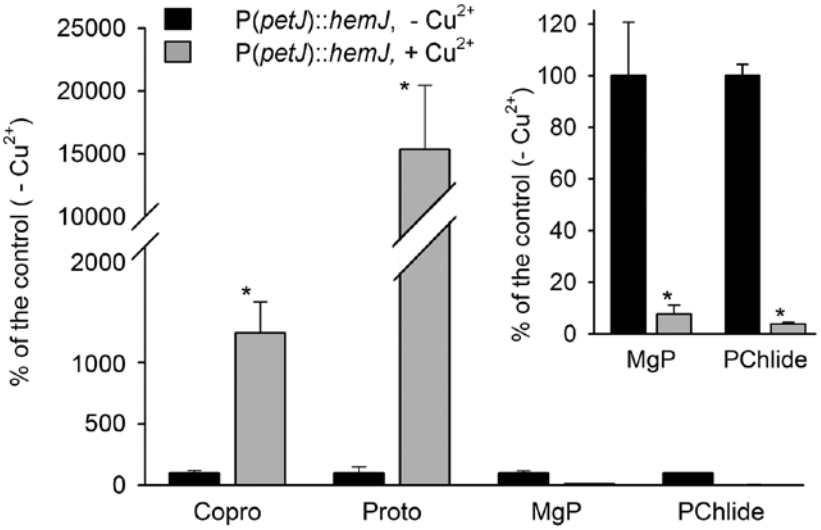

Figure 27

Analysis of heme/chlorophyll precursors in the P(*petJ*)::*hemJ* strain grown photoautotrophically in a medium with or without copper

Heme/chlorophyll precursors were extracted with 70% methanol from the P(*petJ*)::*hemJ* cells at OD_{730} = 0.3 - 0.4 and separated on an HPLC equipped with two fluorescence detectors (Pilný et al., 2015). The amounts of chlorophyll precursors MgP and PChlide were markedly reduced in cells cultivated with the repressed *hemJ* expression when compared with the same mutant cells grown without copper. On the contrary, Proto and Copro massively accumulated in the repressed cells. The inset shows a different scale for the less abundant precursors. *, significance difference tested using a paired *t* test (P = 0.05). Abbreviations of intermediates: Copro, Coproporphyrin III; Proto, Protoporphyrin IX; MgP, Mg-protoporphyrin IX; PChlide, divinyl protochlorophyllide

The HemG complemented strain Δ*hemJ/hemG* grew on glucose slightly slower than WT (Figure 28) and accumulated lower amounts of phycobilins (Figure 28A). Even though the Chl level was comparable to WT, the strain displayed a slightly lower level of photosystem complexes and a significantly lower amount of PSII dimer (Figure 28B). However, the strain did not grow autotrophically (Figure 28C).

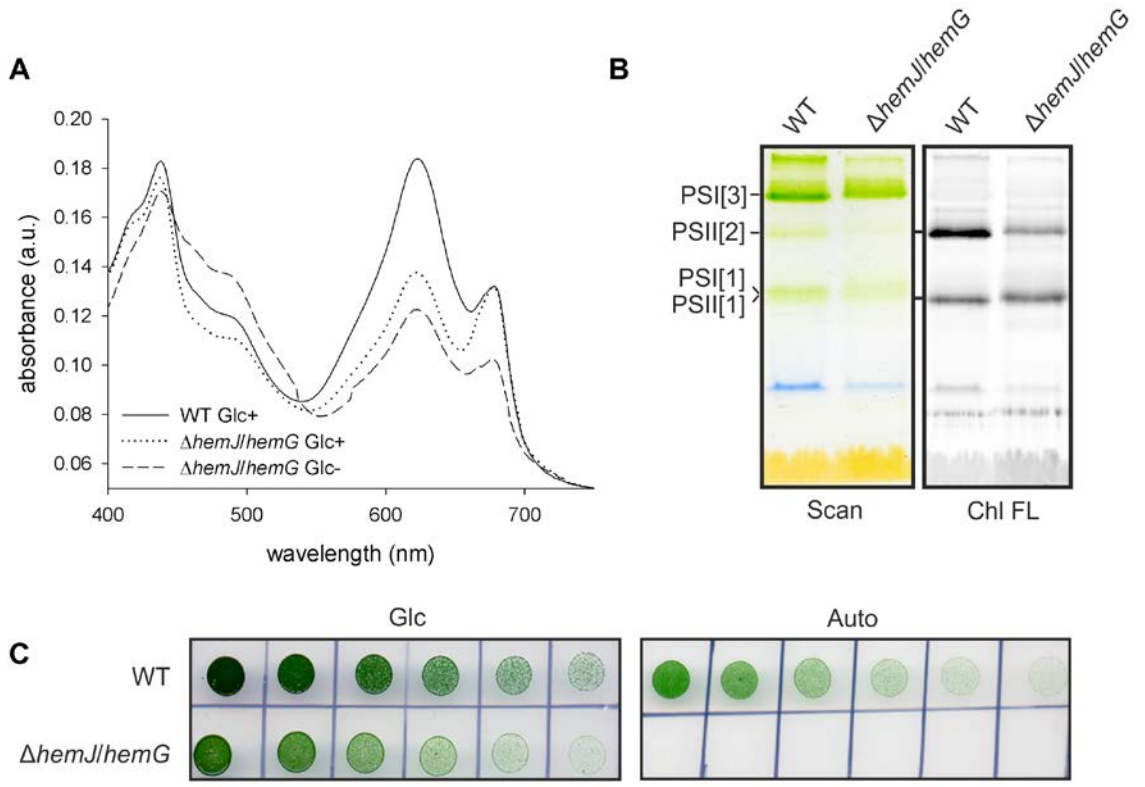

Figure 28

Mixotrophic (5 mM glucose) and photoautotrophic growth (Auto) of WT and Δ*hemJ*/*hemG* strains of *Synechocystis* 6803

Synechocystis 6803 strains grown at 40 µmol of photons $m^{-2}s^{-1}$ and 28 °C were used for whole-cell absorption spectra (A) and clear native gel (CN-PAGE) (B). Chlorophyll is represented by 680 nm peak and phycobiliproteins by the 625 nm peak. Spectra were normalized to light scattering at 750 nm. Glc+ strains were grown with 5 mM glucose and Glc- were measured 3 days after the exchange of the medium for the one without glucose. Membranes from Glc- strains were used for CN-PAGE (B). The gel was scanned (Scan); chlorophyll fluorescence (Chl FL) emitted by PSII was excited by blue light and detected by LAS 4000 Imager (Fuji). (C) Strains precultivated in liquid BG11 supplemented with 5 mM glucose, were subsequently cultivated for 4 days on plates either with (Glc) or without glucose (Auto). 5 µl of the culture OD_{730}= 0.2 was applied to the plate on the left side followed with two-fold serial dilutions.

Designation of complexes: PSI[3] and PSI[1], trimeric and monomeric PSI; PSII[2] and PSII[1], dimeric and monomeric PSII

When the Δ*hemJ/hemG* cells were transferred to the glucose-free medium, the Chl precursors were almost undetectable in the cells, except for MV- Chlide (Figure 29A), most probably originating from Chl *a* recycling from pigment-protein complexes by its dephytylation (Kopečná et al., 2015b). In addition, a large quantity of an unidentified tetrapyrrole eluted at 13.4 minutes on the HPLC profile of the extract from the Δ*hemJ/hemG* strain incubated without glucose (Figure 29). This tetrapyrrole-like compound was completely missing in the WT strain (Figure 29A) as well as in the Δ*hemJ/hemG* mutant grown on glucose (Figure 30). Its absorption spectra resembled that of Copro (Figure 29), however, Copro is eluted at 6.9 – 7 minute (Pilný et al., 2015).

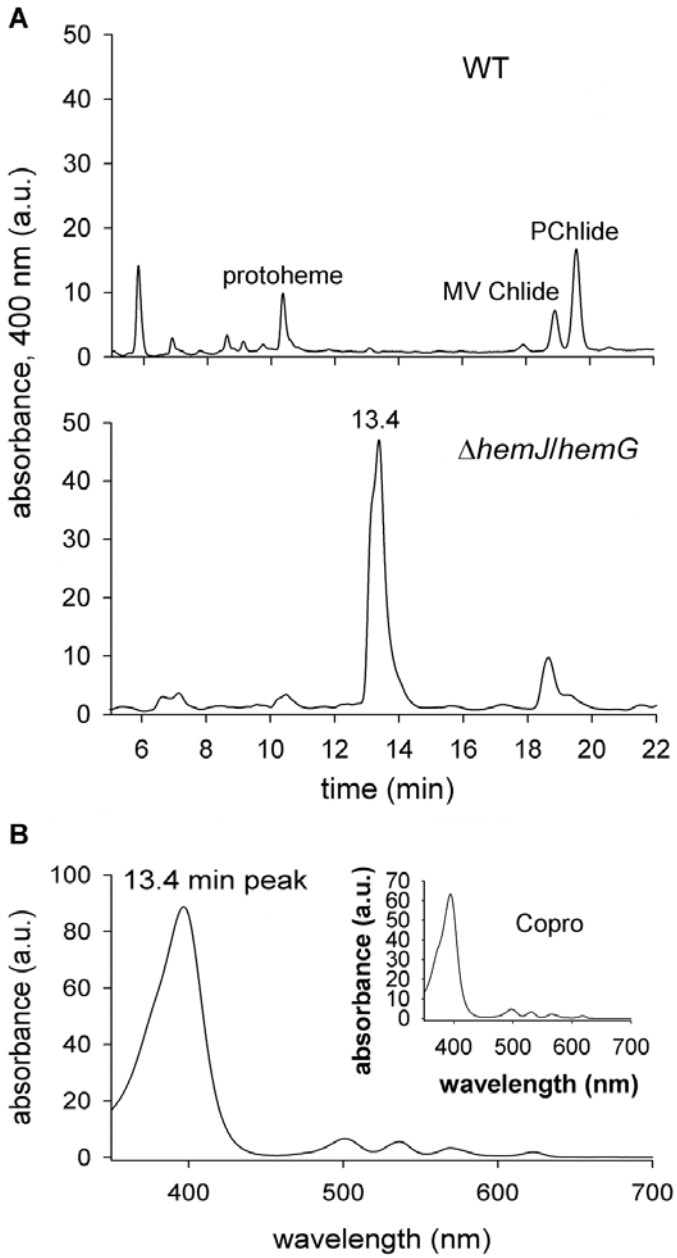

Figure 29

Detection of an unusual tetrapyrrole in the Δ*hemJ*/*hemG* strain incubated without glucose

(A) Polar tetrapyrroles were extracted with 70% methanol from 50 ml of WT and Δ*hemJ/hemG* cells grown photoautotrophically for three days and harvested at OD_{730} = 0.3 - 0.4. The obtained extract was separated on HPLC (see Experimental procedures) and eluted pigments were detected by a diode-array detector at 400 nm. (B) The absorption spectrum of the compound eluting at 13.4 min. The inset shows the absorption spectrum of the Copro standard. Abbreviations of intermediates: Copro, Coproporphyrin III; MV Chlide, monovinyl chlorophyllide; Pchlide, divinyl protochlorophyllide

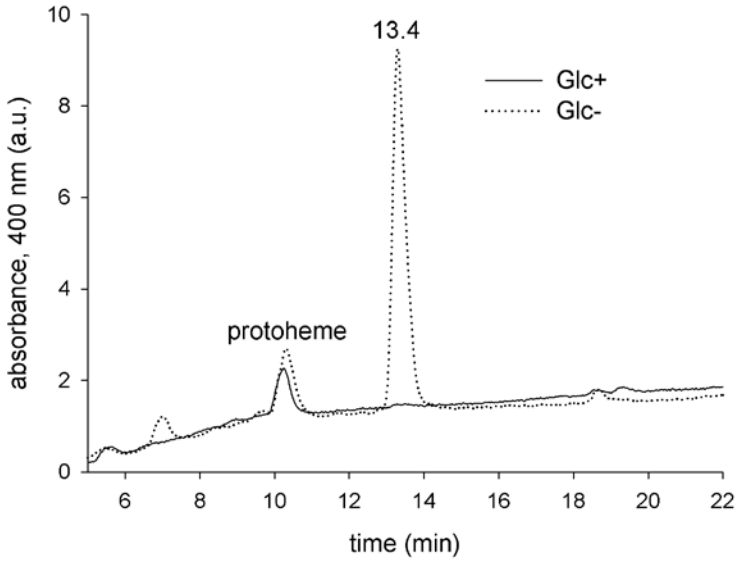

Figure 30

Accumulation of harderoporphyrin in the Δ*hemJ*/*hemG* strain under photoautotrophic conditions

Pigments were extracted from 2 ml of the mutant cells grown in the presence of 5 mM glucose (Glc+) or from cells incubated for three days without glucose (Glc-). Extracted pigments were separated by HPLC and detected by a diode-array detector at 400 nm.

The unknown tetrapyrrole observed in Δ*hemJ*/*hemG* mutant was isolated and analyzed using HPLC coupled to high-resolution tandem mass spectrometry (HPLC-HRMS/MS) and identified as harderoporphyrin (Skotnicová et al., 2018), a spontaneously oxidized intermediate of the CPO reaction, which is normally generating Protogen (see Figure 5).

4.3 Sll1106

I found the Sll1106 protein in eluates of several pull-down assays with the proteins involved in the tetrapyrrole pathway used as bait. It was the major protein co-purified with PPO (4.2 HemJ, Figure 22A, Figure 24) and also with the CAB domain of FeCH (His-C-tn, Figure 31), responsible for FeCH oligomerization (Sobotka et al., 2008b) and expected to bind Chl (Sobotka et al., 2011). This His-C-tn of FeCH was expressed as a stand-alone protein in the strain with the shortened FeCH (Figure 31A) and the eluate was purified by affinity chromatography from membranes solubilized by non-ionic detergent. Eluate was separated by SDS-PAGE and bands were identified by mass spectrometry (made by Peter Koník).

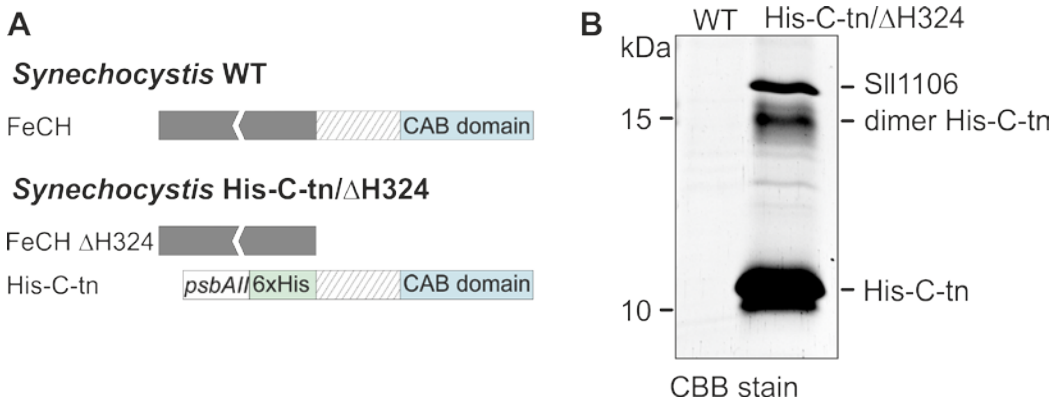

Figure 31

Co-purification of Sll1106 with the CAB domain of ferrochelatase (His-C-tn)

(A) A schematic presentation of the FeCH from WT and His-C-tn/ΔH324 strain. FeCH from WT consists of a catalytic part (dark grey), spacer region (hatched) and CAB domain (blue). The His-C-tn/ΔH324 strain contains a truncated version of FeCH and CAB domain including spacer region expressed as an independent His-tagged protein under the *psbAII* promoter. (B) Sll1106 was co-purified with His-C-tn from the ΔH324 background and identified by mass spectrometry.

To clarify the role of Sll1106, I prepared strain with deleted *sll1106* (Δ*sll1106*). The phenotype of Δ*sll1106* was completely normal. The growth rate at different light and temperature conditions on plates (Figure 32A), as well as the whole-cell absorption spectrum, was identical with WT (data not shown). The strain accumulated normal levels of heme and Chl and also the majority of the precursors (Figure 32B). However, the Δ*sll1106* contained significantly lower level of Proto and decreased level of MgP and Mg PME, the precursors at the beginning of the Chl branch.

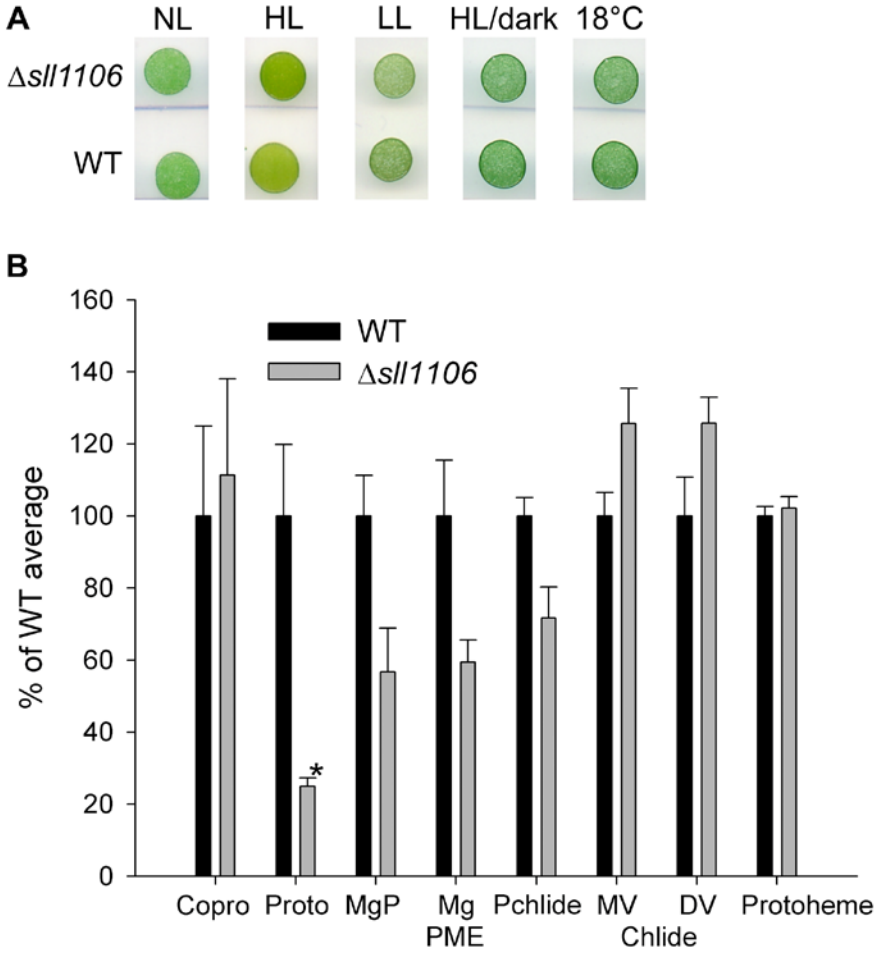

Figure 32

Growth and analysis of heme/chlorophyll precursors of Δ*sll1106* strain

(A) The growth of Δ*sll1106* and WT on plates at different growing conditions (used light in µmol of photons $m^{-2}s^{-1}$: NL and 18°C – 40, HL – 300, LL – 5, HL/dark – 300 swapped with a dark period every 5 minutes). Except for the strain grown at 18 °C, all the plates were kept at 28 °C. (B) Heme/chlorophyll precursors were extracted with 70% methanol from the Δ*sll1106* and WT cells at OD_{730} = 0.3 - 0.4 and separated on an HPLC equipped with two fluorescence detectors (Pilný et al., 2015). The amount of Proto in Δ*sll1106* was markedly reduced. *, significance difference tested using a paired *t* test (P = 0.05). Abbreviations of intermediates: Copro, Coproporphyrin III; Proto, Protoporphyrin IX; MgP, Mg-protoporphyrin IX; Mg PME, Mg protoporphyrin IX monomethyl ester; PChlide, divinyl protochlorophyllide; DV Chlide, divinyl chlorophyllide; MV Chlide, monovinyl chlorophyllide

To investigate the growth of Δ*sll1106* under iron and nitrogen limiting conditions, the strain was grown in liquid culture. Also, a regreening of cells after one month of nitrogen depletion was examined. There was no difference in the growth of WT and Δ*sll1106* strain under these conditions (data not shown). Since *sll1106* is induced by salt-stress (Pandhal et al., 2009), the influence of high salt was explored as well. With 1M NaCl in the medium, the growth rate of Δ*sll1106* strain was half of that of WT.

To confirm the interaction between Sll1106 and enzymes of heme/Chl branchpoint (Figure 5) or their binding partners, I prepared strain expressing Sll1106 with 3x FLAG tag under *psbAII* promoter. As the membrane protein topology servers differed in the predicted Sll1106 topology, I decided to tag Sll1106 on both N- and C-terminal (f.Sll1106 and Sll1106.f, respectively). Both eluates contained more pigments than the background eluate from WT (WT el., Figure 33A), possibly because of the hydrophobic nature of the protein. Eluates were enriched in carotenoids, as demonstrated by increased absorption in the region 450 to 520 nm when Sll1106.f eluates were compared with WT eluate normalized to Sll1106.f level of Chl (675nm). The relatively low level of Chl together with carotenoids in WT eluate comes from photosystems, mainly PSI (see Figure 22), which means that Sll1106.f eluate is specifically enriched in carotenoids not present as a component of photosystems. When Sll1106 eluate was separated by CN-PAGE, there was not visible any specific carotenoids containing band (data not shown), indicating that carotenoids are not bound specifically to Sll1106 or other protein from the eluate.

There was not a significant difference in pigment (Figure 33A) and protein composition between f.Sll1106 and Sll1106.f (data not shown), thus data from the separation of the eluate by SDS-PAGE are presented only for Sll1106.f. Analysis of the Sll1106.f eluate by SDS-PAGE revealed several proteins specifically co-eluted with Sll1106.f from the anti-FLAG resin (Figure 33). A number of proteins were identified by a mass-spectrometry in these protein bands (Table 5). Most of the detected proteins were associated with protein synthesis and translocation through the membrane (ribosomal protein L1, SecD, YidC), proteases involved in quality control and degradation (FtsH2-4), prohibitins, PilA1 and number of proteins with unknown function. Except for proteins discovered by analysis of SDS bands, cytochrome b559 alpha subunit, CurT and Psb28-1 were identified by examination of whole-cell eluates (Table 6).

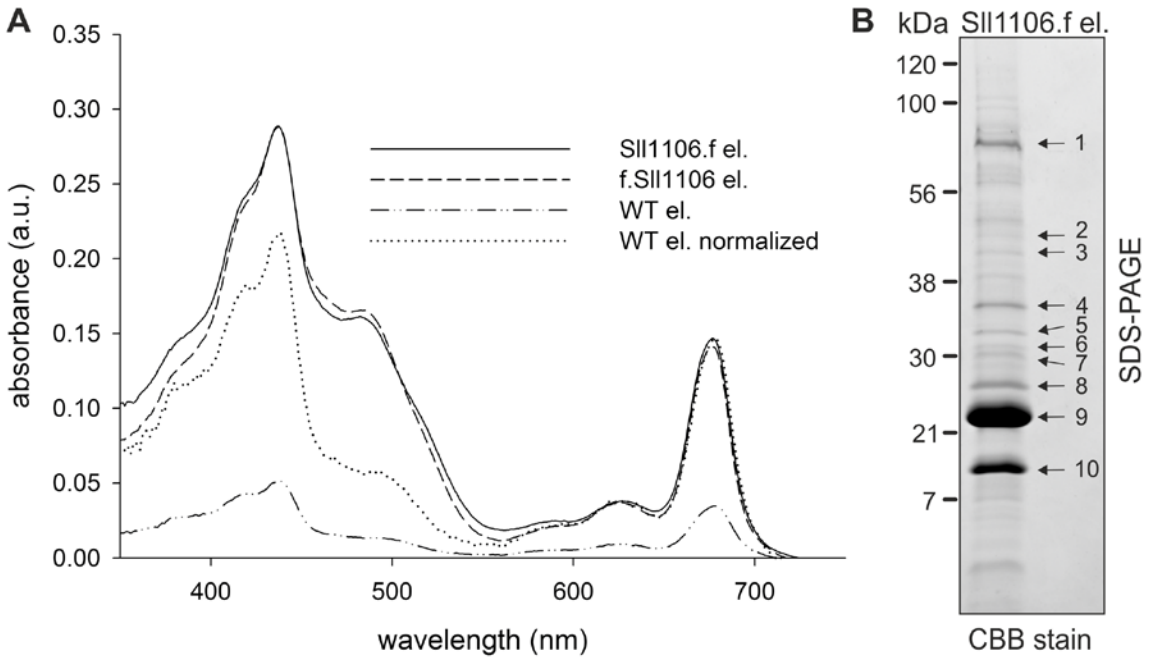

Figure 33

Characterization of Sll1106 eluates

(A) Absorption spectra of Sll1106.f and f.Sll1106 eluates (el.). The peak at 675 nm derives from Chl and region at 450 to 520 nm belongs to carotenoids. WT eluate (WT el.) is also shown when normalized to chlorophyll (675 nm) in Sll1106.f el.. (B) Proteins isolated by affinity chromatography from the membrane fraction of *sll1106.f* strain were separated by 12 to 20% SDS-PAGE, stained with Coomassie brilliant blue (CBB) and the individual proteins bands were identified by mass spectrometry (Table 5).

Table 5

Proteins identified in the bands of Sll1106.f eluate (Figure 33) separated by SDS-PAGE

In the table are presented proteins with the coverage up to 10 %.

	Gene	Protein description	mW (Da)	Peptides	Theoretical Peptides	Coverage (%)
1	*sll1463*	FtsH4 protease	68157	14	60	26.91
	slr0228	FtsH2 protease	68453	10	48	22.65
	slr1604	FtsH3 protease	67209	7	45	12.99
2	*slr0774*	protein export membrane protein SecD	48147	5	28	15.71
	slr0839	ferrochelatase	43896	2	19	10.59
3	*slr1471*	YidC	42599	3	26	13.28
4	*slr1128*	prohibitin 3	35704	8	30	41.74
5	*slr1106*	prohibitin 1	30550	6	24	25.53
	slr1768	prohibitin 2	32807	2	28	19.46
6	*slr0404*	hypothetical protein	34843	4	17	16.82
7	*slr0447*	ABC type urea transport system substrate binding protein	48329	6	29	23.09
	slr0404	hypothetical protein	34843	3	17	12.61
8	*sll1694*	pilin polypeptide PilA1	17562	3	10	17.26
	slr0404	hypothetical protein	34843	3	17	12.61
	sll1744	50S ribosomal protein L1	25835	2	18	12.18
9	*sll1106*	hypothetical protein	18019	5	10	37.43
	sll1571	hypothetical protein	34512	3	11	17.57
10	*sll1106*	hypothetical protein	18019	6	10	43.86

Table 6

Mass spectrometry of whole-cell eluates

Proteins identified in at least 2 of 3 purifications of FLAG-tagged Sll1106 with coverage up to 10% and not present in the control eluate from the WT. A number of peptides and coverage represents the highest values found in the eluates.

Gene	Protein description	mW (Da)	Peptides	Theoretical Peptides	Coverage (%)
sll1106	hypothetical protein	18019	9	10	59.06
slr1128	prohibitin 3	35704	11	30	42.68
sll1463	FtsH4 protease	68157	20	60	40.76
ssr3451	cytochrome b559 alpha subunit	9442	2	5	25.93
slr0483	CurT	16874	4	9	20.81
slr0228	FtsH2 protease	68453	10	48	20.26
sll1398	Psb28-1 PSII assembly factor	12582	2	11	19.64
slr1106	prohibitin 1	30550	4	24	17.02
slr0404	hypothetical protein	34843	2	17	13.21
sll1694	pilin polypeptide PilA1	17562	2	10	12.50
slr1604	FtsH3 protease	67209	5	45	10.06

4.4 CurT

CurT is important for the organization of thylakoid membranes in chloroplast and cyanobacteria (Armbruster et al., 2013; Heinz et al., 2016). Interestingly, I found that CurT also interacts with the proteins associated with the tetrapyrrole pathway. CurT was found in the Sll1106.f eluate (see 4.3 Sll1106) and in the eluate of FLAG-tagged FeCH (FLAG-HemH/Δ*hemH*, Table 7).

Table 7

Proteins identified in FLAG-HemH/Δ*hemH* by mass spectrometry

In the table are proteins found in the FLAG-HemH/Δ*hemH* eluate and were not present in the control eluate from the WT.

Gene	Protein description	mW (Da)	Peptides	Theoretical Peptides	Coverage (%)
slr0839	ferrochelatase	43896	13	19	45.48
slr0483	CurT	16874	2	9	20.13
sll1244	50S ribosomal protein L9	16631	2	11	18.42
sll1921	hypothetical protein	28278	2	22	10.76

To confirm the co-purification of CurT with FeCH, I have prepared strain with FLAG-tagged CurT (*curT*.f). In this strain, I was able to delete the native copy of *curT*, which proves that CurT.f is functional in the cell, as *curT* deletion in WT background was not possible (see further). Moreover, also the level of Chl and PBS in *curT.f*/Δ*curT* was comparable to WT (Figure 34).

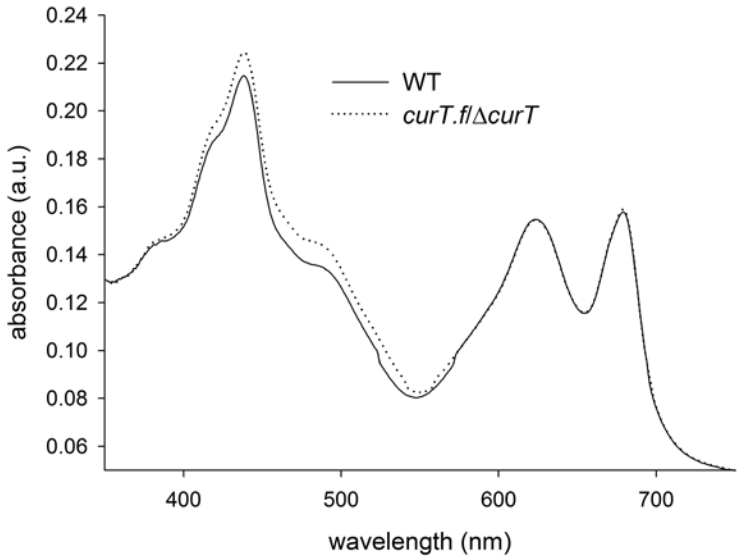

Figure 34

Whole-cell absorption spectra showing complementation of Δ*curT* by FLAG-tagged CurT

A whole-cell absorption spectra of WT and *curT.f*/Δ*curT* grown at 40 µmol of photons $m^{-2}s^{-1}$. Chlorophyll is represented by 680 nm peak and phycobiliproteins by the 625 nm peak. Spectra were normalized to light scattering at 750 nm.

After affinity chromatography of *curT.f*/*ΔcurT* membrane fraction solubilized by non-ionic detergent, proteins in the eluate were identified by mass spectrometry (made by Peter Koník). The eluate contained a number of ribosomal protein subunits, prohibitin 3, Sll1106, FtsH2 and 3 proteases, ATP synthase, POR, transport proteins and a number of proteins with unknown function (Table 8). FeCH was not found among proteins identified in the CurT.f/Δ*curT* eluate by mass spectrometry. However, FeCH was not detected in the whole-cell eluates of HemJ.f and Sll1106.f, yet it was identified by antibody (Figure 24) or in the band from SDS-PAGE (band 2, Table 5), respectively.

Table 8

Proteins co-purified with CurT.f

Proteins identified in the CurT.f eluate from Δ*curT* background with coverage up to 10% and not present in the control eluate from the WT. PilA1 is mentioned even though its coverage is lower than mentioned 10% as this protein is often detected with low coverage, even though there is a high level of protein detected otherwise (Linhartová and Koník, unpublished data).

Gene	Protein description	mW (Da)	Peptides	Theoretical Peptides	Coverage (%)
ssr1399	30S ribosomal protein S18	8375	2	9	43.66
ssr0109	hypothetical protein	6738	1	3	40.32
sll1799	50S ribosomal protein L3	22726	4	16	38.03
slr0637	hypothetical protein	28999	5	17	37.93
slr1128	prohibitin 3	35704	9	30	37.69
sll1323	ATP synthase subunit b of CF 0	16235	4	13	34.27
sll1743	50S ribosomal protein L11	14968	2	13	28.37
sll1456	hypothetical protein	33495	5	15	28.15
sll1106	hypothetical protein	18019	3	10	26.90
slr1678	50S ribosomal protein L21	13660	2	7	25.81
slr0228	FtsH2 protease	68453	10	48	25.68
slr0483	CurT	16874	5	9	25.50
slr1604	FtsH3 protease	67209	10	45	23.70
slr0677	biopolymer transport ExbB2	25058	2	15	21.15
sll1180	toxin secretion ABC transporter ATP binding protein	112019	8	68	20.47
slr0021	protease	30255	3	18	19.49
sll1178	probable carbamoyl transferase	69098	7	42	16.26
slr0506	POR (light operative)	36038	4	31	15.22
sll1324	ATP synthase B chain subunit I of CF 0	19792	2	14	15.08
sll0072	hypothetical protein	25783	2	14	11.89
sll1694	pilin polypeptide PilA1	17562	1	10	7.74

The importance of CurT for *Synechocystis* 6803 can be implied from the fact that the *curT* deletion mutants were very reluctant to segregate (Heinz et al., 2016) or did not segregate (Armbruster et al., 2013). I have prepared my own construct for the *curT* deletion with erythromycin resistance cassette (Table 1). However, I was not able to get fully segregated Δ*curT* strain in the WT background. Although Heinz et al. (2016) described that they were able to fully segregate Δ*curT* at high levels of antibiotic, in my case, even high concentration of erythromycin (300 μg/ml) did not lead to full segregation (data not shown).

As the published fully segregated Δ*curT* had a lower amount of PSII (Heinz et al., 2016), I have decided to try the *curT* deletion in two PSII-less strains lacking PSII subunits, either CP47 or PsbE (ΔCP47 or Δ*psbE*). In both strains, the Δ*curT* construct segregated easily at a common level of antibiotics (10 or 20 μg/ml of erythromycin, Figure 35). To test whether PSII function is the major obstacle for Δ*curT* segregation, I tried segregation in WT background in the presence of PSII inhibitor atrazine. Apparently, PSII inhibitor did not facilitate the segregation of the Δ*curT* mutant (Figure 35).

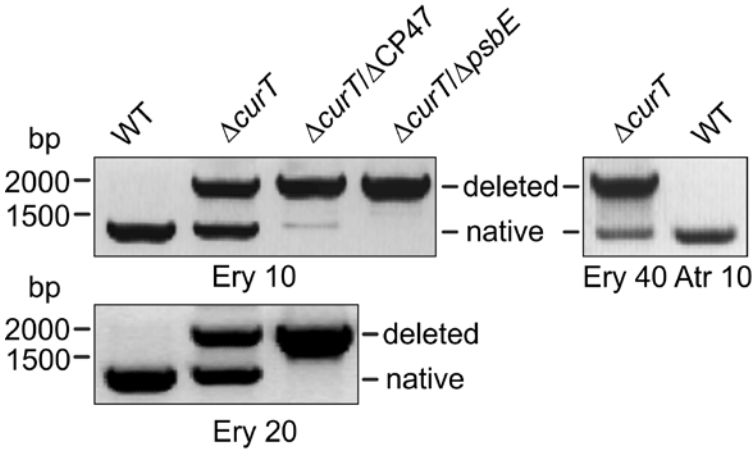

Figure 35

Deletion of *curT* in different backgrounds

Deletion of *curT* was performed by construct containing erythromycin resistance. Segregation was successfully achieved in different ΔPSII backgrounds (ΔCP47, Δ*psbE*) at 10 or 20 μg/ml of erythromycin (Ery 10, 20). Δ*curT* was not possible fully segregate in WT background, even when atrazine (Atr) was added to the medium.

Parallelly, we have obtained the fully segregated Δ*curT* strain with zeocin resistance from the laboratory of Neil Hunter (Hollingshead, unpublished). I have transformed our WT with DNA isolated from the strain. After prolonged segregation at high zeocin levels, I got 5 fully segregated colonies (Δ*curT* R1-R5). Interestingly, these five transformants exhibited markedly different phenotypes.

All five transformants displayed severely retarded growth compared to WT on the plate supplemented with glucose, especially the Δ*curT* R1, R3, and R4 (Figure 36A, Figure 37A). Δ*curT* R2-R5 were able to grow photoautotrophically, even though the photoautotrophic growth of Δ*curT* R5 was highly impaired (Figure 37A). On the other hand, Δ*curT* R1 was not growing photoautotrophically (Figure 36A). Separation of the membrane complexes by CN-PAGE revealed that all the Δ*curT* transformants contained a lower amount of PSI (Figure 36C, Figure 37B). Δ*curT* R2-R5 had decreased level of PSII dimer (Figure 37B) and Δ*curT* R1 lacked PSII entirely (Figure 36C).

As Δ*curT* R1 exhibited the strongest phenotype and did not contain any PSII, I chose this transformant for closer characterization. Interestingly, although the fully assembled PSII complexes in the mutant were not detectable, the mutant still accumulated relatively high levels of unassembled CP43 (Figure 36C). This observation suggested a block in the formation of the early PSII assembly intermediates, as PSII assembly occurs in a stepwise fashion from four preassembled modules and attachment of the CP43 module and is the final step of PSII reaction center core assembly (Figure 1, Komenda et al. (2012)).

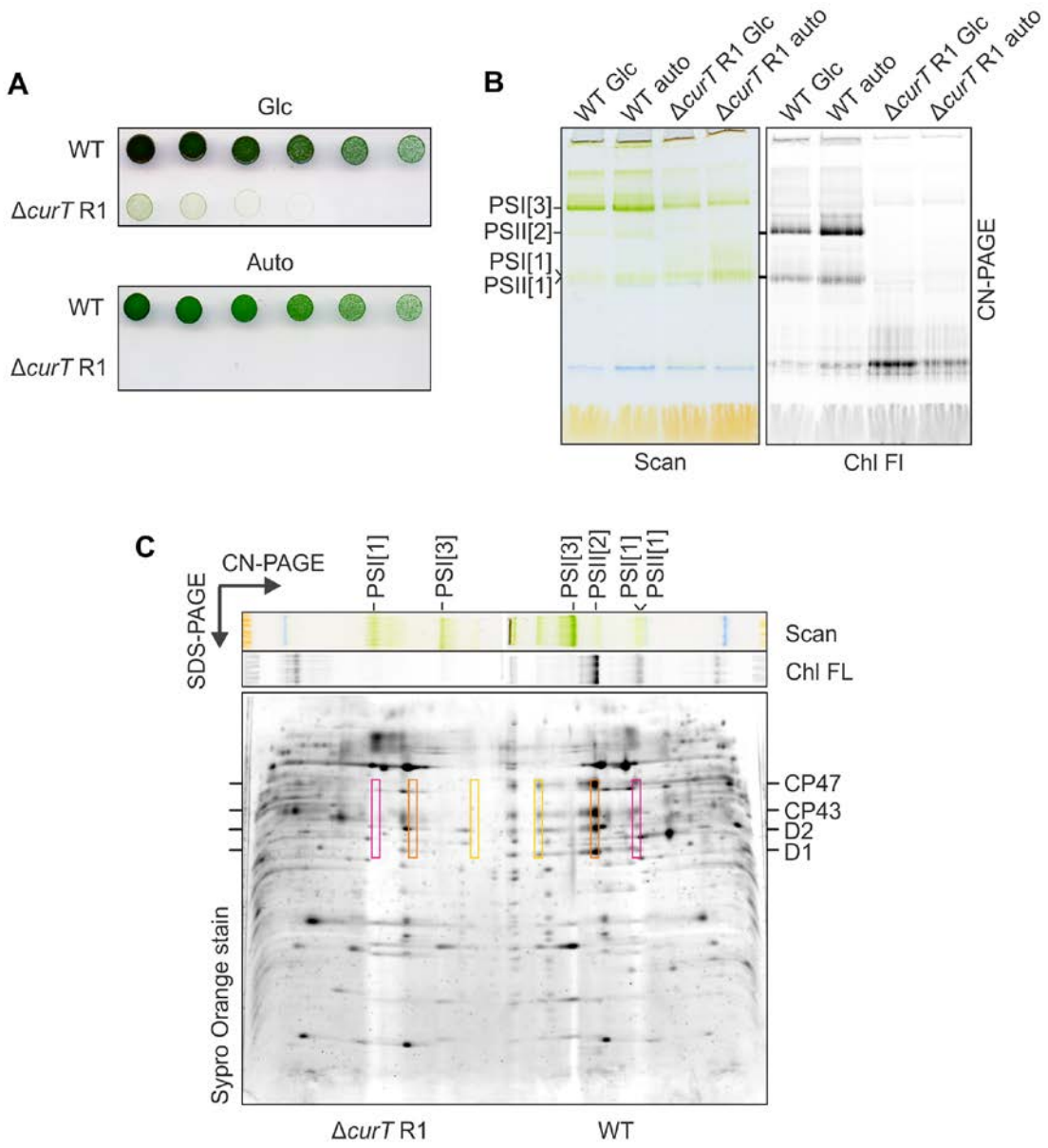

Figure 36

Characterization of Δ*curT* R1 strain

(A) Δ*curT* R1 and WT precultivated in liquid BG11 supplemented with 5 mM glucose, were subsequently cultivated on plates either with (Glc) or without glucose (Auto) at 40 µmol of photons $m^{-2}s^{-}1$ for 4 days. 5 µl of the culture OD_{730}= 0.2 was applied to the plate on the left side followed with two-fold serial dilutions. (B) The membranes of WT and Δ*curT* grown either with glucose or 2 days without glucose (auto) were separated by CN-PAGE. For WT, membranes containing 5 µg of chlorophyll were loaded; for Δ*curT* R1, the amount was recalculated based on the Chl/OD ratio of the strains. The gel was scanned (Scan) and chlorophyll fluorescence (Chl Fl) emitted by PSII was excited by blue light and detected by LAS 4000 Imager (Fuji). (C) CN-bands of WT auto and Δ*curT* R1 auto were separated in the second dimension by SDS-PAGE and stained by Sypro Orange. By pink, orange and yellow rectangles are highlight positions of the main PSII subunits in the monomer, dimer, and supercomplexes, respectively.

Designation of complexes: PSI[3] and PSI[1], trimeric and monomeric PSI; PSII[2] and PSII[1], dimeric and monomeric PSII

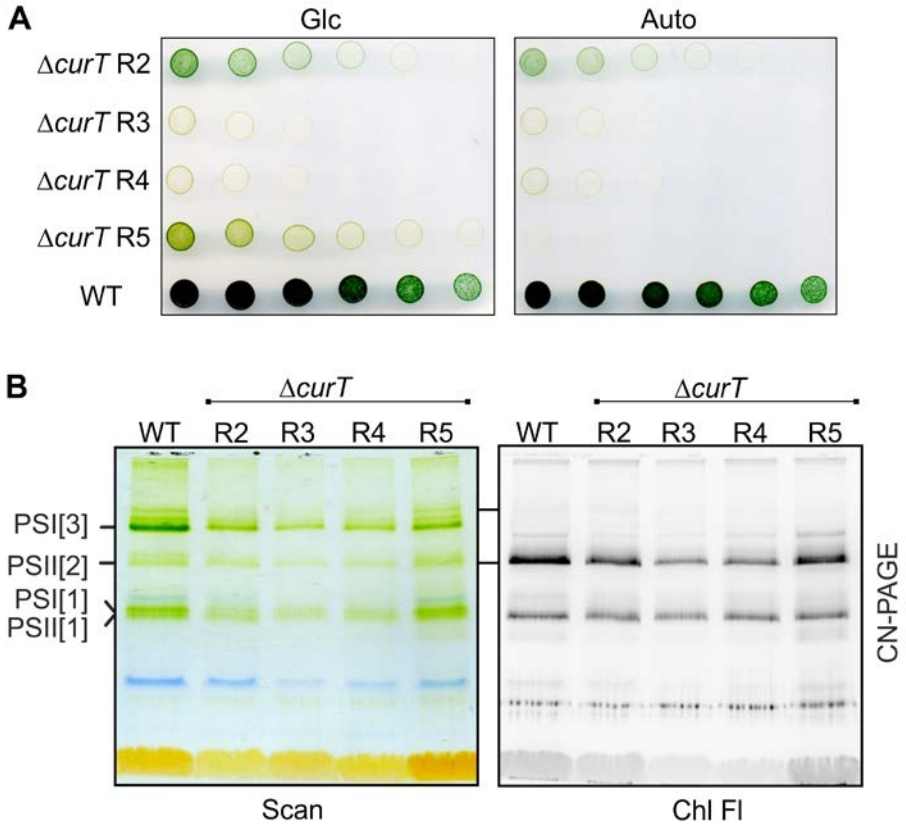

Figure 37

Characterization of Δ*curT* R2-R5

(A) Strains precultivated in liquid BG11 supplemented with 5 mM glucose, were subsequently cultivated for 4 days on plates either with (Glc) or without glucose (Auto) at 40 µmol of photons $m^{-2}s^{-1}$. 5 µl of the culture OD_{730}= 0.2 was applied to the plate on the left side followed with two-fold serial dilutions. (B) Solubilized thylakoids from WT and of Δ*curT* R2-R5 strains were separated by 4-14% clear native gel electrophoresis (CN-PAGE). The gel was scanned (Scan) and chlorophyll fluorescence (Chl Fl) emitted by PSII was excited by blue light and detected by LAS 4000 Imager (Fuji). For WT, membranes containing 5 µg of chlorophyll were loaded; for Δ*curT* R2-R5, the amount was recalculated based on the Chl/OD ratio in the strains.

Designation of complexes: PSI[3] and PSI[1], trimeric and monomeric PSI; PSII[2] and PSII[1], dimeric and monomeric PSII

As the Δ*curT* R1 displayed more severe phenotype than the one described by Heinz et al. (2016), I examined its ultrastructure by transmission electron microscopy (TEM – made by Lenka Bučinská, Figure 38). The Δ*curT* R1 contained fewer membrane sheets than the previously described one (Heinz et al. 2016), otherwise seemed to display similar patterns. Thylakoid membranes sheets in Δ*curT* R1 were arranged in ring-like fashion copying the shape of the cell (Figure 38B, D, E, and F) with concentric circles frequently occurring (C, F). Heinz et al. (2016) claimed that the mutant lacked the convergence zones normally seen in WT (Figure 38A – white arrows), nevertheless, our Δ*curT* R1 occasionally contained structures resembling the convergence zones (B – black arrow).

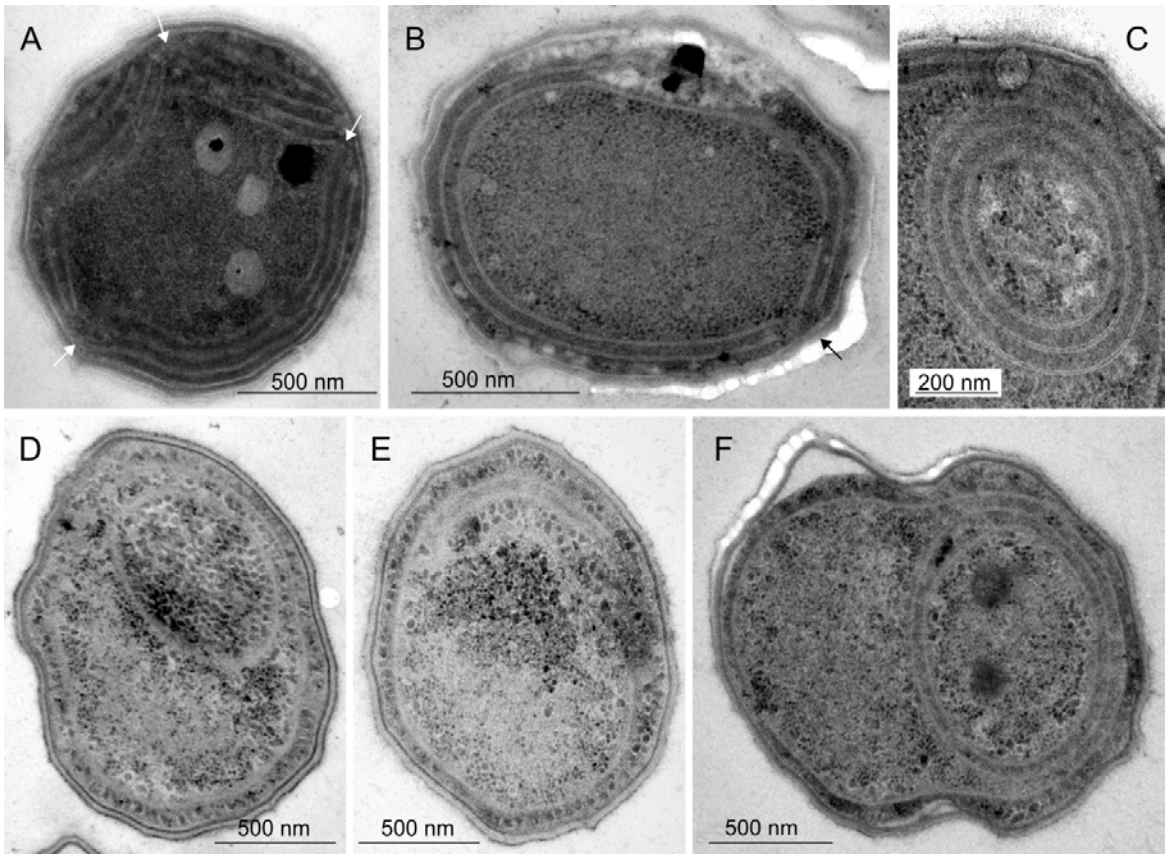

Figure 38

Comparison of WT and Δ*curT* R1 ultrastructure

Ultrastructure of WT (A) and Δ*curT* R1 (B-F) were analyzed by transmission electron microscopy (performed by Lenka Bučinská). Both strains were grown at 40 μmol of photons $m^{-2}s^{-1}$ in the medium supplemented with 5 mM glucose. Arrows show the convergence zones.

The decreased level of photosystems in Δ*curT* R1-R5 is in agreement with downregulation of the tetrapyrrole pathway, demonstrated by lower level of Copro and other heme/Chl precursors (Figure 39). High levels of MV Chlide, originating from Chl recycling, indicate lower proportion of Chl coming from de-novo synthesis in the mutants. Interestingly, Δ*curT* R1 contains barely any Proto, which suggests higher activity of FeCH. It would explain higher level of phycobilins (Figure 40) in Δ*curT* R1 compared to other Δ*curT* transformants with decreased level of tetrapyrrole precursors. In general, all the transformants had significantly decreased level of Chl and mostly also phycobilins. Δ*curT* R1 had also increased level of carotenoids, implying that even 40 μmol of photons $m^{-2}s^{-1}$ presents light stress for the transformant.

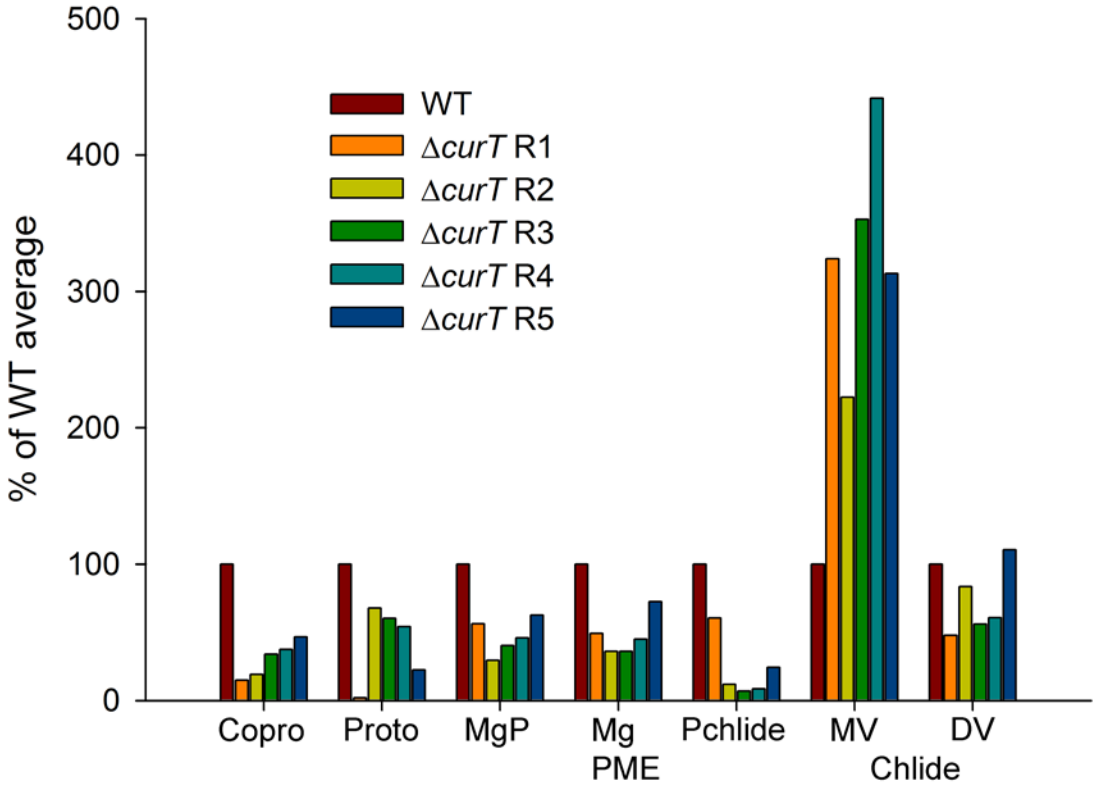

Figure 39

Analysis of heme/chlorophyll precursors of Δ*curT* transformants

Heme/chlorophyll precursors were extracted with 70% methanol from the Δ*curT* R1-R5 and WT cells at OD_{730} = 0.3 - 0.4 and separated on an HPLC equipped with two fluorescence detectors (Pilný et al., 2015). Abbreviations of intermediates: Copro, Coproporphyrin III; Proto, Protoporphyrin IX; MgP, Mg-protoporphyrin IX; Mg PME, Mg protoporphyrin IX monomethyl ester; PChlide, divinyl protochlorophyllide; DV Chlide, divinyl chlorophyllide; MV Chlide, monovinyl chlorophyllide

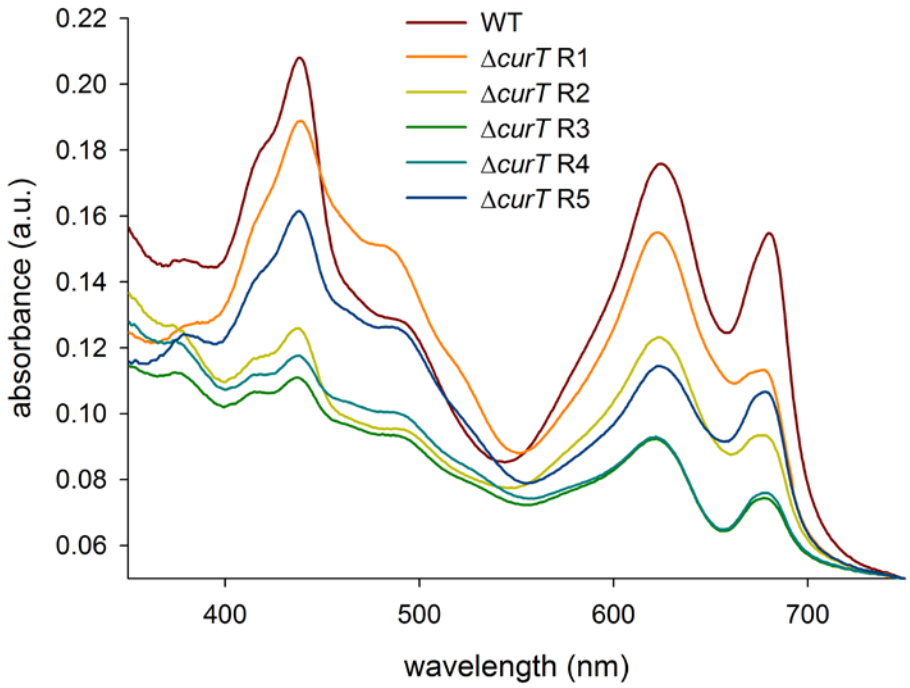

Figure 40

Whole-cell absorption spectra of WT and Δ*curT* R1-R5

The stains were grown at 40 µmol of photons $m^{-2}s^{-1}$ in the medium supplemented with 5mM glucose. Chlorophyll is represented by 680 nm peak and phycobiliproteins by the 625 nm peak. Spectra were normalized to light scattering at 750 nm.

As previously reported (Heinz et al., 2016), also our Δ*curT* R1 mutant lost its transformation competence, thus I could not perform complementation experiment of the deletion strain with WT or tagged copy of *curT* to show if *curT* deletion is solely responsible for Δ*curT* R1 phenotype. Generation of deletion mutants after prolonged segregation process exhibiting different phenotypes indicates that mutants with improved phenotype may contain suppressor mutation. To confirm or exclude such possibility, the whole genome sequencing of the Δ*curT* mutants was performed using the Illumina HiSeq platform.

Analysis of the sequencing data revealed that all Δ*curT* R1-R5 contained such secondary mutation (s). The Δ*curT* R1 mutant has a point mutation in *psbF* gene eliminating the stop codon and leading to the formation of PsbF (cytochrome b559 b subunit) protein fused with the following PsbL. Both PsbF and PsbL are subunits of PSII and it is clear from the 2D gel that their fusion blocks the assembly of PSII (Figure 36B, C).

The Δ*curT* R2 contains 2 mutations, first is the one base insertion in the *btpA* causing frameshift at Val51, the second is one base substitution in *rpaB* (coding Ycf27, also called Rre26) resulting in the substitution of Arg15 for Leu15. As the Δ*curT* R2 had originally pale green color and during cultivation increased its tetrapyrrole content (data not shown), I expect that the primary suppressor mutation was the frameshift in *btpA*

considering the phenotype of the Δ*btpA* strain (Figure 14). The Δ*curT* R3 and R4 bare different one base deletions in *ycf26* coding for Hik33 resulting in a frameshift in Gly239 in case of R3 and in Asp594 in case of R4. Interestingly, both frameshifts yielded the mutants with a similar phenotype (Figure 37, Figure 39, and Figure 40). Unfortunately, we were not able to identify the suppressor mutation in Δ*curT* R5 as the preparation of the sequencing library failed.

5. Discussion

5.1 BtpA

BtpA is a peripheral membrane protein (Zak et al., 1999) forming the TIM-barrel structure. It has been previously described to form oligomers (Schwabe et al., 2003). In my pull-down experiments, BtpA.f was co-purified with its native form indicating that BtpA forms at least dimer (Figure 18). Both BtpA and BtpA.f form a double band on SDS gel (Figure 18). This could be explained by insufficient denaturation of the protein by SDS. However, as a boiling of the sample did not change the pattern (data not shown), I favor posttranslational modification of BtpA as the cause for the observed mobility shift. BtpA was identified as a phosphoprotein by peptide mass fingerprinting (Mikkat et al., 2014). As an introduction of the negative charge by phosphorylation decrease the amount of SDS molecules bound to the protein (Lee et al., 2019), the double band might represent phosphorylated and non-phosphorylated version of BtpA.

BtpA was originally described as a protein connected to the assembly or stability of PSI reaction center proteins. The *btpA* deletion mutant (Zak and Pakrasi, 2000) had significantly reduced Chl content compared to WT. It also exhibited a reduced level of the majority of PSI subunits and impaired PSI activity, whereas its PSII-mediated oxygen evolution was similar to WT. Unlike WT, the mutant was not able to grow photoautotrophically at low temperature and its transfer from normal to low temperature led to degradation of PsaA and PsaB subunits of PSI. Although our Δ*btpA* mutant is based on the same construct obtained as a gift from the Pakrasi lab, it exhibits much stronger phenotype. It has an extremely low level of pigments, both photosystems and thylakoid membranes (Figure 14). In my hands, the most prominent feature of the Δ*btpA* was the lack of Chl, indicating that BtpA is rather connected to the tetrapyrrole pathway than just to the PSI assembly.

As Chl is essential for the accumulation of Chl-binding proteins (Eichacker et al., 1996; Herrin et al., 1992), its lack could explain the lower accumulation of PsaA and PsaB protein in Δ*btpA* (Zak and Pakrasi, 2000). Also transfer from normal to low growth temperature resulting in a reduction of Chl content in WT to half (Zak and Pakrasi, 2000) could lead to such low Chl levels in their Δ*btpA* that did not sustain the photoautotrophic growth at low temperature.

The idea that BtpA is connected to tetrapyrrole pathway was further strengthened by the fact that BtpA.f was co-purified by affinity chromatography with the GluTR protein, the enzyme located at the beginning of tetrapyrrole pathway (Figure 4). As GluTR catalyzes the introductory reaction of the tetrapyrrole pathway, its reaction is considered as an important rate-limiting step within the pathway (Tanaka and Tanaka, 2007). Accordingly, GluTR is the subject of multiple regulations (see Introduction).

The evidence that BtpA interacts with GluTR is also coming from several other findings. Firstly, BtpA and GluTR apparently co-migrate during native electrophoresis of the BtpA.f eluate followed by SDS-PAGE in a 2D gel (Figure 19,Table 3). Moreover, their interaction was also shown by reverse purification of GluTR.f (Kopečná, 2012), which I reconfirmed (Figure 20).

Further proof for the functional connection of BtpA and GluTR was provided by a study of Δ*btpA* suppressor mutants. The poorly growing Δ*btpA* strain easily generated suppressor mutants containing a secondary mutation leading to improvement of its phenotype. Two of complementing mutations were localized within region encoding GluTR. Mutation in suppressor mutant P1 lies at -10 element region responsible for transcription initiation. It leads to an increase of the GluTR transcript (Srivastava, unpublished data). Mutation in P2 suppressor mutant lies in the GluTR dimerization domain (Moser et al., 2001). Even though the exchange of Val352 for Leu352 is conservative, it can have an impact on protein-protein interaction or protein stability. Dimerization domain has been proposed to interact with the anticodon region of glutamyl-tRNA (Moser et al., 2001). In plants, binding of the FLU protein to the GluTR C-terminal, including its dimerization domain, mediates GluTR inhibition, possibly through preventing the binding of glutamyl-tRNA^{Glu} (Zhang et al., 2015).

The last suppressor mutant P3 contained a mutation in FtsH3 protease. FtsHs are universally conserved trans-membrane metalloproteases responsible for quality control of membrane- and membrane-associated proteins. They form homo-/hetero-oligomeric complexes with distinct functions (Kato and Sakamoto, 2018; Krynická et al., 2014). Mutation in Δ*btpA* P3 mapped to FtsH3 led to the replacement of Ser502 with Pro502 located in proximity to its zinc-binding motif (Figure 41). In *E. coli*, mutation in the FtsH zinc-binding motif led to its markedly decreased proteolytic activity (Akiyama et al., 1996). The cyclic structure of proline's side chain gives proline an exceptional conformational rigidity resulting in its disrupting properties on secondary structures as α helices and β sheets. Therefore, the introduction of proline might have a significant impact on the function of the protease. Since FtsH3 is essential in *Synechocystis* 6803 (Mann et al., 2000), it is likely that its activity is not completely aborted in the Δ*btpA* P3 suppressor mutant. The possible effect of FtsH3 on the stability of GluTR might also explain the inability to purify GluTR.f without metalloprotease inhibitor. Regulated proteolysis is one of the posttranslational regulatory mechanisms facilitating responses to external influences (Langklotz et al., 2012). Nevertheless, the evaluation of the role of FtsH3 protease in the regulation of the tetrapyrrole pathway will need further examination.

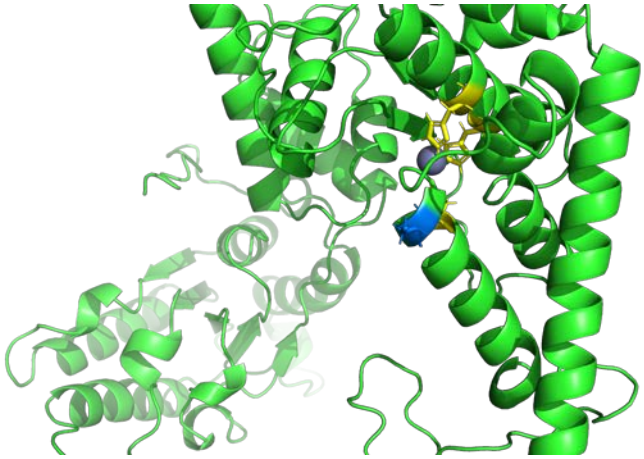

Figure 41

Position of the suppressor mutation in FtsH3 of the Δ*btpA* P3 strain

Zn ion is represented by a violet sphere. Yellow color displays amino acids involved in Zn binding and blue color shows the position of the suppressor mutation in the native FtsH3. Model was created by PyMOL (pymol.org).

As our Δ*btpA* mutant formed suppressor mutants with high frequencies, it was extremely challenging to maintain and characterize the Δ*btpA* strain. It was necessary to take the strain regularly from the frozen stock and frequently check for any changes in Chl accumulation. Such behavior may indicate the possibility that also the originally characterized Δ*btpA* (Zak and Pakrasi, 2000) was suppressor mutant, explaining its less severe phenotype.

GluTR is not detectable by a specific antibody in Δ*btpA*, whereas it is present in the Δ*btpA* P1-P3 suppressor mutants (Srivastava, unpublished data). This implies that low level of tetrapyrroles in Δ*btpA* mutant might be caused by the lower accumulation of GluTR and examined suppressor mutants bypassed that by a mutation in GluTR, higher transcription of GluTR, or by the lower proteolytic activity of FtsH3 protease. BtpA protein might thus act as a chaperon, stabilize the GluTR directly, or protect it against protease(s), similar to the suggested function of GluBP and cpSRP43 in plants (Apitz et al., 2016; Wang et al., 2018). Even though there might be a functional resemblance with plants, neither of the protein known to be involved in the regulation of GluTR accumulation (GluBP and cpSRP43) or activity (FLU) has a homolog in *Synechocystis* 6803. It can be expected that also in cyanobacteria there is the need for balancing the ALA synthesis with the level of tetrapyrrole pathway end products. It was shown that GluTR purified from *Synechocystis* 6803 was inhibited by heme (Rieble and Beale, 1991). An indication that inhibition by heme might occur also in vivo comes from the study of a truncated FeCH (Sobotka et al., 2008b). The truncation resulted in reduced FeCH activity and led to the increased accumulation of ALA. Even though other protein-protein interaction might be provided by less stable transient interactions or at different growth condition of the strain, from my results the rate-limiting step of GluTR seems to

be preferentially interconnected by protein-protein interactions with the nitrogen metabolism in *Synechocystis* 6803.

Interesting is the unexpected co-purification of BtpA and GluTR with enzymes involved in the metabolism of nitrogen. Nitrogen is the critical macronutrient required in high amounts in all organisms. In addition to being the component of DNA and proteins, large amounts of nitrogen in cyanobacteria and plants are found in tetrapyrroles, particularly in Chl. Lack of nitrogen limits the growth and leads to chlorosis, which includes the degradation of photosynthetic pigments (Schwarz and Forchhammer, 2005). BtpA.f was co-purified with all three subunits of urease and 2 of its 4 accessory proteins (Table 3), which are necessary for the functional incorporation of urease metallocenter (Lee et al., 1992). Urease degrades urea to CO_2 and ammonium, which is a preferred nitrogen source of cyanobacteria (Flores and Herrero, 2005) and which can be directly used for incorporation into organic compounds. Urea can be actively gained from the environment by inducible high-affinity permease under nitrogen-limiting conditions (Valladares et al., 2002). In contrast, expression and activity of urease in cyanobacteria is constitutive (Ludwig and Bryant, 2012; Valladares et al., 2002) and it was suggested that urease plays an important role in the catabolism of urea produced internally (Quintero et al., 2000; Solomon et al., 2010). In most organisms, urea is produced intracellularly by the urea cycle and/or by purine catabolism. In cyanobacteria, however, the degradation of purines is completely unknown and the presence of the urea-producing enzyme arginase in cyanobacteria is questionable (Quintero et al., 2000). Instead, an arginine dihydrolase ArgZ was identified as a major arginine-degrading enzyme in *Synechocystis*, which catalyzes the conversion of arginine directly into ornithine and ammonia without the urea intermediate (Zhang and Yang, 2019). Currently, the only confirmed urea generating enzyme is agmatinase on the metabolic pathway from arginine to putrescine and other polyamines (Quintero et al., 2000). Interestingly, the respective *Synechocystis* 6803 agmatinase knockout mutant (*sll0228*) exhibited impaired growth when grown on arginine as the sole nitrogen source indicating possible problems with conversion from arginine to urea (Zhang and Yang, 2019).

ArgJ (Figure 20B), an enzyme in the arginine biosynthetic pathway catalyzing two steps in the conversion of glutamate to ornithine (Shin and Lee, 2014) was co-purified with GluTR. Arginine serves not only as a precursor for the synthesis of proteins and polyamines, but it is also used for the synthesis of nitrogen storage molecule cyanophycin (Simon and Weathers, 1976). Metabolites of the arginine biosynthetic pathway were markedly increased after nitrate addition to nitrogen depleted cultures (Zhang and Yang, 2019).

The co-purification of BtpA with urease subunits and its accessory proteins and co-purification of GluTR with ArgJ suggests interconnection of early steps of the tetrapyrrole pathway with nitrogen metabolism. This connection might ensure fast decrease of the tetrapyrrole pathway, which occurs within hours after nitrogen limitation

(Sobotka, unpublished data), and the restart of the tetrapyrrole pathway after the supply of nitrogen. Moreover, it can also affect protein synthesis. Glutamyl-tRNA^{Glu}, the substrate of GluTR, has to be distributed among protein synthesis and tetrapyrrole pathway dependent on current need of their products. As the levels of Chl and glutamyl-tRNA^{Glu} are not co-regulated (O'Neill and Söll, 1990), other mechanisms may be responsible for routing the tRNA into separate pathways. Also arginine pool is used for both protein synthesis and cyanophycin production. Interaction of ArgJ with GluTR may affect activity or localization either of the enzymes and provide one of the mechanisms how to balance tetrapyrrole and protein biosynthesis with nitrogen storage.

The size of BtpA.f/GluTR complex ranged the size from 500 kDa to more than 1000 kDa according to its mobility during native electrophoresis (Figure 19). GluTR forms a dimer (Moser et al., 2001). Nevertheless, the size of native GluTR complex described by Rieble and Beale (1991) was approximately 350 kDa. Also, BtpA probably forms oligomers (Schwabe et al., 2003) and its amount seems to correlate with the amount of GluTR (Figure 18). It is possible that GluTR and BtpA create molecules of higher oligomeric state with the dimer as a basic unit. Such detected large complex can easily accommodate oligomers of GluTR and BtpA.f together with components of nitrogen metabolism pathway.

5.2 HemJ

HemJ was the last discovered variant of PPO, even though it is present in many proteobacteria and cyanobacteria (Dailey et al., 2017). There is only little information about its structure and function. To characterize HemJ from *Synechocystis* 6803, I have homologously overexpressed Flag-tagged HemJ and purified it from the solubilized membranes. I have used the strain containing both WT and tagged variant of HemJ to potentially co-isolate tagged HemJ.f together with the native form of the protein, given that oligomeric states have previously been described for other PPO variants (Möbius et al., 2010). Indeed, the isolated complex forms an oligomer, most likely tetramer, according to its separation in the second dimension (Figure 25). As HemJ is hydrophobic membrane protein, it cannot be ruled out that tetramer formation is the result of unnatural aggregation. However, the formation of a dimer is highly probable as a dimeric form of HemJ is stable even after SDS electrophoresis (Figure 24A).

The natively isolated eluate of HemJ.f was reddish thanks to bound tetrapyrrole (Figure 23), which was identified as heme *b* (Skotnicová et al., 2018). It is consistent with the fact that *E. coli* overexpressing HemJ from *R. sphaeroides* resulted in its color change into pink (Gomelsky and Kaplan, 1996). Surprisingly, Kato et al. (2010) did not describe any coloring of *E.coli* or eluate, when they purified *R. sphaeroides* HemJ variant from *E.coli*. Unfortunately, there are no available data about spectroscopic analysis of their eluate or its protein composition.

From the reduced absorbance spectra (Figure 23B), it seems that HemJ contains six-coordinated heme *b* with a ligand on the distal side, probably an amino acid side chain. We expect that heme *b* is redox-active and involved in electron transfer. Alternatively, the heme bound to HemJ.f may have a regulatory function and serve for example as an inhibitor. Nevertheless, some cofactor is needed for the PPO reaction and UV/VIS spectra did not reveal any other cofactor than heme (Figure 23). Moreover, the amount of bound heme was estimated 0.85 per subunit (Skotnicová et al., 2018), which considering the probable partial heme loss during isolation suits the model where HemJ binds one heme *b*. This fits better into the picture of heme *b* as a functional, rather than a regulatory component of HemJ.

HemG and HemY have been shown to be coupled with the electron transport chain and plastoquinone pool, respectively (Brzezowski et al., 2019; Möbius et al., 2010). Protoporphyrinogen oxidase reaction in *R. sphaeroides* (containing HemJ) was inhibited upon extraction of quinones and Protogen was able to reduce cytochromes during the assay. This implies close linkage of HemJ reaction with components of the respiratory electron transport chain in *R. sphaeroides* (Jacobs and Jacobs, 1981). Unfortunately, we were not able to measure the activity of HemJ isolated from solubilized membranes (Skotnicová et al., 2018). This is in line with no enzymatic activity detected in *R. sphaeroides* membranes solubilized by Triton (Jacobs and Jacobs, 1981). PPO activity

from the membrane fraction of *R. sphaeroides* was inhibited by respiratory inhibitors and by extraction of quinones from the membrane by pentane. This implies HemJ linkage to electron transport chain as it was already described for HemG.

Even though we were not able to measure the activity of purified HemJ.f, my data further show that HemJ functions as protoporphyrinogen oxidase. Its downregulation resulted in Copro and Proto accumulation and at the same time also decrease of Chl precursors (Figure 27), which proofs further that measured Proto originates from oxidation of Protogen in the cell or during measurement and not enzymatic reaction (Figure 10). Accumulation of Proto and not Protogen was also described when other PPO variants were deleted or inhibited (Lee et al., 1993; Nishimura et al., 1995). Massive accumulation of not only Proto but also Copro after HemJ downregulation (Figure 27) inclines, that whole pathway is upregulated as a response to missing Proto or its further products.

To see whether HemJ can be complemented by HemG, I tried to delete HemJ from the strain with previously introduced HemG. In this strain I was able to achieve full segregation of *hemJ* deletion, which is not possible in WT background, suggesting that HemG is functional in *Synechocystis* 6803. The Δ*hemJ*/*hemG* strain contained enough pigments to assemble the photosystems, even though in a lower amount than in WT (Figure 28B). Nevertheless, the strain was not photosynthetically complemented as it grew only in media supplemented with glucose (Figure 28C). When the strain was transferred to the medium without glucose the Chl precursors decreased (represented by Pchlide in Figure 29A). Additionally, the unusual porphyrin identified as harderoporphyrin (Skotnicová et al., 2018) started to accumulate (Figure 29, Figure 30). Harderoporhyrin is most probably a product of autooxidation of harderoporphyrinogen, which is an intermediate of two-step decarboxylation of Coprogen, catalyzed by CPO (Rand et al., 2010). There are two CPOs in *Synechocystis* 6803 named HemN and HemF, nevertheless, HemF is the prevalent CPO under aerobic conditions (Goto et al., 2010). Complex formation of CPO with PPO and FeCH enabling direct channeling of photoactive intermediates was suggested by Ferreira et al. (1988). Harderoporphyrin accumulation indicates that such a connection might exist among HemF and HemJ, and it is disrupted in Δ*hemJ*/*hemG*. CPO uses Coprogen as well as harderoporphyrinogen as a substrate. Binding of HemG instead of HemJ might destabilize HemF active site leading to release of harderoporphyrinogen (latter oxidized to harderoporphyrin), similar to human mutant HemF, where the accumulation of harderoporphyrin was attributed to reduced affinity to harderoporphyrinogen (Schmitt et al., 2005).

A possible explanation for harderoporhyrin accumulation only at photoautotrophic condition comes from the study of red algae *Galdieria sulphuraria*. This alga excretes Copro to the medium when grown mixotrophically on glucose (Sarian et al., 2016). This excretion is avoided when intensive aeration is used. This organism possesses HemN as well as HemF, similarly to *Synechocystis* 6803. It has been shown that the activity of

HemN and HemF forms differ among oxic/anoxic conditions (Goto et al., 2010). I expect, that during growth on glucose, available oxygen is preferentially used to gain energy from glucose by glycolysis, Krebs cycle and oxidative phosphorylation, leading to inactivation of oxygen-dependent coproporphyrinogen oxidase (Sarian et al., 2016), which uses oxygen as an electron acceptor for its reaction (Breckau et al., 2003). An identical situation occurs probably also in *Synechocystis* 6803. For the transition between photoautotrophic and photomixotrophic growth as well as between oxic and microoxic conditions is responsible two-component regulatory histidine kinase Hik31 (Kahlon et al., 2006; Summerfield et al., 2011). When transferred from oxic to microoxic condition, *hemF* mRNA levels are increased in Δ*hik31* compared to WT showing that *hemF* is a target of Hik31 downregulation at low oxygen condition. I expect that in glucose-supplemented *Synechocystis* 6803 culture, the active form of CPO is HemN as a consequence of a decreased oxygen level.

These results together indicate the importance of substrate channeling in tetrapyrrole biosynthesis under different environmental conditions and serious consequences any disbalance could have. Interesting is that HemJ uses heme *b*, the product of its subsequent enzymatic reaction as a cofactor. The occurrence of heme *b* with the enzyme of the heme biosynthetic pathway was also described by Kühner et al. (2014) in heterodimeric AhbAB (siroheme decarboxylase) complex catalyzing the decarboxylation of siroheme to 12,18-didecarboxysiroheme. Also, the heme biosynthetic pathway using HemG is coupled to the respiratory system highly dependent on heme-containing proteins (Möbius et al., 2010). However, this is probably only a coincidence as heme proteins are generally important for redox reactions.

I aimed to identify HemJ partners within tetrapyrrole pathway by affinity chromatography of FLAG-tagged HemJ as complex formation of CPO, PPO and FeCH was proposed (Ferreira et al., 1988) and some evidence exists for complex formation between FeCH and other PPO variants (Kim et al., 2018; Masoumi et al., 2008; Medlock et al., 2015). I was able to detect FeCH in HemJ.f eluate by specific antibody (Figure 24B). The amount of co-isolated FeCH was significantly higher in ΔPSI background, possibly reflecting the higher flow into heme branch in this background lacking most of the chlorophyll. Nevertheless, a further proof will be needed to prove the complex formation of HemJ with FeCH in *Synechocystis* 6803.

5.3 Sll1106

Sll1106 is a membrane protein. As membrane topology prediction servers predict that Sll1106 contains one or two membrane helices affecting the relative orientation of its termini we tagged Sll1106 on both N- or C- termini. Comparable results of both pull-down experiments imply that Sll1106 contains probably two membrane-spanning helices providing the same orientation of N- and C-termini.

I found Sll1106 in high amount in eluates of His tagged CAB domain of FeCH (Hli-C-tn, Figure 31) and HemJ.f eluate (Figure 24, Table 4). Connection with FeCH was confirmed by identification of several fragments of FeCH in one protein band from SDS-PAGE of the Sll1106.f eluate (band 2, Table 5), even though the amount of FeCH in reverse purification was probably low as it was not identified in whole-cell eluates (Table 6). The connection of Sll1106 with HemJ was not confirmed by reverse purification. This might be caused by a difference in their quantity in the cell. Whereas the level of enzymes like FeCH and HemJ in the cell is quite low, Sll1106 is quite abundant. At standard conditions, its amount is slightly higher than that of D1 protein of PSII (Krynická and Jackson, unpublished data). Moreover, according to their data, HemJ is significantly less abundant than FeCH.

Another indication, that Sll1106 may be functionally connected with the branchpoint of tetrapyrrole biosynthesis is the precursor analysis, where the Δ*sll1106* mutant displayed a significantly lower amount of Proto and also decreased level of MgP and Mg PME (Figure 32B). This lower level of Proto did not lead to any growth defects at standard growth conditions and the steady-state levels of protoheme and Chl were comparable to WT (Figure 32A). Interestingly, the lower level of Proto was reported for ΔH347 mutant of FeCH (later only ΔH347), which lacks the CAB domain (Sobotka et al. (2011), Figure 31A). A possible explanation for the decreased level of Proto is an increased activity of either FeCH or MgCH, as decreased activity of PPO, the enzyme catalyzing the Proto formation would lead to Proto accumulation from spontaneous oxidation of Protogen (Figure 10, Figure 27). Since Δ*sll1106* has also slightly decreased level of MgP and Mg PME, the lower level of Proto may be caused by increased activity of FeCH like in ΔH347, where truncated FeCH exhibited much higher turnover number k_{cat} of ΔH347 than the full-length FeCH (Storm et al., 2013). It is possible, that lower Proto level in ΔH347 might be caused by the inability of the truncated FeCH to interact with Sll1106, as Sll1106 binds the CAB domain of FeCH (Figure 31). As eluates of FLAG-tagged Sll1106 contain high level of carotenoids, it is probable that Sll1106 lies in the region specifically enriched with carotenoids to deal with potentially harmful molecules as it is Proto and other tetrapyrrole intermediates.

The only condition where Δ*sll1106* exhibited impaired growth was salt stress. This is in agreement with the induction of its expression by short-term salt stress (Pandhal et al., 2009). Interestingly, *Arabidopsis thaliana FeCH1*-encoded isoform has a

significant function during salt stress (Fan et al., 2019). During stress, increased level of Proto might be utilized by FeCH to generate heme-derived antioxidant biomolecules for defense. Indeed, increased expression of PPO (HemY) in rice increased tolerance to drought-induced stress (Phung et al., 2011). It is possible that the lower level of Proto in Δ*sll1106* increase the sensitivity to salt stress. Connection to the stress response is suggested also by co-purification with Slr0404 protein. Even though the function of Slr0404 in *Synechocystis* 6803 is unknown, it belongs to DUF1517 superfamily consisting of several glycine rich plant and bacterial proteins, which in plants have a significant role in response to various stress conditions (Czolpinska and Rurek, 2018).

It has been shown that tolerance to salt stress in *Synechocystis* 6803 is associated with the synthesis of proteins (Hagemann et al., 1991). One of the proteins found in the eluate was PilA1, which was suggested to be involved in but not required for, biogenesis and/or stabilization of Chl-binding complex (He and Vermaas, 1999). Co-purification of Sll1106 with PilA1 was confirmed by reverse purification (Linhartová, unpublished results). Also, deletion of PilA1 in the background with normal Chl level had no obvious phenotype (He and Vermaas, 1999). Connection to protein biogenesis and photosystems also demonstrate the presence of YidC, SecD (protein translocation), FtsH proteases (D1 degradation during PSII repair (Komenda et al., 2012), acclimation to iron stress (Krynická et al., 2014)), cytochrome b559 (component of PSII), Psb28-1 (PSII assembly factor, Dobáková et al. (2009)), CurT (membrane architecture, Heinz et al. (2016)) and prohibitins in the Sll1106 eluates. Prohibitins form the large ring-shaped complexes in mitochondria (Tatsuta et al., 2005). They were proposed to act as a general scaffold that stabilizes protein complexes (Van Aken et al., 2010). Nevertheless, the role of prohibitins is still rather enigmatic. In *Synechocystis* 6803 it was postulated that prohibitin 2 is involved in the maintenance of thylakoid membrane (Bryan et al., 2011) and prohibitin 3 in the maintenance of cell fitness under excess excitation (Wang et al., 2008).

The role of Sll1106 is not clear. We can speculate that it plays some role in convergence zones, particularly under stress conditions.

5.4 CurT

Based on analysis of CurT fused with a fluorescent tag, CurT is preferentially located in the cell in the regions with low Chl autofluorescence, slightly above thylakoid membranes, suggesting its localization at the thylakoid membrane/plasma membrane interface (Heinz et al., 2016). In plants, CurT1A is mainly localized at grana margins (Pribil et al., 2014), which are also depleted in Chl-containing complexes (Koochak et al., 2019). The localization of CurT at the thylakoid membrane/plasma membrane interface, its ability to curve the membrane (Armbruster et al., 2013), and the tendency of Δ*curT* mutant to create round membranes without so-called convergence zones, where thylakoid membranes converge close to the plasma membrane (Heinz et al., 2016), strongly suggests that CurT is an important part of convergence zones in *Synechocystis* 6803. Also, our Δ*curT* R1 suppressor mutant displays similar membrane organization, even though it occasionally contains structure resembling the convergence zones (Figure 38B). Thanks to the atypical membrane organization in the cell with fewer membrane sheets, also the convergence zones might be less abundant and are not easily identified by the TEM of a single section. Nevertheless, the convergence zones in Δ*curT* seem to be either entirely missing or at least highly depleted. However, at this point it is difficult to distinguish the effect of *curT* deletion and PsbF-PsbL fusion on the membrane organization of Δ*curT* R1.

The exact role of convergence zones is not clear. The common feature of all *curT* deletion mutants is their transformation incompetence, which might be caused either by incompetence to uptake DNA or to perform homology recombination. Both processes are little understood. It is accepted that type IV pili system plays important role in natural transformability, as many of its components were shown to affect transformation and some, such as PilA1, plays a critical role in the process since its deletion causes incompetence for natural transformation (Yoshihara et al., 2001). Recently the convergence zones were visualized by cryo-electron tomography as highly curved membrane structures connected to the multiple thylakoid tips (Rast et al., 2019). Some of the convergence membranes were in close contact with the plasma membrane, bridged by small densities of unknown identity. It is possible that the connection between thylakoid and plasma membrane is important for transformability of the cell and thus *curT* mutants lacking these connections are incompetent for transformation. It is likely that such connections may be important for DNA uptake.

The general importance of CurT protein for the cell is obvious also from the fact that it is challenging to prepare the *curT* deletion strain. Armbruster et al. (2013) were not able to get fully segregated Δ*curT* strain in *Synechocystis* 6803. On the other hand, Heinz et al. (2016) were able to get the fully segregated mutant when they used high levels of antibiotic during segregation (more than 10 times higher than is usual). In my experiments, I was not able to get fully segregated Δ*curT* using construct with

erythromycin resistance cassette and the fully segregated deletion mutants gained with zeocin resistance cassette differed significantly and they bore suppressor mutation(s). The phenotypic differences seen between my Δ*curT* strains and the Δ*curT* strain created by (Heinz et al., 2016) could be attributable to a number of factors. The first might be differences in the *Synechocystis* 6803 WT substrains used in different labs (Morris et al., 2014; Tichý et al., 2016). Hollingshead et al. (2016) demonstrated that these WT substrains might have diverse tolerance for deletion of particular functionally important genes. It is possible that WT substrain used by Heinz et al. (2016) already contained some mutation making the *curT* segregation possible. The discrepancy in obtaining Δ*curT* mutants might be also connected to the method of gene deletion. I have used the deletion of the native gene where the major part of the gene is replaced by the antibiotic resistance. On the other hand, Heinz et al. (2016) used insertional mutation at the 159 bp from the N-terminus. In rare cases, inactivation of the gene by insertion of antibiotic cassette might result in a partially functional protein. There has been described differences in phenotype between insertional and deletion mutant (Boehm et al., 2009; Bryan et al., 2011). However, the most likely explanation is that during prolonged segregation, the Δ*curT* mutants generated suppressor mutation(s), although the authors claimed that all the colonies displayed the same phenotype.

When Δ*curT* was transformed into background missing PSII subunits (CP47, PsbE), full segregation of the *curT* deletion was achieved at standard antibiotic concentration. Conversely, the addition of atrazine, which binds to plastoquinone binding site of D1 and leads to inhibition of electron transport in PSII (Shukla and Devine, 2008), did not facilitate full segregation of the Δ*curT* deletion. Therefore, CurT is probably not connected to PSII function. Rather it looks like that once the PSII assembly is disrupted in the PSII mutant, there is no longer the strict need to keep the *curT* gene. This would fit the theories, that CurT defined domains at convergence zones are the place of PSII assembly and possibly also repair (Heinz et al., 2016; Rast et al., 2019). In agreement with this, convergence zones are not photosynthetically active (Rast et al., 2019). However, they have membrane-associated ribosomes. In plants, the grana margins, which are enriched with CurT1A protein and FtsH proteases (Yoshioka and Yamamoto, 2011), contain preferentially PSII monomers and CP43-free core of PSII (Koochak et al., 2019). It is expected that PSII is channeled to this grana margin location for repair.

We believe that CurT is indispensable under normal conditions. Intriguing question is, why it is indispensable and what special conditions allow full segregation of Δ*curT*. Clearly, CurT is dispensable in the mutants lacking assembled PSII like in ΔCP47 and Δ*psbE* mutants. The complementing mutation, fusing PsbF with PsbL in the Δ*curT* R1 suppressor mutant also falls into this category. PsbF/PsbL fusion would yield a protein with two transmembrane helices resulting in the antiparallel orientation of PsbF or PsbL. Moreover, PsbF and PsbL are included in different PSII assembly modules (Figure 1). Obviously, according to the lack of early PSII assembly modules in the Δ*curT* R1

(Figure 36 B, C), such an arrangement prevents assembly of PSII, similarly to the situation in Δ*psbE*. In the second group of suppressor mutants Δ*curT* R2 - R4 the complementing mutation did not influence PSII assembly, at least not directly. In Δ*curT* R2 the frameshift in *btpA* most probably resulted in nonfunctional BtpA similar to our Δ*btpA* mutant with completely bleached phenotype (Figure 14). From the course of segregation in Δ*curT* R2 it seems that the second mutation found in the Δ*curT* R2 actually alleviated its bleached phenotype. This second mutation led to Arg15Leu substitution in response regulator Rre26 paired with histidine kinase Hik33 in two-component signal transduction system. Interestingly, also in Δ*curT* R3 and R4, the complementing mutation was found in the same Hik33-Rre26 signal transduction pair, this time in Hik33. The suppressor mutants contained frameshifts at the position 239 in Δ*curT* R3 and at the position 594 in Δ*curT* R4 (of total 663 amino acids). As the Hik33 kinase cannot function without its C-terminal ATPase domain starting around amino acid 538, the Hik33 in Δ*curT* R3 will be nonfunctional. Interestingly, phenotypes of both Δ*curT* R3 and R4 are very similar (Figure 37, Figure 39, and Figure 40), indicating that Hik33 is inactive in both strains. This means that the effect of this suppressor mutation can be directly compared with the phenotype of the thoroughly studied Δ*hik33* mutant.

The histidine kinase Hik33 plays a central role in acclimation to changing environments in cyanobacteria (Ge et al., 2018). The Hik33/Rre26 two-component system controls the expression of genes encoding proteins related to PSI and II and some electron transport genes (Riediger et al., 2018). Deletion of *hik33* severely affects photosynthetic oxygen evolution of PSII and the mutant is unable to survive at high light conditions (Hsiao et al., 2004). Δ*hik33* also accumulates significantly lower amounts of Chl (Ge et al., 2018).

Absence of PSII in ΔCP47, Δ*psbE*, and in Δ*curT* R1 clearly facilitated deletion of *curT*. However, Δ*curT* R2 and R5 accumulated significant amount of PSII, so it is not PSII accumulation per se, what is preventing *curT* deletion. All the Δ*curT* suppressor mutants exhibited decreased accumulation of Chl and tetrapyrrole precursors (Figure 39 and Figure 40). Also, various PSII-less mutants have a decreased level of Chl and tetrapyrrole precursors (Clarke and Eaton-Rye, 2000; Sobotka et al., 2005).

Taken together, low level of tetrapyrrole precursors are apparently required to achieve full segregation of *curT*. The assembly of photosystems and tetrapyrrole pathway are deeply interconnected (Chidgey et al., 2014). As Chl and its intermediates are highly toxic, possible organization of Chl pathway in a multienzymatic complex enabling passing of the toxic intermediate from one enzyme to another ending with co-translational insertion of Chl into proteins was discussed (Sobotka, 2014). It is possible that in Δ*curT* strain, synthesis of Chl-binding protein or/and PSII assembly are impaired due to the absence of the convergence zones and that toxic intermediates accumulate. Then

downregulation of the tetrapyrrole pathway, affecting the whole assembly/synthesis process, could be beneficial.

Proposed location of the CurT domain as the place of PSII assembly and Chl delivery fits co-purification of CurT with FeCH and POR, an enzyme of Chl biosynthesis. Both FeCH and POR were localized in thylakoid as well as plasma membrane (Pisareva et al., 2011) suggesting special properties of the convergence zones. Also, FtsH2 and FtsH3 proteases, involved in quality control of PSII (Komenda et al., 2006) and found in the CurT.f eluate (Table 8), were localized at the interface between plasma and thylakoid membrane (Sacharz et al., 2015). All this suggest the importance of the CurT domain for a proper function of the tetrapyrrole biosynthesis and PSII assembly.

6. Conclusions

Heme and Chl are critical components of the cellular metabolism in the photosynthetic cell. Nevertheless, Chl and intermediates of Chl/heme biosynthesis are phototoxic, thus this pathway has to be strictly regulated and balanced with other cellular processes. Several connections of the tetrapyrrole pathway with other processes in the cell were also demonstrated in my work. I also showed impacts of disruption of this highly regulated system.

First, I studied BtpA protein which was formerly characterized as a protein involved in the stabilization of PsaA and PsaB protein of PSI (Zak and Pakrasi, 2000). Yet, the *btpA* deletion mutant barely contains any pigments suggesting a connection with the tetrapyrrole pathway. This was confirmed by isolation of suppressor mutants containing the suppressor mutation within the GluTR region and by co-purification of FLAG-tagged BtpA with GluTR. GluTR is an enzyme operating at the beginning of the tetrapyrrole pathway and regulation of its activity or stability seems to be crucial for controlling the total flux through the pathway. Complex formation between BtpA and GluTR was further confirmed by reverse purification of GluTR.f. Unexpected was co-purification of BtpA and GluTR with several proteins of the nitrogen metabolism. Possible regulatory connection of the tetrapyrrole pathway with nitrogen utilization is logical but completely unexplored.

Another important regulatory step is the branchpoint of heme and Chl pathway. Proto, the product of Protogen oxidation, is the last common precursor of both pathways. In *Synechocystis* 6803 PPO reaction is catalyzed by HemJ. This enzyme was only poorly characterized. Purification of homologously expressed FLAG-tagged HemJ revealed that it contains heme *b* as a cofactor. Moreover, I was able to complement HemJ by HemG, non-homologous PPO from *E.coli*. Yet when grown photoautotrophically, complemented strain accumulated high levels of harderoporphyrin, an oxidized intermediate of the previous step catalyzed by CPO. This supports the idea of functional coupling between CPO and PPO which was disrupted by replacement of HemJ by its analog, HemG.

Further, I studied proteins physically associated with the proteins above by pull-down assays. CurT protein was localized at the interface of plasma and thylakoid membranes (Heinz et al., 2016), where it contributes to the formation of the convergence zones. These structures are anticipated to function in PSII assembly and/or repair (Rast et al., 2019; Sacharz et al., 2015; Stengel et al., 2012). In agreement with that, I have co-purified CurT.f with FtsH2 and 3 proteases (Table 8), which are involved in PSII quality control (Komenda et al., 2006). Interestingly, also Sll1106.f was co-purified with the FtsH proteases together with CurT itself, PSII assembly factor Psb28-1 and components of protein translocation machinery (Table 5 and Table 6).

If the convergence zones are the place of the PSII assembly/repair, they should also provide protein translocation machinery together with Chl delivery for

co-translational insertion. This is supported by CurT co-purification with FeCH and POR, enzymes of the tetrapyrrole biosynthesis, and also by co-purification of HemJ.f with FtsH proteases and Sll1106 mentioned above. Moreover, predicted location of the convergence zones at the interface of plasma and thylakoid membrane would bring the machinery close to transport systems for the supply of the necessary ions. In agreement with that PilA1 protein found in the eluates (Table 5, Table 6, and Table 8) is among other functions also involved in manganese and iron acquisition (Lamb et al., 2014; Lamb and Hohmann-Marriott, 2017). Through PilA1, CurT can be also connected to transformability of the *Synechocystis* 6803, as not only deletion of *curT* but also deletion of *pilA1* results in the loss of transformation competence (Heinz et al., 2016; Yoshihara et al., 2001).

7. References

Adams, N. B., Brindley, A. A., Hunter, C. N., and Reid, J. D. (2016). The catalytic power of magnesium chelatase: a benchmark for the AAA(+) ATPases. *FEBS Lett* **590**, 1687-93.

Akiyama, Y., Kihara, A., Tokuda, H., and Ito, K. (1996). FtsH (HflB) Is an ATP-dependent protease selectively acting on SecY and some other membrane proteins. *J Biol Chem* **271**, 31196-31201.

Al-Karadaghi, S., Franco, R., Hansson, M., Shelnutt, J. A., Isaya, G., and Ferreira, G. C. (2006). Chelatases: distort to select? *Trends Biochem Sci* **31**, 135-42.

Aoki, R., Goto, T., and Fujita, Y. (2011). A heme oxygenase isoform is essential for aerobic growth in the cyanobacterium *Synechocystis* sp. PCC 6803: modes of differential operation of two isoforms/enzymes to adapt to low oxygen environments in cyanobacteria. *Plant Cell Physiol* **52**, 1744-56.

Aoki, R., Takeda, T., Omata, T., Ihara, K., and Fujita, Y. (2012). MarR-type transcriptional regulator ChlR activates expression of tetrapyrrole biosynthesis genes in response to low-oxygen conditions in cyanobacteria. *J Biol Chem* **287**, 13500-7.

Apitz, J., Nishimura, K., Schmied, J., Wolf, A., Hedtke, B., van Wijk, K. J., and Grimm, B. (2016). Posttranslational control of ALA synthesis includes GluTR degradation by Clp protease and stabilization by GluTR-binding protein. *Plant Physiol* **170**, 2040-51.

Armbruster, U., Labs, M., Pribil, M., Viola, S., Xu, W. T., Scharfenberg, M., Hertle, A. P., Rojahn, U., Jensen, P. E., Rappaport, F., Joliot, P., Dormann, P., Wanner, G., and Leister, D. (2013). Arabidopsis CURVATURE THYLAKOID1 proteins modify thylakoid architecture by inducing membrane curvature. *Plant Cell* **25**, 2661-2678.

Bartsevich, V. V., and Pakrasi, H. B. (1997). Molecular identification of a novel protein that regulates biogenesis of photosystem I, a membrane protein complex. *J Biol Chem* **272**, 6382-7.

Bečková, M., Gardian, Z., Yu, J., Koník, P., Nixon, P. J., and Komenda, J. (2017). Association of Psb28 and Psb27 proteins with PSII-PSI supercomplexes upon exposure of *Synechocystis* sp. PCC 6803 to high light. *Mol Plant* **10**, 62-72.

Bhaya, D., Dufresne, A., Vaulot, D., and Grossman, A. (2002). Analysis of the hli gene family in marine and freshwater cyanobacteria. *FEMS Microbiol Lett* **215**, 209-19.

Boehm, M., Nield, J., Zhang, P. P., Aro, E. M., Komenda, J., and Nixon, P. J. (2009). Structural and mutational analysis of band 7 proteins in the cyanobacterium *Synechocystis* sp strain PCC 6803. *J Bacteriol* **191**, 6425-6435.

Boynton, T. O., Daugherty, L. E., Dailey, T. A., and Dailey, H. A. (2009). Identification of *Escherichia coli* HemG as a novel, menadione-dependent flavodoxin with protoporphyrinogen oxidase activity. *Biochemistry* **48**, 6705-6711.

Boynton, T. O., Gerdes, S., Craven, S. H., Neidle, E. L., Phillips, J. D., and Dailey, H. A. (2011). Discovery of a gene involved in a third bacterial protoporphyrinogen oxidase activity through comparative genomic analysis and functional complementation. *Appl Environ Microbiol* **77**, 4795-801.

Breckau, D., Mahlitz, E., Sauerwald, A., Layer, G., and Jahn, D. (2003). Oxygen-dependent coproporphyrinogen III oxidase (HemF) from *Escherichia coli* is stimulated by manganese. *J Biol Chem* **278**, 46625-31.

Bryan, S. J., Burroughs, N. J., Evered, C., Sacharz, J., Nenninger, A., Mullineaux, C. W., and Spence, E. M. (2011). Loss of the SPHF homologue Slr1768 leads to a catastrophic failure in the maintenance of thylakoid membranes in *Synechocystis* sp. PCC 6803. *PLoS One* **6**, e19625-e19625.

Brzezowski, P., Ksas, B., Havaux, M., Grimm, B., Chazaux, M., Peltier, G., Johnson, X., and Alric, J. (2019). The function of PROTOPORPHYRINOGEN IX OXIDASE in chlorophyll biosynthesis requires oxidised plastoquinone in *Chlamydomonas reinhardtii*. *Commun Biol* **2**, 159.

Brzezowski, P., Richter, A. S., and Grimm, B. (2015). Regulation and function of tetrapyrrole biosynthesis in plants and algae. *Biochim Biophys Acta* **1847**, 968-985.

Bučinská, L., Kiss, E., Koník, P., Knoppová, J., Komenda, J., and Sobotka, R. (2018). The ribosome-bound protein Pam68 promotes insertion of chlorophyll into the CP47 subunit of Photosystem II. *Plant Physiol*.

Burillo, S., Luque, I., Fuentes, I., and Contreras, A. (2004). Interactions between the nitrogen signal transduction protein PII and N-acetyl glutamate kinase in organisms that perform oxygenic photosynthesis. *J Bacteriol* **186**, 3346-54.

Clarke, S. M., and Eaton-Rye, J. J. (2000). Amino acid deletions in loop C of the chlorophyll a-binding protein CP47 alter the chloride requirement and/or prevent the assembly of photosystem II. *Plant Mol Biol* **44**, 591-601.

Collier, J. L., and Grossman, A. R. (1992). Chlorosis induced by nutrient deprivation in *Synechococcus* sp. strain PCC 7942: not all bleaching is the same. *J Bacteriol* **174**, 4718-26.

Cornah, J. E., Terry, M. J., and Smith, A. G. (2003). Green or red: what stops the traffic in the tetrapyrrole pathway? *Trends Plant Sci* **8**, 224-230.

Crooks, G. E., Hon, G., Chandonia, J. M., and Brenner, S. E. (2004). WebLogo: a sequence logo generator. *Genome Res* **14**, 1188-90.

Czarnecki, O., and Grimm, B. (2012). Post-translational control of tetrapyrrole biosynthesis in plants, algae, and cyanobacteria. *J Exp Bot* **63**, 1675-1687.

Czarnecki, O., Hedtke, B., Melzer, M., Rothbart, M., Richter, A., Schroter, Y., Pfannschmidt, T., and Grimm, B. (2011). An *Arabidopsis* GluTR binding protein mediates spatial separation of 5-aminolevulinic acid synthesis in chloroplasts. *Plant Cell* **23**, 4476-4491.

Czolpinska, M., and Rurek, M. (2018). Plant glycine-rich proteins in stress response: an emerging, still prospective story. *Front Plant Sci* **9**, 302.

Dailey, H. A., Dailey, T. A., Gerdes, S., Jahn, D., Jahn, M., O'Brian, M. R., and Warren, M. J. (2017). Prokaryotic heme biosynthesis: multiple pathways to a common essential product. *Microbiol Mol Biol Rev* **81**, 62.

Dekker, J. P., and Boekema, E. J. (2005). Supramolecular organization of thylakoid membrane proteins in green plants. *Biochim Biophys Acta* **1706**, 12-39.

Dobáková, M., Sobotka, R., Tichý, M., and Komenda, J. (2009). Psb28 protein is involved in the biogenesis of the photosystem II inner antenna CP47 (PsbB) in the cyanobacterium *Synechocystis* sp PCC 6803. *Plant Physiol* **149**, 1076-1086.

Eichacker, L. A., Helfrich, M., Rudiger, W., and Muller, B. (1996). Stabilization of chlorophyll a-binding apoproteins P700, CP47, CP43, D2, and D1 by chlorophyll a or Zn-pheophytin a. *J Biol Chem* **271**, 32174-32179.

Enami, I., Okumura, A., Nagao, R., Suzuki, T., Iwai, M., and Shen, J. R. (2008). Structures and functions of the extrinsic proteins of photosystem II from different species. *Photosynth Res* **98**, 349-63.

Ermakova-Gerdes, S., and Vermaas, W. (1999). Inactivation of the open reading frame *slr0399* in *Synechocystis* sp PCC 6803 functionally complements mutations near the Q(A) niche of photosystem II - A possible role of *slr0399* as a chaperone for quinone binding. *J Biol Chem* **274**, 30540-30549.

Fan, T., Roling, L., Meiers, A., Brings, L., Ortega-Rodes, P., Hedtke, B., and Grimm, B. (2019). Complementation studies of the Arabidopsis fc1 mutant substantiate essential functions of ferrochelatase 1 during embryogenesis and salt stress. *Plant Cell Environ* **42**, 618-632.

Ferreira, G. C., Andrew, T. L., Karr, S. W., and Dailey, H. A. (1988). Organization of the terminal two enzymes of the heme biosynthetic pathway. Orientation of protoporphyrinogen oxidase and evidence for a membrane complex. *J Biol Chem* **263**, 3835-9.

Flores, E., and Herrero, A. (2005). Nitrogen assimilation and nitrogen control in cyanobacteria. *Biochem Soc Trans* **33**, 164-7.

Forcada-Nadal, A., Llácer, J. L., Contreras, A., Marco-Marín, C., and Rubio, V. (2018). The P(II)-NAGK-PipX-NtcA regulatory axis of cyanobacteria: A tale of changing partners, allosteric effectors and non-covalent interactions. *Front Mol Biosci* **5**, 91-91.

Forchhammer, K., and Schwarz, R. (2019). Nitrogen chlorosis in unicellular cyanobacteria - a developmental program for surviving nitrogen deprivation. *Environ Microbiol* **21**, 1173-1184.

Frankenberg-Dinkel, N., and Terry, M. J. (2009). Synthesis and role of bilins in photosynthetic organisms. *In* "Tetrapyrroles: Birth, Life and Death" (M. J. Warren and A. G. Smith, eds.), pp. 208-220. Springer New York, New York, NY.

Fujita, Y., Tsujimoto, R., and Aoki, R. (2015). Evolutionary aspects and regulation of tetrapyrrole biosynthesis in cyanobacteria under aerobic and anaerobic environments. *Life (Basel)* **5**, 1172-203.

Ge, H., Fang, L., Huang, X., Wang, J., Chen, W., Zhang, Y., Wang, X., Sui, N., Xu, W., He, Q., and Wang, Y. (2018). Activation of the oxidative pentose phosphate pathway is critical for photomixotrophic growth of a *hik33*-deletion mutant of *Synechocystis* sp. PCC 6803. *Proteomics* **18**, e1800046.

Gomelsky, M., and Kaplan, S. (1996). The *Rhodobacter sphaeroides* 2.4.1 rho gene: Expression and genetic analysis of structure and function. *J Bacteriol* **178**, 1946-1954.

Gorchein, A. (1972). Magnesium protoporphyrin chelatase activity in *Rhodopseudomonas spheroides*. Studies with whole cells. *Biochem J* **127**, 97-106.

Goslings, D., Meskauskiene, R., Kim, C. H., Lee, K. P., Nater, M., and Apel, K. (2004). Concurrent interactions of heme and FLU with Glu tRNA reductase (HEMA1), the target of metabolic feedback inhibition of tetrapyrrole biosynthesis, in dark- and light-grown *Arabidopsis* plants. *Plant J* **40**, 957-967.

Goto, T., Aoki, R., Minamizaki, K., and Fujita, Y. (2010). Functional differentiation of two analogous coproporphyrinogen III oxidases for heme and chlorophyll biosynthesis pathways in the cyanobacterium *Synechocystis* sp PCC 6803. *Plant Cell Physiol* **51**, 650-663.

Griffin, T. J., Gygi, S. P., Ideker, T., Rist, B., Eng, J., Hood, L., and Aebersold, R. (2002). Complementary profiling of gene expression at the transcriptome and proteome levels in *Saccharomyces cerevisiae*. *Mol Cell Proteomics* **1**, 323-33.

Grotjohann, I., and Fromme, P. (2005). Structure of cyanobacterial photosystem I. *Photosynth Res* **85**, 51-72.

Grzybowska, E., Gora, M., Plochocka, D., and Rytka, J. (2002). *Saccharomyces cerevisiae* ferrochelatase forms a homodimer. *Arch Biochem Biophys* **398**, 170-8.

Hagemann, M., Techel, D., and Rensing, L. (1991). Comparison of salt-induced and heat-induced alterations of protein-synthesis in the cyanobacterium *Synechocystis* sp PCC-6803 *Arch Microbiol* **155**, 587-592.

Hanaichi, T., Sato, T., Iwamoto, T., Malavasi-Yamashiro, J., Hoshino, M., and Mizuno, N. (1986). A stable lead by modification of Sato's method. *J Electron Microsc (Tokyo)* **35**, 304-6.

He, Q., and Vermaas, W. (1999). Genetic deletion of proteins resembling Type IV pilins in *Synechocystis* sp. PCC 6803: their role in binding or transfer of newly synthesized chlorophyll. *Plant Mol Biol* **39**, 1175-1188.

Heinz, S., Rast, A., Shao, L., Gutu, A., Gugel, I. L., Heyno, E., Labs, M., Rengstl, B., Viola, S., Nowaczyk, M. M., Leister, D., and Nickelsen, J. (2016). Thylakoid membrane architecture in *Synechocystis* depends on CurT, a homolog of the granal CURVATURE THYLAKOID1 proteins. *Plant Cell* **28**, 2238-2260.

Herrin, D. L., Battey, J. F., Greer, K., and Schmidt, G. W. (1992). Regulation of chlorophyll apoprotein expression and accumulation. Requirements for carotenoids and chlorophyll. *J Biol Chem* **267**, 8260-9.

Heyes, D. J., Hunter, C. N., vanStokkum, I. H. M., vanGrondelle, R., and Groot, M. L. (2003). Ultrafast enzymatic reaction dynamics in protochlorophyllide oxidoreductase. *Nat Struct Biol* **10**, 491-492.

Hollingshead, S., Kopečná, J., Armstrong, D. R., Bučinská, L., Jackson, P. J., Chen, G. E., Dickman, M. J., Williamson, M. P., Sobotka, R., and Hunter, C. N. (2016). Synthesis of chlorophyll-binding proteins in a fully segregated Δ*ycf54* strain of the cyanobacterium *Synechocystis* PCC 6803. *Front Plant Sci* **7**.

Hoober, J. K., Kahn, A., Ash, D. E., Gough, S., and Kannangara, C. G. (1988). Biosynthesis of delta-aminolevulinate in greening barley leaves. IX. Structure of the substrate, mode of gabaculine inhibition, and the catalytic mechanism of glutamate 1-semialdehyde aminotransferase. *Carlsberg Res Commun* **53**, 11-25.

Horáková, E., Changmai, P., Vancová, M., Sobotka, R., Van Den Abbeele, J., Vanhollebeke, B., and Lukeš, J. (2017). The *Trypanosoma brucei* TbHrg protein is a heme transporter involved in the regulation of stage-specific morphological transitions. *J Biol Chem* **292**, 6998-7010.

Hsiao, H. Y., He, Q., Van Waasbergen, L. G., and Grossman, A. R. (2004). Control of photosynthetic and high-light-responsive genes by the histidine kinase DspA: negative and positive regulation and interactions between signal transduction pathways. *J Bacteriol* **186**, 3882-8.

Chidgey, J. W., Linhartová, M., Komenda, J., Jackson, P. J., Dickman, M. J., Canniffe, D. P., Koník, P., Pilný, J., Hunter, C. N., and Sobotka, R. (2014). A cyanobacterial chlorophyll synthase-HliD complex associates with the Ycf39 protein and the YidC/Alb3 insertase. *Plant Cell* **26**, 1267-79.

Ikegami, A., Yoshimura, N., Motohashi, K., Takahashi, S., Romano, P. G., Hisabori, T., Takamiya, K., and Masuda, T. (2007). The CHLI1 subunit of *Arabidopsis thaliana* magnesium chelatase is a target protein of the chloroplast thioredoxin. *J Biol Chem* **282**, 19282-91.

Jacobs, N. J., and Jacobs, J. M. (1981). Protoporphyrinogen oxidation in *Rhodopseudomonas spheroides*, a step in heme and bacteriochlorophyll synthesis. *Arch Biochem Biophys* **211**, 305-311.

Jensen, P. E., Gibson, L. C., and Hunter, C. N. (1999). ATPase activity associated with the magnesium-protoporphyrin IX chelatase enzyme of *Synechocystis* PCC 6803:

evidence for ATP hydrolysis during Mg2+ insertion, and the MgATP-dependent interaction of the ChlI and ChlD subunits. *Biochem J* **339 (Pt 1)**, 127-34.

Jordan, P., Fromme, P., Witt, H. T., Klukas, O., Saenger, W., and Ktrauss, N. (2001). Three-dimensional structure of cyanobacterial photosystem I at 2.5 A resolution. *Nature* **411**, 909-917.

Kahlon, S., Beeri, K., Ohkawa, H., Hihara, Y., Murik, O., Suzuki, I., Ogawa, T., and Kaplan, A. (2006). A putative sensor kinase, Hik31, is involved in the response of *Synechocystis* sp. strain PCC 6803 to the presence of glucose. *Microbiology* **152**, 647-55.

Kato, K., Tanaka, R., Sano, S., Tanaka, A., and Hosaka, H. (2010). Identification of a gene essential for protoporphyrinogen IX oxidase activity in the cyanobacterium *Synechocystis* sp. PCC6803. *Proc Natl Acad Sci USA* **107**, 16649-54.

Kato, Y., and Sakamoto, W. (2018). FtsH protease in the thylakoid membrane: physiological functions and the regulation of protease activity. *Front Plant Sci* **9**, 855.

Kauss, D., Bischof, S., Steiner, S., Apel, K., and Meskauskiene, R. (2012). FLU, a negative feedback regulator of tetrapyrrole biosynthesis, is physically linked to the final steps of the Mg++-branch of this pathway. *FEBS Lett* **586**, 211-216.

Kim, H., Kim, H., and Lee, J. K. (2018). Biochemical characterization of protoporphyrinogen dehydrogenase and protoporphyrin ferrochelatase of *Vibrio vulnificus* and the critical complex formation between these enzymes. *Biochim Biophys Acta Gen Subj* **1862**, 2674-2687.

Kim, S., Jeon, T. J., Oberai, A., Yang, D., Schmidt, J. J., and Bowie, J. U. (2005). Transmembrane glycine zippers: physiological and pathological roles in membrane proteins. *Proc Natl Acad Sci USA* **102**, 14278-83.

Klotz, A., Georg, J., Bučinská, L., Watanabe, S., Reimann, V., Januszewski, W., Sobotka, R., Jendrossek, D., Hess, W. R., and Forchhammer, K. (2016). Awakening of a dormant cyanobacterium from nitrogen chlorosis reveals a genetically determined program. *Curr Biol* **26**, 2862-2872.

Knoppová, J., Sobotka, R., Tichý, M., Yu, J., Koník, P., Halada, P., Nixon, P. J., and Komenda, J. (2014). Discovery of a chlorophyll binding protein complex involved in the early steps of photosystem II assembly in *Synechocystis*. *Plant Cell* **26**, 1200-12.

Kobayashi, K., and Masuda, T. (2016). Transcriptional regulation of tetrapyrrole biosynthesis in *Arabidopsis thaliana*. *Front Plant Sci* **7**.

Kobayashi, K., Masuda, T., Tajima, N., Wada, H., and Sato, N. (2014). Molecular phylogeny and intricate evolutionary history of the three isofunctional enzymes involved in the oxidation of protoporphyrinogen IX. *Genome Biol Evol* **6**, 2141-55.

Komenda, J., Barker, M., Kuvikova, S., de Vries, R., Mullineaux, C. W., Tichy, M., and Nixon, P. J. (2006). The FtsH protease *slr0228* is important for quality control of photosystem II in the thylakoid membrane of *Synechocystis* sp PCC 6803. *J Biol Chem* **281**, 1145-1151.

Komenda, J., Krynická, V., and Zakar, T. (2019). Isolation of thylakoid membranes from the cyanobacterium *Synechocystis* sp. PCC 6803 and analysis of their photosynthetic pigment-protein complexes by Clear Native-PAGE. *Bio Protoc* **9**, e3126.

Komenda, J., and Sobotka, R. (2016). Cyanobacterial high-light-inducible proteins--Protectors of chlorophyll-protein synthesis and assembly. *Biochim Biophys Acta* **1857**, 288-95.

Komenda, J., and Sobotka, R. (2019). Chapter Seven - Chlorophyll-binding subunits of photosystem I and II: Biosynthesis, chlorophyll incorporation and assembly. *In* "Advances in Botanical Research" (B. Grimm, ed.), Vol. 91, pp. 195-223. Academic Press.

Komenda, J., Sobotka, R., and Nixon, P. J. (2012). Assembling and maintaining the Photosystem II complex in chloroplasts and cyanobacteria. *Curr Opin Plant Biol* **15**, 245-251.

Koochak, H., Puthiyaveetil, S., Mullendore, D. L., Li, M., and Kirchhoff, H. (2019). The structural and functional domains of plant thylakoid membranes. *Plant J* **97**, 412-429.

Kopečná, J. (2012). Regulation of the chlorophyll biosynthesis in the cyanobacterium *Synechocystis* sp. PCC 6803. Ph.D. thesis, University of South Bohemia, České Budějovice, Czech Republic.

Kopečná, J., Cabeza de Vaca, I., Adams, N. B., Davison, P. A., Brindley, A. A., Hunter, C. N., Guallar, V., and Sobotka, R. (2015a). Porphyrin binding to Gun4 protein, facilitated by a flexible loop, controls metabolite flow through the chlorophyll biosynthetic pathway. *J Biol Chem* **290**, 28477-88.

Kopečná, J., Komenda, J., Bučinská, L., and Sobotka, R. (2012). Long-term acclimation of the cyanobacterium *Synechocystis* sp PCC 6803 to high light is accompanied by an enhanced production of chlorophyll that is preferentially channeled to trimeric Photosystem I. *Plant Physiol* **160**, 2239-2250.

Kopečná, J., Pilný, J., Krynická, V., Tomčala, A., Kis, M., Gombos, Z., Komenda, J., and Sobotka, R. (2015b). Lack of phosphatidylglycerol inhibits chlorophyll biosynthesis at multiple sites and limits chlorophyllide reutilization in the cyanobacterium *Synechocystis* 6803. *Plant Physiol*.

Kopečná, J., Sobotka, R., and Komenda, J. (2013). Inhibition of chlorophyll biosynthesis at the protochlorophyllide reduction step results in the parallel depletion of Photosystem I and Photosystem II in the cyanobacterium *Synechocystis* PCC 6803. *Planta* **237**, 497-508.

Kopf, M., Klahn, S., Scholz, I., Matthiessen, J. K., Hess, W. R., and Voss, B. (2014). Comparative analysis of the primary transcriptome of *Synechocystis* sp. PCC 6803. *DNA Res* **21**, 527-39.

Krieger-Liszkay, A. (2005). Singlet oxygen production in photosynthesis. *J Exp Bot* **56**, 337-346.

Krieger-Liszkay, A., Fufezan, C., and Trebst, A. (2008). Singlet oxygen production in photosystem II and related protection mechanism. *Photosynth Res* **98**, 551-564.

Krynická, V., Tichý, M., Krafl, J., Yu, J., Kaňa, R., Boehm, M., Nixon, P. J., and Komenda, J. (2014). Two essential FtsH proteases control the level of the Fur repressor during iron deficiency in the cyanobacterium *Synechocystis* sp. PCC 6803. *Mol Microbiol* **94**, 609-24.

Kufryk, G. I., and Vermaas, W. F. J. (2001). A novel protein involved in the functional assembly of the oxygen-evolving complex of photosystem II in *Synechocystis* sp PCC 6803. *Biochemistry* **40**, 9247-9255.

Kühner, M., Haufschildt, K., Neumann, A., Storbeck, S., Streif, J., and Layer, G. (2014). The alternative route to heme in the methanogenic archaeon *Methanosarcina barkeri*. *Archaea*, 13.

Lamb, J. J., Hill, R. E., Eaton-Rye, J. J., and Hohmann-Marriott, M. F. (2014). Functional role of PilA in iron acquisition in the cyanobacterium *Synechocystis* sp. PCC 6803. *PLoS One* **9**, e105761.

Lamb, J. J., and Hohmann-Marriott, M. F. (2017). Manganese acquisition is facilitated by PilA in the cyanobacterium *Synechocystis* sp. PCC 6803. *PLoS One* **12**, e0184685.

Langklotz, S., Baumann, U., and Narberhaus, F. (2012). Structure and function of the bacterial AAA protease FtsH. *Biochim Biophys Acta* **1823**, 40-8.

Larkin, R. M., Alonso, J. M., Ecker, J. R., and Chory, J. (2003). GUN4, a regulator of chlorophyll synthesis and intracellular signaling. *Science* **299**, 902-906.

Latifi, A., Ruiz, M., and Zhang, C. C. (2009). Oxidative stress in cyanobacteria. *FEMS Microbiol Rev* **33**, 258-78.

Layer, G., Verfurth, K., Mahlitz, E., and Jahn, D. (2002). Oxygen-independent coproporphyrinogen-III oxidase HemN from *Escherichia coli*. *J Biol Chem* **277**, 34136-42.

Lee, C.-R., Park, Y.-H., Min, H., Kim, Y.-R., and Seok, Y.-J. (2019). Determination of protein phosphorylation by polyacrylamide gel electrophoresis. *J Microbiol* **57**, 93-100.

Lee, H. J., Duke, M. V., and Duke, S. O. (1993). Cellular localization of protoporphyrinogen-oxidizing activities of etiolated barley (*Hordeum vulgare L.*) leaves (Relationship to mechanism of action of protoporphyrinogen oxidase-inhibiting herbicides). *Plant Physiol* **102**, 881-889.

Lee, J., Lee, H. J., Shin, M. K., and Ryu, W. S. (2004). Versatile PCR-mediated insertion or deletion mutagenesis. *Biotechniques* **36**, 398-400.

Lee, M. H., Mulrooney, S. B., Renner, M. J., Markowicz, Y., and Hausinger, R. P. (1992). *Klebsiella aerogenes* urease gene cluster: sequence of *ureD* and demonstration that four accessory genes (*ureD*, *ureE*, *ureF*, and *ureG*) are involved in nickel metallocenter biosynthesis. *J Bacteriol* **174**, 4324-30.

Lermontova, I., and Grimm, B. (2006). Reduced activity of plastid protoporphyrinogen oxidase causes attenuated photodynamic damage during high-light compared to low-light exposure. *Plant J* **48**, 499-510.

Ludwig, M., and Bryant, D. (2012). Acclimation of the global transcriptome of the cyanobacterium *Synechococcus* sp. strain PCC 7002 to nutrient limitations and different nitrogen sources. *Front Microbiol* **3**.

Luer, C., Schauer, S., Mobius, K., Schulze, J., Schubert, W. D., Heinz, D. W., Jahn, D., and Moser, J. (2005). Complex formation between glutamyl-tRNA reductase and glutamate-1-semialdehyde 2,1-aminomutase in *Escherichia coli* during the initial reactions of porphyrin biosynthesis. *J Biol Chem* **280**, 18568-18572.

Luque, I., and Ochoa de Alda, J. A. (2014). CURT1,CAAD-containing aaRSs, thylakoid curvature and gene translation. *Trends Plant Sci* **19**, 63-6.

Maheswaran, M., Ziegler, K., Lockau, W., Hagemann, M., and Forchhammer, K. (2006). PII-regulated arginine synthesis controls accumulation of cyanophycin in *Synechocystis* sp. strain PCC 6803. *J Bacteriol* **188**, 2730-2734.

Mahmoudi, K., Garvey, K. L., Bouras, A., Cramer, G., Stepp, H., Jesu Raj, J. G., Bozec, D., Busch, T. M., and Hadjipanayis, C. G. (2019). 5-aminolevulinic acid photodynamic therapy for the treatment of high-grade gliomas. *J Neurooncol* **141**, 595-607.

Malavath, T., Caspy, I., Netzer-El, S. Y., Klaiman, D., and Nelson, N. (2018). Structure and function of wild-type and subunit-depleted photosystem I in *Synechocystis*. *Biochim Biophys Acta*.

Mann, N. H., Novac, N., Mullineaux, C. W., Newman, J., Bailey, S., and Robinson, C. (2000). Involvement of an FtsH homologue in the assembly of functional

photosystem I in the cyanobacterium *Synechocystis* sp PCC 6803. *FEBS Lett* **479**, 72-77.

Mareš, J., Strunecký, O., Bučinská, L., and Wiedermannová, J. (2019). Evolutionary patterns of thylakoid architecture in cyanobacteria. *Front Microbiol* **10**, 277.

Masoumi, A., Heinemann, I. U., Rohde, M., Koch, M., Jahn, M., and Jahn, D. (2008). Complex formation between protoporphyrinogen IX oxidase and ferrochelatase during haem biosynthesis in *Thermosynechococcus elongatus*. *Microbiol-Sgm* **154**, 3707-3714.

Medlock, A. E., Shiferaw, M. T., Marcero, J. R., Vashisht, A. A., Wohlschlegel, J. A., Phillips, J. D., and Dailey, H. A. (2015). Identification of the mitochondrial heme metabolism complex. *PLoS One* **10**.

Meskauskiene, R., and Apel, K. (2002). Interaction of FLU, a negative regulator of tetrapyrrole biosynthesis, with the glutamyl-tRNA reductase requires the tetratricopeptide repeat domain of FLU. *FEBS Lett* **532**, 27-30.

Meskauskiene, R., Nater, M., Goslings, D., Kessler, F., den Camp, R. O., and Apel, K. (2001). FLU: A negative regulator of chlorophyll biosynthesis in *Arabidopsis thaliana*. *P Natl Acad Sci USA* **98**, 12826-12831.

Mikkat, S., Fulda, S., and Hagemann, M. (2014). A 2D gel electrophoresis-based snapshot of the phosphoproteome in the cyanobacterium *Synechocystis* sp. strain PCC 6803. *Microbiology* **160**, 296-306.

Minamizaki, K., Mizoguchi, T., Goto, T., Tamiaki, H., and Fujita, Y. (2008). Identification of two homologous genes, chlAI and chlA(II), that are differentially involved in isocyclic ring formation of chlorophyll a in the cyanobacterium *Synechocystis* sp PCC 6803. *J Biol Chem* **283**, 2684-2692.

Möbius, K., Arias-Cartin, R., Breckau, D., Hännig, A. L., Riedmann, K., Biedendieck, R., Schröder, S., Becher, D., Magalon, A., Moser, J., Jahn, M., and Jahn, D. (2010). Heme biosynthesis is coupled to electron transport chains for energy generation. *Proc Natl Acad Sci USA* **107**, 10436-10441.

Morris, J. N., Crawford, T. S., Jeffs, A., Stockwell, P. A., Eaton-Rye, J. J., and Summerfield, T. C. (2014). Whole genome re-sequencing of two 'wild-type' strains of the model cyanobacterium *Synechocystis* sp. PCC 6803. *New Zeal J Bot* **52**, 36-47.

Moser, J., Schubert, W. D., Beier, V., Bringemeier, I., Jahn, D., and Heinz, D. W. (2001). V-shaped structure of glutamyl-tRNA reductase, the first enzyme of tRNA-dependent tetrapyrrole biosynthesis. *EMBO J* **20**, 6583-6590.

Muro-Pastor, M. I., Reyes, J. C., and Florencio, F. J. (2001). Cyanobacteria perceive nitrogen status by sensing intracellular 2-oxoglutarate levels. *J Biol Chem* **276**, 38320-8.

Nishimura, K., Nakayashiki, T., and Inokuchi, H. (1995). Cloning and identification of the *hemG* gene encoding protoporphyrinogen oxidase (PPO) of *Escherichia coli* K-12. *DNA Res* **2**, 1-8.

Nixon, P. J., Michoux, F., Yu, J. F., Boehm, M., and Komenda, J. (2010). Recent advances in understanding the assembly and repair of photosystem II. *Ann Bot* **106**, 1-16.

Nogaj, L. A., and Beale, S. I. (2005). Physical and kinetic interactions between glutamyl-tRNA reductase and glutamate-1-semialdehyde aminotransferase of *Chlamydomonas reinhardtii*. *J Biol Chem* **280**, 24301-24307.

O'Neill, G. P., and Söll, D. (1990). Expression of the *Synechocystis* sp. strain PCC 6803 tRNA(Glu) gene provides tRNA for protein and chlorophyll biosynthesis. *J Bacteriol* **172**, 6363-71.

Olmedo-Verd, E., Santamaria-Gomez, J., de Alda, J., de Pouplana, L. R., and Luque, I. (2011). Membrane anchoring of aminoacyl-tRNA synthetases by convergent acquisition of a novel protein domain. *J Biol Chem* **286**, 41057-41068.

Ouchane, S., Steunou, A. S., Picaud, M., and Astier, C. (2004). Aerobic and anaerobic Mg-protoporphyrin monomethyl ester cyclases in purple bacteria: a strategy adopted to bypass the repressive oxygen control system. *J Biol Chem* **279**, 6385-94.

Ozawa, S., Onishi, T., and Takahashi, Y. (2010). Identification and characterization of an assembly intermediate subcomplex of photosystem I in the green alga *Chlamydomonas reinhardtii*. *J Biol Chem* **285**, 20072-9.

Pandhal, J., Noirel, J., Wright, P. C., and Biggs, C. A. (2009). A systems biology approach to investigate the response of *Synechocystis* sp. PCC6803 to a high salt environment. *Saline Syst* **5**, 8.

Panek, H., and O'Brian, M. R. (2002). A whole genome view of prokaryotic haem biosynthesis. *Microbiology* **148**, 2273-82.

Papenbrock, J., Mock, H. P., Kruse, E., and Grimm, B. (1999). Expression studies in tetrapyrrole biosynthesis: inverse maxima of magnesium chelatase and ferrochelatase activity during cyclic photoperiods. *Planta* **208**, 264-273.

Papenbrock, J., Pfundel, E., Mock, H. P., and Grimm, B. (2000). Decreased and increased expression of the subunit CHL I diminishes Mg chelatase activity and reduces chlorophyll synthesis in transgenic tobacco plants. *Plant J* **22**, 155-164.

Pazderník, M., Mareš, J., Pilný, J., and Sobotka, R. (2019). The antenna-like domain of the cyanobacterial ferrochelatase can bind chlorophyll and carotenoids in an energy-dissipative configuration. *J Biol Chem* **294**, 11131-11143.

Peter, E., and Grimm, B. (2009). GUN4 is required for posttranslational control of plant tetrapyrrole biosynthesis. *Mol Plant* **2**, 1198-210.

Phung, T. H., Jung, H. I., Park, J. H., Kim, J. G., Back, K., and Jung, S. (2011). Porphyrin biosynthesis control under water stress: sustained porphyrin status correlates with drought tolerance in transgenic rice. *Plant Physiol* **157**, 1746-64.

Pilný, J., Kopečná, J., Noda, J., and Sobotka, R. (2015). Detection and quantification of heme and chlorophyll precursors using a High Performance Liquid Chromatography (HPLC) system equipped with two fluorescence detectors. *Bio Protoc* **5**, e1390.

Pisareva, T., Kwon, J., Oh, J., Kim, S., Ge, C. R., Wieslander, A., Choi, J. S., and Norling, B. (2011). Model for membrane organization and protein sorting in the cyanobacterium *Synechocystis* sp PCC 6803 inferred from proteomics and multivariate sequence analyses. *J Proteome Res* **10**, 3617-3631.

Pontoppidan, B., and Kannangara, C. G. (1994). Purification and partial characterisation of barley glutamyl-tRNA(Glu) reductase, the enzyme that directs glutamate to chlorophyll biosynthesis. *Eur J Biochem* **225**, 529-537.

Pribil, M., Labs, M., and Leister, D. (2014). Structure and dynamics of thylakoids in land plants. *J Exp Bot* **65**, 1955-72.

Proctor, M. S., Chidgey, J. W., Shukla, M. K., Jackson, P. J., Sobotka, R., Hunter, C. N., and Hitchcock, A. (2018). Plant and algal chlorophyll synthases function in *Synechocystis* and interact with the YidC/Alb3 membrane insertase. *FEBS Lett* **592**, 3062-3073.

Prosecka, J., Orlov, A. V., Fantin, Y. S., Zinchenko, V. V., Babykin, M. M., and Tichy, M. (2009). A novel ATP-binding cassette transporter is responsible for resistance to viologen herbicides in the cyanobacterium *Synechocystis* sp. PCC 6803. *FEBS J* **276**, 4001-11.

Quintero, M. J., Muro-Pastor, A. M., Herrero, A., and Flores, E. (2000). Arginine catabolism in the cyanobacterium *Synechocystis* sp strain PCC 6803 involves the urea cycle and arginase pathway. *J Bacteriol* **182**, 1008-1015.

Rand, K., Noll, C., Schiebel, H. M., Kemken, D., Dulcks, T., Kalesse, M., Heinz, D. W., and Layer, G. (2010). The oxygen-independent coproporphyrinogen III oxidase HemN utilizes harderoporphyrinogen as a reaction intermediate during conversion of coproporphyrinogen III to protoporphyrinogen IX. *Biol Chem* **391**, 55-63.

Rast, A., Schaffer, M., Albert, S., Wan, W., Pfeffer, S., Beck, F., Plitzko, J. M., Nickelsen, J., and Engel, B. D. (2019). Biogenic regions of cyanobacterial thylakoids form contact sites with the plasma membrane. *Nat Plants* **5**, 436-446.

Ricchelli, F. (1995). Photophysical properties of porphyrins in biological membranes. *J Photochem Photobiol B* **29**, 109-18.

Rieble, S., and Beale, S. I. (1991). Purification of glutamyl-tRNA reductase from *Synechocystis* sp. PCC 6803. *J Biol Chem* **266**, 9740-5.

Riediger, M., Hihara, Y., and Hess, W. (2018). From cyanobacteria and algae to land plants: The RpaB/Ycf27 regulatory network in transition. *Perspectives in Phycology* **5**.

Richter, A. S., Banse, C., and Grimm, B. (2019). The GluTR-binding protein is the heme-binding factor for feedback control of glutamyl-tRNA reductase. *Elife* **8**.

Richter, C. V., Bals, T., and Schunemann, D. (2010). Component interactions, regulation and mechanisms of chloroplast signal recognition particle-dependent protein transport. *Eur J Cell Biol* **89**, 965-73.

Sacharz, J., Bryan, S. J., Yu, J., Burroughs, N. J., Spence, E. M., Nixon, P. J., and Mullineaux, C. W. (2015). Sub-cellular location of FtsH proteases in the cyanobacterium *Synechocystis* sp. PCC 6803 suggests localised PSII repair zones in the thylakoid membranes. *Mol Microbiol* **96**, 448-62.

Sarian, F. D., Rahman, D. Y., Schepers, O., and van der Maarel, M. (2016). Effects of oxygen limitation on the biosynthesis of photo pigments in the red microalgae *Galdieria sulphuraria* strain 074G. *PLoS One* **11**, 10.

Sasarman, A., Letowski, J., Czaika, G., Ramirez, V., Nead, M. A., Jacobs, J. M., and Morais, R. (1993). Nucleotide sequence of the *hemG* gene involved in the protoporphyrinogen oxidase activity of *Escherichia coli* K12. *Can J Microbiol* **39**, 1155-61.

Shen, G. Z., Boussiba, S., and Vermaas, W. F. J. (1993). *Synechocystis* sp PCC-6803 strains lacking Photosystem-I and phycobilisome function. *Plant Cell* **5**, 1853-1863.

Shepherd, M., McLean, S., and Hunter, C. N. (2005). Kinetic basis for linking the first two enzymes of chlorophyll biosynthesis. *FEBS J* **272**, 4532-4539.

Shin, J. H., and Lee, S. Y. (2014). Metabolic engineering of microorganisms for the production of L-arginine and its derivatives. *Microb Cell Fact* **13**, 166.

Shlyk, A. A. (1971). Biosynthesis of chlorophyll *b*. *Annu Rev Plant Physiol* **22**, 169-&.

Shukla, A., and Devine, M. D. (2008). Chapter 9 - Basis of crop selectivity and weed resistance to triazine herbicides. *In* "The Triazine Herbicides" (H. M. LeBaron, J. E. McFarland and O. C. Burnside, eds.), pp. 111-118. Elsevier, San Diego.

Shukla, M. K., Llansola-Portoles, M. J., Tichy, M., Pascal, A. A., Robert, B., and Sobotka, R. (2018). Binding of pigments to the cyanobacterial high-light-inducible protein HliC. *Photosynth Res* **137**, 29-39.

Schmitt, C., Gouya, L., Malonova, E., Lamoril, J., Camadro, J. M., Flamme, M., Rose, C., Lyoumi, S., Da Silva, V., Boileau, C., Grandchamp, B., Beaumont,

C., Deybach, J. C., and Puy, H. (2005). Mutations in human CPO gene predict clinical expression of either hepatic hereditary coproporphyria or erythropoietic harderoporphyria. *Hum Mol Genet* **14**, 3089-3098.

Schöttler, M. A., Albus, C. A., and Bock, R. (2011). Photosystem I: its biogenesis and function in higher plants. *J Plant Physiol* **168**, 1452-61.

Schwabe, T. M. E., Gloddek, K., Schluesener, D., and Kruip, J. (2003). Purification of recombinant BtpA and Ycf3, proteins involved in membrane protein biogenesis in *Synechocystis* PCC 6803. *J Chromatogr B Analyt Technol Biom Life Sci* **786**, 45-59.

Schwarz, R., and Forchhammer, K. (2005). Acclimation of unicellular cyanobacteria to macronutrient deficiency: emergence of a complex network of cellular responses. *Microbiology* **151**, 2503-14.

Simon, R. D., and Weathers, P. (1976). Determination of the structure of the novel polypeptide containing aspartic acid and arginine which is found in Cyanobacteria. *Biochim Biophys Acta* **420**, 165-76.

Skotnicová, P., Sobotka, R., Shepherd, M., Hájek, J., Hrouzek, P., and Tichý, M. (2018). The cyanobacterial protoporphyrinogen oxidase HemJ is a new *b*-type heme protein functionally coupled with coproporphyrinogen III oxidase. *J Biol Chem* **293**, 12394-12404.

Sobotka, R. (2014). Making proteins green; biosynthesis of chlorophyll-binding proteins in cyanobacteria. *Photosynth Res* **119**, 223-32.

Sobotka, R., Duerhring, U., Komenda, J., Peter, E., Gardian, Z., Tichý, M., Grimm, B., and Wilde, A. (2008a). Importance of the cyanobacterial GUN4 protein for chlorophyll metabolism and assembly of photosynthetic complexes. *J Biol Chem* **283**, 25794-25802.

Sobotka, R., Komenda, J., Bumba, L., and Tichý, M. (2005). Photosystem II assembly in CP47 mutant of *Synechocystis* sp PCC 6803 is dependent on the level of chlorophyll precursors regulated by ferrochelatase. *J Biol Chem* **280**, 31595-31602.

Sobotka, R., McLean, S., Žuberová, M., Hunter, C. N., and Tichý, M. (2008b). The C-terminal extension of ferrochelatase is critical for enzyme activity and for functioning of the tetrapyrrole pathway in *Synechocystis* strain PCC 6803. *J Bacteriol* **190**, 2086-2095.

Sobotka, R., Tichý, M., Wilde, A., and Hunter, C. N. (2011). Functional assignments for the carboxyl-terminal domains of the ferrochelatase from *Synechocystis* PCC 6803: The CAB domain plays a regulatory role, and region II is essential for catalysis. *Plant Physiol* **155**, 1735-1747.

Solomon, C. M., Collier, J. L., Berg, G. M., and Glibert, P. M. (2010). Role of urea in microbial metabolism in aquatic systems: a biochemical and molecular review. *Aquat Microb Ecol* **59**, 67-88.

Spät, P., Klotz, A., Rexroth, S., Macek, B., and Forchhammer, K. (2018). Chlorosis as a developmental program in cyanobacteria: The proteomic fundament for survival and awakening. *Mol Cell Proteomics* **17**, 1650-1669.

Staleva, H., Komenda, J., Shukla, M. K., Slouf, V., Kaňa, R., Polívka, T., and Sobotka, R. (2015). Mechanism of photoprotection in the cyanobacterial ancestor of plant antenna proteins. *Nat Chem Biol* **11**, 287-91.

Stengel, A., Gugel, I. L., Hilger, D., Rengstl, B., Jung, H., and Nickelsen, J. (2012). Initial steps of photosystem II de novo assembly and preloading with manganese take place in biogenesis centers in Synechocystis. *Plant Cell* **24**, 660-75.

Storm, P., Tibiletti, T., Hall, M., and Funk, C. (2013). Refolding and enzyme kinetic studies on the ferrochelatase of the cyanobacterium *Synechocystis* sp. PCC 6803. *PLoS One* **8**.

Summerfield, T. C., Nagarajan, S., and Sherman, L. A. (2011). Gene expression under low-oxygen conditions in the cyanobacterium *Synechocystis* sp. PCC 6803 demonstrates Hik31-dependent and -independent responses. *Microbiology* **157**, 301-12.

Sun, Z., and Blanchard, J. L. (2014). Strong genome-wide selection early in the evolution of *Prochlorococcus* resulted in a reduced genome through the loss of a large number of small effect genes. *PLoS One* **9**, e88837.

Tanaka, R., and Tanaka, A. (2007). Tetrapyrrole biosynthesis in higher plants. *In* "Annu Rev Plant Biol", Vol. 58, pp. 321-346.

Tatsuta, T., Model, K., and Langer, T. (2005). Formation of membrane-bound ring complexes by prohibitins in mitochondria. *Mol Biol Cell* **16**, 248-59.

Terry, M. J., and Kendrick, R. E. (1999). Feedback inhibition of chlorophyll synthesis in the phytochrome chromophore-deficient aurea and yellow-green-2 mutants of tomato. *Plant Physiol* **119**, 143-152.

Tichý, M., Bečková, M., Kopečná, J., Noda, J., Sobotka, R., and Komenda, J. (2016). Strain of *Synechocystis* PCC 6803 with aberrant assembly of Photosystem II contains tandem duplication of a large chromosomal region. *Front Plant Sci* **7**, 648.

Tichý, M., and Vermaas, W. (2000). Combinatorial mutagenesis and pseudorevertant analysis to characterize regions in loop E of the CP47 protein in *Synechocystis* sp PCC 6803. *Eur J Biochem* **267**, 6296-6301.

Tolonen, A. C., Aach, J., Lindell, D., Johnson, Z. I., Rector, T., Steen, R., Church, G. M., and Chisholm, S. W. (2006). Global gene expression of *Prochlorococcus* ecotypes in response to changes in nitrogen availability. *Mol Syst Biol* **2**, 53.

Umena, Y., Kawakami, K., Shen, J. R., and Kamiya, N. (2011). Crystal structure of oxygen-evolving photosystem II at a resolution of 1.9 A. *Nature* **473**, 55-60.

Valladares, A., Montesinos, M. L., Herrero, A., and Flores, E. (2002). An ABC-type, high-affinity urea permease identified in cyanobacteria. *Mol Microbiol* **43**, 703-15.

Van Aken, O., Whelan, J., and Van Breusegem, F. (2010). Prohibitins: mitochondrial partners in development and stress response. *Trends Plant Sci* **15**, 275-82.

van de Meene, A. M. L., Hohmann-Marriott, M. F., Vermaas, W. F. J., and Roberson, R. W. (2006). The three-dimensional structure of the cyanobacterium *Synechocystis* sp PCC 6803. *Arch Microbiol* **184**, 259-270.

Vavilin, D., and Vermaas, W. (2007). Continuous chlorophyll degradation accompanied by chlorophyllide and phytol reutilization for chlorophyll synthesis in *Synechocystis* sp PCC 6803. *BBA-Bioenergetics* **1767**, 920-929.

Verdecia, M. A., Larkin, R. M., Ferrer, J. L., Riek, R., Chory, J., and Noel, J. P. (2005). Structure of the Mg-chelatase cofactor GUN4 reveals a novel hand-shaped fold for porphyrin binding. *PLoS Biol* **3**, e151.

Vidal, R., Lopez-Maury, L., Guerrero, M. G., and Florencio, F. J. (2009). Characterization of an alcohol dehydrogenase from the cyanobacterium *Synechocystis* sp. strain PCC 6803 that responds to environmental stress conditions via the Hik34-Rre1 two-component system. *J Bacteriol* **191**, 4383-91.

Vothknecht, U. C., Kannangara, C. G., and von Wettstein, D. (1998). Barley glutamyl tRNA(Glu) reductase: Mutations affecting haem inhibition and enzyme activity. *Phytochemistry* **47**, 513-519.

Wang, L. Y., Elliott, M., and Elliott, T. (1999). Conditional stability of the HemA protein (glutamyl-tRNA reductase) regulates heme biosynthesis in *Salmonella typhimurium*. *J Bacteriol* **181**, 1211-1219.

Wang, P., and Grimm, B. (2015). Organization of chlorophyll biosynthesis and insertion of chlorophyll into the chlorophyll-binding proteins in chloroplasts. *Photosynth Res* **126**, 189-202.

Wang, P., Liang, F. C., Wittmann, D., Siegel, A., Shan, S. O., and Grimm, B. (2018). Chloroplast SRP43 acts as a chaperone for glutamyl-tRNA reductase, the rate-limiting enzyme in tetrapyrrole biosynthesis. *Proc Natl Acad Sci U S A* **115**, E3588-E3596.

Wang, Q., Jantaro, S., Lu, B., Majeed, W., Bailey, M., and He, Q. (2008). The high light-inducible polypeptides stabilize trimeric photosystem I complex under high light conditions in *Synechocystis* PCC 6803. *Plant Physiol* **147**, 1239-50.

Warren, M. J., and Smith, A. G., eds. (2009). "Tetrapyrroles: Birth, life and death," pp. 1-406. Springer-Verlag New York.

Watzer, B., and Forchhammer, K. (2018). Cyanophycin: A Nitrogen-Rich Reserve Polymer.

Wierenga, R. K. (2001). The TIM-barrel fold: a versatile framework for efficient enzymes. *FEBS Lett* **492**, 193-8.

Wilson, A., Ajlani, G., Verbavatz, J. M., Vass, I., Kerfeld, C. A., and Kirilovsky, D. (2006). A soluble carotenoid protein involved in phycobilisome-related energy dissipation in cyanobacteria. *Plant Cell* **18**, 992-1007.

Yao, D., Kieselbach, T., Komenda, J., Promnares, K., Prieto, M. A. H., Tichý, M., Vermaas, W. F. J., and Funk, C. (2007). Localization of the small CAB-like proteins in photosystem II. *J Biol Chem* **282**, 267-276.

Yoshihara, S., Geng, X., Okamoto, S., Yura, K., Murata, T., Go, M., Ohmori, M., and Ikeuchi, M. (2001). Mutational analysis of genes involved in pilus structure, motility and transformation competency in the unicellular motile cyanobacterium *Synechocystis* sp. PCC6803. *Plant Cell Physiol* **42**, 63-73.

Yoshioka, M., and Yamamoto, Y. (2011). Quality control of Photosystem II: where and how does the degradation of the D1 protein by FtsH proteases start under light stress?--Facts and hypotheses. *J Photochem Photobiol B* **104**, 229-35.

Zak, E., Norling, B., Andersson, B., and Pakrasi, H. B. (1999). Subcellular localization of the BtpA protein in the cyanobacterium *Synechocystis* sp. PCC 6803. *Eur J Biochem* **261**, 311-316.

Zak, E., and Pakrasi, H. B. (2000). The BtpA protein stabilizes the reaction center proteins of photosystem I in the cyanobacterium *Synechocystis* sp PCC 6803 at low temperature. *Plant Physiol* **123**, 215-222.

Zhang, C. C., Zhou, C. Z., Burnap, R. L., and Peng, L. (2018). Carbon/nitrogen metabolic balance: Lessons from cyanobacteria. *Trends Plant Sci* **23**, 1116-1130.

Zhang, H., and Yang, C. (2019). Arginine and nitrogen mobilization in cyanobacteria. *Mol Microbiol* **111**, 863-867.

Zhang, M., Zhang, F., Fang, Y., Chen, X., Chen, Y., Zhang, W., Dai, H. E., Lin, R., and Liu, L. (2015). The non-canonical tetratricopeptide repeat (TPR) domain of fluorescent (FLU) mediates complex formation with glutamyl-tRNA reductase. *J Biol Chem* **290**, 17559-65.

Zhao, A., Fang, Y., Chen, X., Zhao, S., Dong, W., Lin, Y., Gong, W., and Liu, L. (2014). Crystal structure of *Arabidopsis* glutamyl-tRNA reductase in complex with its stimulator protein. *Proc Natl Acad Sci U S A* **111**, 6630-5.

Zwerschke, D., Karrie, S., Jahn, D., and Jahn, M. (2014). *Leishmania major* possesses a unique HemG-type protoporphyrinogen IX oxidase. *Bioscience Rep* **34**, 391-400.

8. Published results

Skotnicová, P., Sobotka, R., Shepherd, M., Hájek, J., Hrouzek, P., and Tichý, M. (2018). The cyanobacterial protoporphyrinogen oxidase HemJ is a new *b*-type heme protein functionally coupled with coproporphyrinogen III oxidase. *Journal of Biological Chemistry* **293**, 12394-12404.

JBC ARTICLE

The cyanobacterial protoporphyrinogen oxidase HemJ is a new *b*-type heme protein functionally coupled with coproporphyrinogen III oxidase

Received for publication, April 12, 2018, and in revised form, June 14, 2018 Published, Papers in Press, June 20, 2018, DOI 10.1074/jbc.RA118.003441

Petra Skotnicová[‡§], Roman Sobotka[‡§], Mark Shepherd[¶], Jan Hájek[‡§], Pavel Hrouzek[‡§], and Martin Tichý[‡§1]

From the [‡]Czech Academy of Sciences, Institute of Microbiology, Centre Algatech, 379 81 Třeboň, Czech Republic, the [§]Faculty of Science, University of South Bohemia, 370 05 České Budějovice, Czech Republic, and the [¶]School of Biosciences, RAPID Group, University of Kent, Canterbury CT2 7NZ,United Kingdom

Edited by Chris Whitfield

Protoporphyrinogen IX oxidase (PPO), the last enzyme that is common to both chlorophyll and heme biosynthesis pathways, catalyzes the oxidation of protoporphyrinogen IX to protoporphyrin IX. PPO has several isoforms, including the oxygen-dependent HemY and an oxygen-independent enzyme, HemG. However, most cyanobacteria encode HemJ, the least characterized PPO form. We have characterized HemJ from the cyanobacterium *Synechocystis* sp. PCC 6803 (*Synechocystis* 6803) as a *bona fide* PPO; HemJ down-regulation resulted in accumulation of tetrapyrrole precursors and in the depletion of chlorophyll precursors. The expression of FLAG-tagged *Synechocystis* 6803 HemJ protein (HemJ.f) and affinity isolation of HemJ.f under native conditions revealed that it binds heme *b*. The most stable HemJ.f form was a dimer, and higher oligomeric forms were also observed. Using both oxygen and artificial electron acceptors, we detected no enzymatic activity with the purified HemJ.f, consistent with the hypothesis that the enzymatic mechanism for HemJ is distinct from those of other PPO isoforms. The heme absorption spectra and distant HemJ homology to several membrane oxidases indicated that the heme in HemJ is redox-active and involved in electron transfer. HemJ was conditionally complemented by another PPO, HemG from *Escherichia coli.* If grown photoautotrophically, the complemented strain accumulated tripropionic tetrapyrrole harderoporphyrin, suggesting a defect in enzymatic conversion of coproporphyrinogen III to protoporphyrinogen IX, catalyzed by coproporphyrinogen III oxidase (CPO). This observation supports the hypothesis that HemJ is functionally coupled with CPO and that this coupling is disrupted after replacement of HemJ by HemG.

The last common step for heme and chlorophyll biosynthesis (1), conversion of protoporphyrinogen IX (Protogen)[2] into protoporphyrin IX (Proto), is catalyzed by the enzyme protoporphyrinogen IX oxidase (Fig. 1). Although the six-electron oxidation of Protogen occurs also spontaneously, its enzymatic conversion is apparently necessary for the correct channeling of Proto to chelatases for metal insertion (Fig. 1). Three analogous enzymes HemY, HemG, and lastly HemJ (recently reannotated as PgoX, PgdH1, and PgdH2 (2)), exhibiting no mutual homology, have been found to serve as a protoporphyrinogen oxidase (3–5). HemY is an oxygen-dependent enzyme of ~55 kDa, creating membrane bound dimers and using FAD as a co-factor (6). HemY occurs in most of bacteria phyla and in almost all eukaryotes (7).

HemG (21 kDa) is mostly found in γ-proteobacteria (7). The protein forms membrane-associated oligomers (8, 9) and uses noncovalently bound flavin mononucleotide as a co-factor (9). HemG is functional in oxic as well as anoxic conditions (9). Electrons from the Proto oxidation catalyzed by HemG are withdrawn via ubiquinone, cytochrome *bo*, and cytochrome *bd* oxidases to oxygen or under anoxic conditions to the terminal electron acceptors fumarate and nitrate by corresponding reductases (8).

Most recently, the *slr1790* gene from the cyanobacterium *Synechocystis* 6803 has been described as the third PPO and named *hemJ* (3). Although HemJ is the most common PPO variant in cyanobacteria, in cyanobacterial GenBank genomes, we found 435 *hemJ* genes and only 47 *hemY* genes, and its origin and spread within cyanobacteria is not clear. It is assumed that HemJ evolved within α-proteobacteria and spread to cyanobacteria and various proteobacteria through multiple horizontal gene transfers (7). In contrast, the phylogenetic tree of HemY for cyanobacteria is consistent with the cyanobacterial phylogeny, and HemY was probably the ancestral PPO in cyanobacteria (7). For completeness, eight genomes of the *Synechococcus–Prochlorococcus* lineage contain the HemG PPO variant probably obtained by horizontal gene transfer.

As with other PPOs, *hemJ* appears to be essential and could not be inactivated in *Synechocystis* 6803 (3). A partially segregated *Synechocystis* 6803 strain contained less than half of the chlorophyll content compared with WT, and although it accumulated Proto, it probably originated from nonenzymatic oxi-

This work was supported by Project P501/12/G055 of the Czech Science Foundation and by Czech Ministry of Education Projects LO1416 and LM2015055. The authors declare that they have no conflicts of interest with the contents of this article.

This article contains text, references, Tables S1 and S2, and Figs. S1–S8.

[1] To whom correspondence should be addressed: Institute of Microbiology, CAS, Centre Algatech, Novohradská 237, Opatovický mlýn, 37981 Třeboň, Czech Republic. Tel.: 420384340433; E-mail: tichym@alga.cz.

[2] The abbreviations used are: Protogen, protoporphyrinogen IX; Proto, protoporphyrin IX; PPO, protoporphyrinogen IX oxidase; CPO, coproporphyrinogen III oxidase; Coprogen, coproporphyrinogen III; CN, clear native; PSI, Photosystem I; PSII, Photosystem II; Copro, coproporphyrin III; DDM, *n*-dodecyl-β-D-maltoside; CBB, Coomassie Brilliant Blue; FeCH, ferrochelatase.

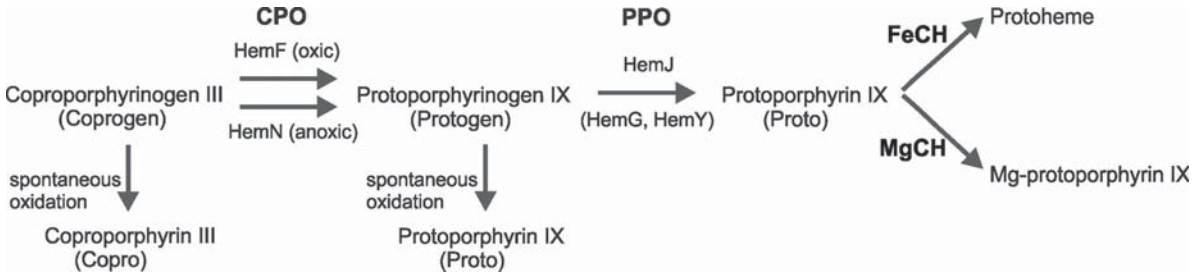

Figure 1. Late steps of tetrapyrrole biosynthesis in cyanobacteria (*Synechocystis* 6803). Conversion of Coprogen to Protogen is catalyzed by CPO. In *Synechocystis* 6803, HemF works as the sole CPO under oxic conditions, and HemN works under anoxic conditions. The CPO product Protogen is oxidized to Proto by PPO. In most cyanobacteria, this reaction is performed by HemJ PPO isoform, in others by HemG or HemY. Proto is than channeled to ferrochelatase (*FeCH*) leading to Protoheme or to magnesium-chelatase (*MgCH*), first enzyme of the dedicated chlorophyll pathway. Coprogen and Protogen can be spontaneously oxidized to Copro and Proto, respectively.

dation of Protogen (Fig. 1). Accordingly, the *hemJ* deletion strain from *Acinetobacter baylyi* exhibited auxotrophy for hemin and accumulated porphyrins when supplemented with 5-aminolevulinic acid (10).

To demonstrate that HemJ is a *bona fide* PPO, HemJ mutants were complemented with other PPO isoforms: several *hemY* variants and *hemG* rescued hemin auxotrophy in *A. baylyi* (10), and expression of *Arabidopsis thaliana hemY* in *Synechocystis* 6803 enabled *hemJ* inactivation. This mutant strain accumulated Proto when treated with HemY inhibitor acifluorfen (3). This accumulation of intermediates is consistent with substrate channeling between the terminal enzymes of heme synthesis. Formation of the multienzyme heme biosynthetic complex, containing the three terminal enzymes CPO, PPO, and ferrochelatase (FeCH) is predicted (11) and partly documented (12, 13). For prokaryotes, identification of such complexes is further complicated by the existence of multiple enzyme isoforms and different heme biosynthetic pathways (2). In addition to PPOs there are two forms of CPOs in *Synechocystis* 6803 as in most organisms performing oxygenic photosynthesis: HemN and HemF (14). Under micro-oxic conditions, the conversion of coproporphyrinogen III (Coprogen) to Protogen is catalyzed by an oxygen-independent CPO encoded by *hemN*, whereas oxidative decarboxylation of the substrate requires oxygen and is catalyzed by HemF, an enzyme structurally and functionally unrelated to HemN (14, 15) (Fig. 1). HemN is a monomeric, iron–sulfur cluster–containing protein (16), HemF is a dimeric protein with two independent active sites (17). Herein, we report the biochemical characterization of HemJ homologously expressed in *Synechocystis* 6803 and the results of complementation of *hemJ* mutant by expression of *hemG* from *Escherichia coli*. We also show that there is a functional coupling between *Synechocystis* 6803 CPO and HemJ.

Results

Synechocystis 6803 HemJ forms a heme-binding oligomer

Because heterologous expression of HemJ proteins from various organisms frequently resulted in no or poor expression (3, 10), we expressed the HemJ enzyme fused on its C terminus with 3× FLAG tag (HemJ.f) homologously in *Synechocystis* 6803 under *psbAII* promoter. After full segregation of the *hemJ.f* strain, it was possible to delete the WT copy of the *hemJ* gene, demonstrating that the HemJ.f protein is functional (Fig. S1). However, for the HemJ isolation, a strain containing both WT and tagged variants of HemJ was used to potentially co-isolate HemJ.f, together with the native form of the protein (see below): oligomeric states have previously been described for other PPO variants (8). After affinity chromatography of *hemJ.f* membrane fraction solubilized by nonionic detergent, the purified HemJ.f eluate was markedly reddish. Native separation of the eluate on clear native gel (CN–PAGE) resulted in two reddish bands: CN1 and only slightly visible CN2 (Fig. 2). Photosystem I (PSI) was shown to bind nonspecifically to the anti-FLAG affinity resin (18). Hence, HemJ.f was also isolated from a strain lacking PSI (ΔPSI) to achieve maximum purity (Fig. 2). Absorption spectra of the eluted HemJ.f protein showed an absorption maximum at 412 nm (Fig. 3*A*), which was presumed to be the Soret band of a bound tetrapyrrole. After deletion of PSI only a small amounts of chlorophyll (absorbing at 671 nm) and variable amount of carotenoids (absorbance 450–520 nm) co-eluted with HemJ.f (Fig. 3*A*). The bound tetrapyrrole was extracted by acetone and was identified as protoheme by HPLC (Fig. S2) (protoheme is referred as heme *b*, when it is bound to a protein). To spectroscopically characterize this bound heme further, absorption spectra of the HemJ.f eluate from the ΔPSI strain were measured after oxidation by air or after reduction by dithionite (Fig. 3*B*). The oxidized spectrum indicates a high spin heme *b* (λ_{max} = 411 nm), and the reduced spectrum (λ_{max} = 424 nm) is typical for a ferrous six-coordinate *b*-type heme. To assess the stoichiometry of heme binding to HemJ.f, protein isolated by affinity chromatography was further purified by size-exclusion chromatography (Fig. 4*A*). Fractions with the highest absorption at 415 nm were collected and used for heme and protein quantification. The protein concentration was estimated from the absorbance at 280 nm using calculated extinction coefficient for HemJ.f. The estimated molar ratio of heme to HemJ.f monomer was 0.85 ± 0.05. Eluted fractions did not display any sign of chlorophyll or carotenoids (Fig. 4*B*). Size-exclusion chromatography was also used to estimate the size of the native HemJ complex (Fig. 4*A*). The main elution peak corresponds to a protein of ~150 kDa, indicating a higher oligomeric state of HemJ.f (27 kDa monomer) even when taking into account its association with detergent. Analysis of the HemJ.f eluate by SDS–PAGE revealed that several proteins specifically co-eluted from the anti-FLAG resin with HemJ.f (Fig. 5*A*). These protein bands were identified by

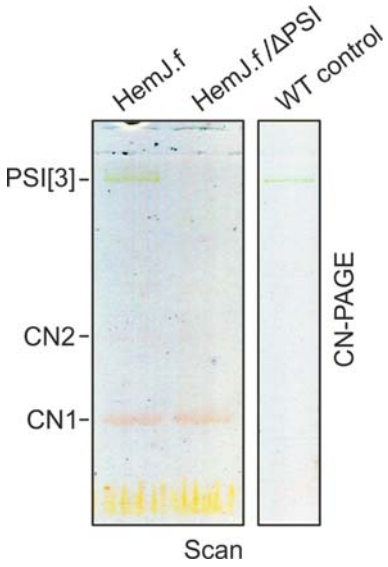

Figure 2. Separation of the purified HemJ.f by clear native gel electrophoresis. Native isolations of HemJ.f from WT and ΔPSI backgrounds that resulted in a reddish eluate were further separated by 4–14% clear native gel electrophoresis (CN–PAGE). Reddish bands CN1 and CN2 (poorly visible) were identified as HemJ.f. As already reported (18), a small amount of trimeric PSI (PSI[3]) is a typical contamination of FLAG eluates obtained from *Synechocystis* 6803. The gel was scanned in transmittance mode (Scan) using an LAS 4000 Imager (Fuji).

MS as Sll1106, FtsH proteases, and ATP synthase subunits (Table S1). Sll1106, together with HemJ, was also identified by MS in the CN1 band from CN–PAGE (Fig. 2). Nevertheless, the reddish CN1 band was present even when HemJ.f was purified from a Δ*sll1106* background (Fig. S3), indicating that heme is associated with HemJ.f. Furthermore, when a gel strip from CN–PAGE (Fig. 2) was separated in a second dimension by SDS–PAGE (Fig. 5*B*), colored CN1 and CN2 bands dissociated into two spots, apparently representing monomer and dimer of the HemJ.f (27 kDa). The presence of the HemJ.f dimer, even on the denaturing SDS gel, suggests its remarkable stability. The upper CN2 band contains the HemJ.f oligomer, most probably a tetramer, which is in agreement with the size of the complex determined by the size-exclusion chromatography (Fig. 4*A*).

In vitro PPO activity of the purified HemJ.f

Because previous studies provided conflicting results regarding the ability of the isolated HemJ to perform Protogen oxidation/dehydrogenation, we attempted to measure PPO activity of the eluted HemJ.f. However, no measurable PPO activity in the eluate was detected with or without artificial electron acceptors menadione or benzoquinone. Marginal activity comparable with the spontaneous oxidation of Protogen was detected in *Synechocystis* 6803 crude extracts and in the membrane fraction, although this activity was probably an artifact, because it was present also in these fractions after heat treatment (90 °C, 3 min). Recombinant human HemY (19) was used as a positive control for the PPO activity measurement.

The HemJ is not fully replaceable by HemG

Because we were not able to detect HemJ activity, we decided to confirm the function of HemJ via complementation with the

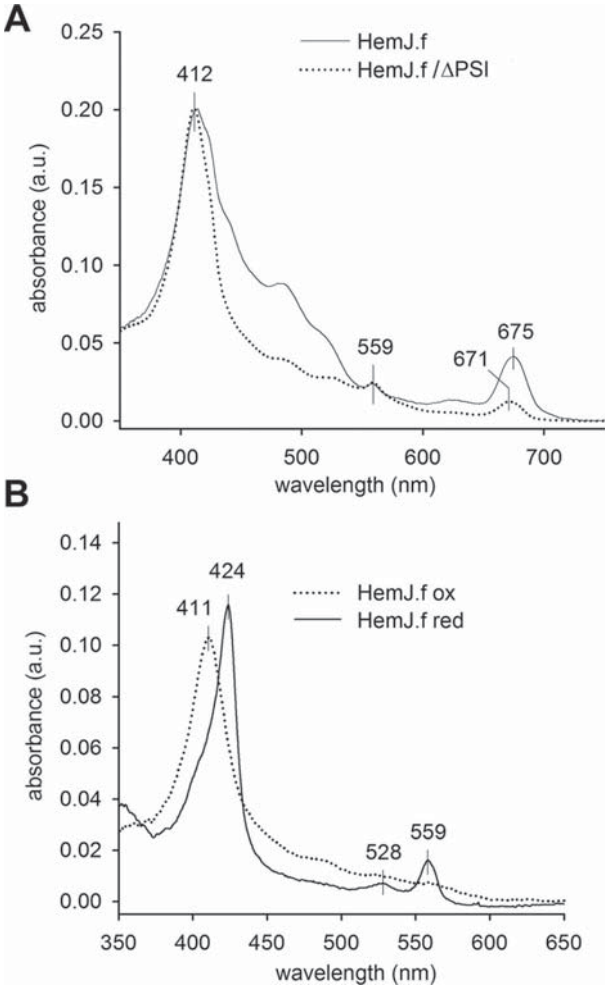

Figure 3. Spectroscopy analysis of the purified HemJ.f. *A*, absorption spectra of HemJ.f eluate. The peak at 675 nm derives from chlorophyll, whereas the peaks at 412 and 559 nm are characteristic for heme. The eluate with lower carotenoid content (absorption at 450–520 nm) was used for spectroscopy analysis. *B*, absorption spectra of oxidized and reduced eluate obtained from the ΔPSI genetic background. *a.u.*, absorbance units.

PPO analog HemG. Two strains were engineered: one with the *Synechocystis* 6803 *hemJ* gene placed under a copper-regulated promoter (*petJ*) and the second expressing *hemG* from *E. coli* under the *psbAII* promoter. In both strains it was possible to delete the WT *hemJ* gene, indicating that both constructs were functional. In the P(*petJ*)::*hemJ* strain, it was possible to decrease the amount of *hemJ* by adding copper to the growth medium. This led to lower amounts of enzymatically produced Proto, followed by decreases in the levels of phycobilins and chlorophyll and lower levels of major chlorophyll-binding photosynthetic complexes, especially trimeric PSI (Fig. S4, *A* and *B*). To identify how the repression of *hemJ* expression affects tetrapyrrole biosynthesis, the accumulation of chlorophyll/heme intermediates was analyzed in the P(*petJ*)::*hemJ* strain suppressed by copper (Fig. 6). The suppressed strain exhibited significantly decreased levels of the chlorophyll precursors magnesium–protoporphyrin IX and monovinyl protochloro-

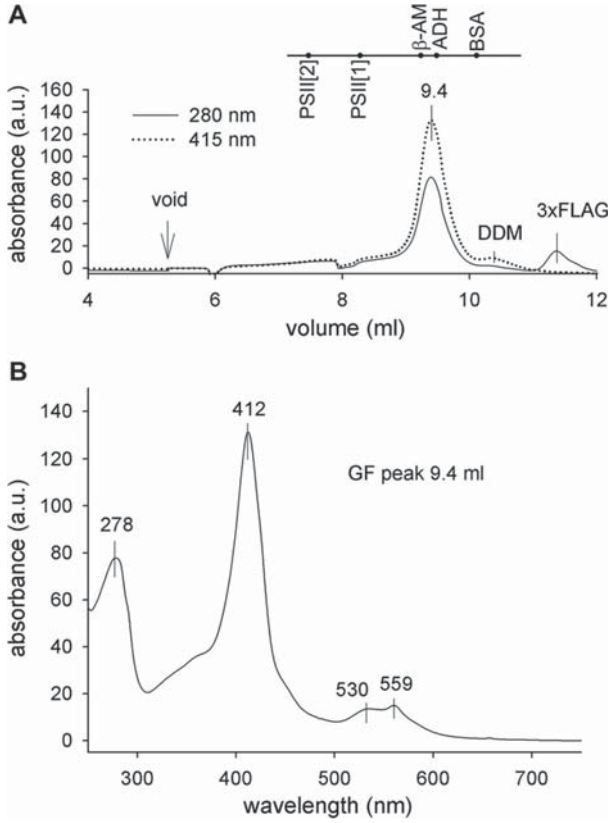

Figure 4. Separation of the purified HemJ.f protein by size-exclusion chromatography. *A*, the HemJ.f pulldown obtained from the ΔPSI genetic background was loaded on a size-exclusion chromatography column, and eluted proteins/complexes were detected by absorbance 280 and 415 nm. Positions of standards are shown at the *top* of the graph: *PSII[2]*, PSII dimer (600 kDa); *PSII[1]*, PSII monomer (300 kDa); *β-AM*, *β*-amylase (200 kDa); *ADH*, alcohol dehydrogenase (150 kDa); *BSA*, BSA (66 kDa); *DDM*, micelle of dodecyl-*β*-maltoside; *3xFLAG*, 3× FLAG peptide used to elute HemJ.f from the anti-FLAG-M2 agarose resin. *B*, absorption spectrum of 9.4 ml size-exclusion chromatography fraction was recorded by a HPLC diode-array detector.

phyllide along with an accumulation of coproporphyrin III (Copro) and Proto; the latter tetrapyrrole was also visibly excreted into the medium. Detection of both Copro and Proto was likely to result from the accumulation and nonenzymatic oxidation of their reduced precursors in the cell (3, 20).

The HemG complementation strain Δ*hemJ/hemG* grew on glucose slightly slower than WT (Fig. S5) and accumulated lower amounts of chlorophyll and phycobilins (Fig. S4*C*). However, the strain did not grow autotrophically (Fig. S5). When the Δ*hemJ/hemG* cells were transferred to glucose-free medium, the cellular level of chlorophyll-binding photosynthetic complexes gradually decreased (Fig. S4*D*). Also chlorophyll precursors were almost undetectable in the cells, except for monovinyl chlorophyllide (Fig. 7), most probably originating from chlorophyll *a* recycling from pigment–protein complexes by its dephytylation (21). In addition, a large quantity of an unidentified tetrapyrrole with absorption spectrum resembling Copro eluted at 13.4 min on the HPLC profile of the extract from the Δ*hemJ/hemG* strain incubated without glucose (Fig. 7). This compound was completely missing in the WT strain (Fig. 7*A*), as well as in the Δ*hemJ/hemG* mutant grown on glucose (Fig. S6).

Harderoporphyrin accumulation in the ΔhemJ/hemG strain

The unknown tetrapyrrole observed in Δ*hemJ/hemG* mutant was isolated and analyzed using HPLC coupled to high resolution tandem MS (HPLC–HRMS/MS). The compound exhibited a *m/z* value of 609.2708 corresponding to the elemental composition $C_{35}H_{37}N_4O_6$. Based on the similarity of this elemental composition to Copro ($C_{36}H_{39}N_4O_8$), the fragmentation spectra of these two molecules were compared (Fig. 8*A* and Table S2). Fragmentation of the Copro molecular ion led to successive benzylic cleavages with the loss of a $^{\bullet}CH_2COOH$ radical (Δ 59 Da) from all four propionic acid residues (*m/z* 655 → 596 → 537 → 478 → 419) as described previously (22). The queried compound exhibited only three consecutive losses of $^{\bullet}CH_2COOH$ radicals, suggesting the presence of only three propionic groups. From the difference in the molecular weight of both compounds, it can be assumed that the fourth propionic acid group of the tetrapyrrole ring is substituted by a vinyl group. Such substitution is consistent with that described for harderoporphyrin (23), although the exact position of the vinyl group on the tetrapyrrole ring cannot be determined via MS/MS experiments. Hence, the compound accumulating in the Δ*hemJ/hemG* strain with a molecular weight of 609 is likely to be harderoporphyrin, a spontaneously oxidized intermediate of the CPO reaction, which is normally generating Protogen.

Discussion

We have isolated tagged HemJ protein from solubilized *Synechocystis* 6803 membranes and found that it forms an oligomeric, most likely tetrameric complex (Figs. 4*A* and 5*B*). Because of the hydrophobic nature of this enzyme, it is unclear whether the tetramer is the native form or results from nonphysiological aggregation. However, the HemJ dimer is very stable even after SDS electrophoresis (Fig. 5*B*). Distantly related HemJ homologs with known three-dimensional structure (see below) have previously been shown to form dimers (24, 25).

The natively isolated HemJ complex was reddish in color (Fig. 2) because of the presence of heme *b* (Fig. 3). Interestingly, Gomelsky and Kaplan (26) previously overexpressed a *Rhodobacter sphaeroides hemJ* gene (*orf1*) located upstream of their gene of interest and noted that the *E. coli* strain overproducing this protein turned pink. Our rough estimate of heme stoichiometry indicated a ratio of 0.85 heme *b* per subunit. It seems plausible that HemJ binds a single heme *b* with partial heme loss occurring during isolation. Even though HemJ.f eluate contained also chlorophyll and variable amounts of carotenoids (Fig. 3*A*), neither was detected in HemJ.f fraction from size-exclusion chromatography (Fig. 4*B*); thus we expect these pigments to be bound unspecifically.

To predict the localization of the observed heme *b* within HemJ, we have modeled the three-dimensional structure of HemJ protein (Fig. 9). The modeling was performed on the HemJ peptide from *R. sphaeroides* (WP_023003745), which contains only four helices, as is found for most of the proteins of the HemJ family. The *Synechocystis* 6803 fifth helix, which is present only in cyanobacteria, did not provide enough coverage

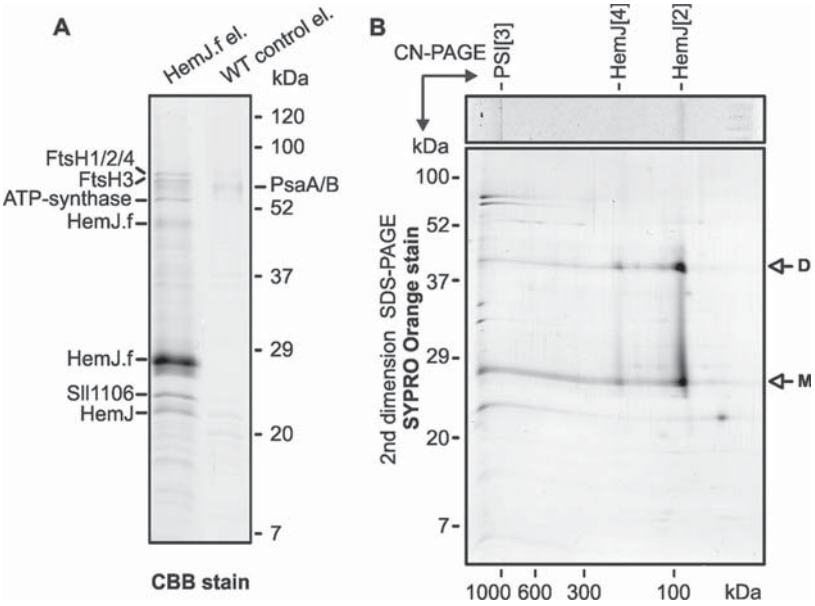

Figure 5. One-dimensional SDS–PAGE and two-dimensional CN/SDS–PAGE separation of HemJ.f eluate. *A*, proteins isolated by affinity chromatography from HemJ.f strain and from WT control cells were separated by 12 to 20% SDS–PAGE and stained with CBB, and the individual proteins bands were identified by MS (Table S1). *B*, the gel strip from CN–PAGE (see Fig. 1) was further separated in a second dimension by 12–20% SDS–PAGE and stained with SYPRO Orange. HemJ.f bands (marked as CN1 and CN2 in Fig. 1) were tentatively assigned as dimeric (HemJ[2]) and tetrameric (HemJ[4]) HemJ.f oligomers, respectively.

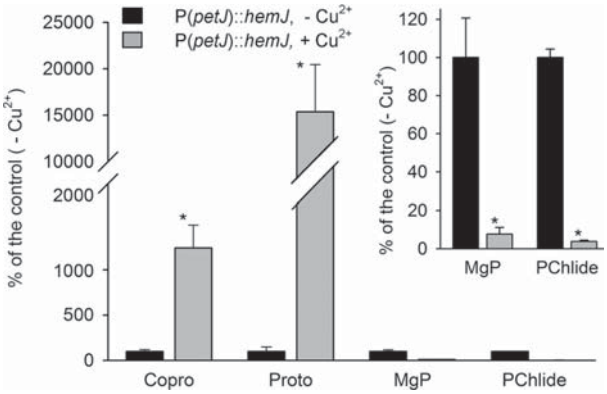

Figure 6. Analysis of heme/chlorophyll precursors in the P(*petJ*)::*hemJ* strain grown photoautotrophically in medium with or without copper. Heme/chlorophyll precursors were extracted with 70% methanol from the P(*petJ*)::*hemJ* cells at OD_{730} = 0.3–0.4 and separated on a HPLC equipped with two fluorescence detectors (48). The amounts of later chlorophyll precursors magnesium-protoporphyrin IX (*MgP*) and monovinyl protochlorophyllide (*PChlide*) were markedly reduced in cells cultivated with the repressed *hemJ* expression when compared with the same mutant cells grown without copper. On the contrary, Proto and Copro massively accumulated in the repressed cells. The *inset* shows a different scale for the less abundant precursors. *, significance difference tested using a paired *t* test (p = 0.05).

for co-evolutionary modeling, and also the overall homology in this helix was much lower (see supplemental information for details). The HemJ protein forms a very common structural motif in membrane proteins, a four–α-helix bundle. The overlay of the predicted structures from *R. sphaeroides* and *Synechocystis* 6803 showed very good agreement within this four–α-helix bundle (Fig. S8*E*), indicating that this domain is sufficient for basic HemJ function. Advanced alignment and secondary structure prediction methods (27) revealed distant homology of HemJ to other heme-binding membrane redox proteins. In several of our models, the invariant His-16 of HemJ (His-12 in Fig. S7) was aligned with heme-binding His residues of such distantly related templates. Because His is the most common residue providing at least one of the usual two heme ligands (28) and because His-16 is the only invariant His in the PF03653 Pfam family, we believe that His-16 of HemJ also ligates heme *b*. This would bury the observed heme *b* in the middle of the membrane, oriented perpendicularly to the membrane surface (Fig. 9). Please note that we are using the term "remote homolog" for HemJ without showing that it has common ancestry with other heme-binding redox membrane proteins. Observed structural similarity and one similarly placed His residue can simply be the result of convergent evolution of a heme-binding membrane protein. Absorbance spectra of reduced HemJ (Fig. 3*B*) indicate the presence of a ferrous six-coordinate heme *b* with the second ligand probably provided by another amino acid side chain. Interestingly, from five amino acids (His, Met, Cys, Tyr, and Lys) that can act as axial heme ligands of hemoproteins (28), there is an invariant Lys-94 (Lys-91 in Fig. S7) located on the distal side of the proposed heme location. This Lys could provide the sixth ligand of HemJ. Moreover, conserved Trp-90 (Trp-87 in Fig. S7), rarely substituted by Phe in other members of the Pfam family, may stabilize the heme pocket, as aromatic residues (phenylalanine, tyrosine, and tryptophan) play important roles in protein–heme interactions through stacking interactions with the porphyrin (28). The distant homology to several membrane oxidases together with heme absorption spectra indicate that the heme *b* in HemJ is redox-active and is involved in electron transfer.

This is in agreement with the expected oxidase/dehydrogenase activity of HemJ, which is still poorly understood. Before

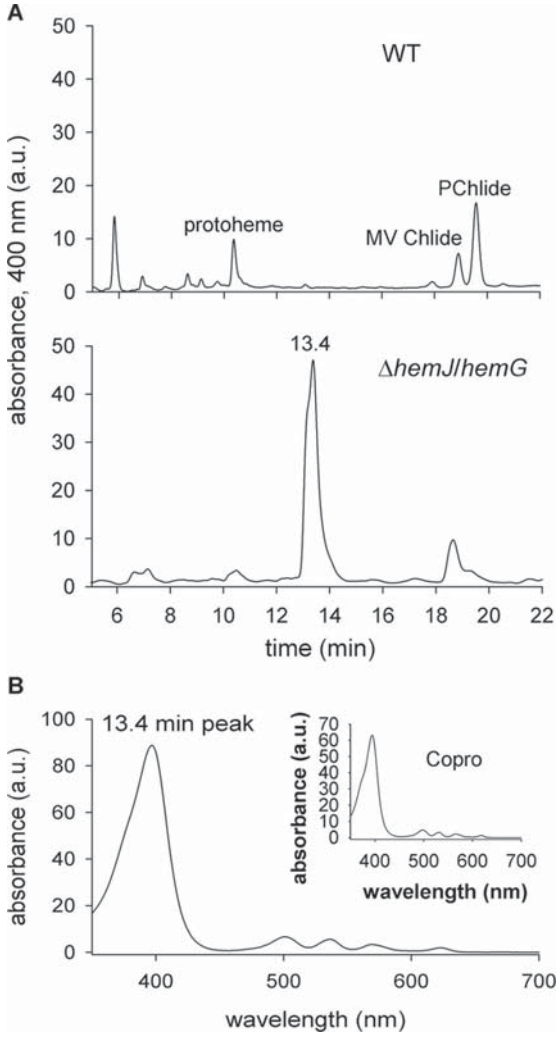

Figure 7. Detection of an unusual tetrapyrrole in the Δ*hemJ*/*hemG* strain incubated without glucose. *A*, polar tetrapyrroles were extracted with 70% methanol from 50 ml of WT and Δ*hemJ/hemG* cells grown photoautotrophically for 3 days and harvested at OD_{730} = 0. 3–0.4. The obtained extract was separated on a HPLC (see "Experimental procedures"), and eluted pigments were detected by a diode-array detector at 400 nm. *MV Chlide*, monovinyl chlorophyllide; *Pchlide*, monovinyl protochlorophyllide. *B*, absorption spectrum of the compound eluting at 13.4 min. The *inset* shows absorption spectrum of the Copro standard.

the enzyme identity was known, PPO activity belonging to HemJ was characterized in the membrane fraction of *R. sphaeroides* (29). This activity was inhibited by respiratory inhibitors and also by extraction of quinones from membranes with pentane, and no enzyme activity was detected after membrane solubilization (29). This indicated that PPO activity in *R. sphaeroides* is closely linked with components of the respiratory electron transport chain. In *A. baylyi*, both membrane and soluble fractions were necessary to detect HemJ activity, suggesting that a soluble factor may be required. In another study, authors documented oxygen-dependent PPO activity of purified HemJ from *R. sphaeroides* (3). However, detected specific PPO activity was much lower than that for the combined fractions in *A. baylyi* mentioned above (10), and the authors also did not note the presence of a colored co-factor in the purified enzyme. We were not able to detect any oxygen-dependent PPO activity of the HemJ protein isolated from solubilized membranes. No activity was detected even in the presence of menadione, a soluble analog of menaquinone probably serving as the electron acceptor for HemG (9). This is in line with the report that HemJ does not complement an *E. coli* Δ*hemG* mutant, suggesting that the connection of HemJ to the respiratory chain is distinct from that of HemG (8).

Even though we were not able to measure PPO activity in our eluate, the data presented herein (Fig. 6 and Fig. S4, *A* and *B*) further document that HemJ is indeed a *bona fide* PPO as indicated previously (3, 10). As would be expected for PPO, HemJ down-regulation resulted in accumulation of tetrapyrrole precursors Copro and Proto at the same time as depletion of chlorophyll precursors occurred (Fig. 6). The HemJ protein is indispensable, and complete inactivation of the encoding gene was possible only after expression of another copy of HemJ or HemG. Although we were able to complement missing HemJ with HemG as shown before (10), this replacement was not without consequences. The resulting Δ*hemJ*/*hemG* strain did not grow autotrophically (Fig. S5), and the tetrapyrrole biosynthetic pathway was disturbed (Fig. 7*A*).

Reactive protoporphyrin intermediates generally do not accumulate in strains with an undisturbed tetrapyrrole biosynthetic pathway. Mutation of genes encoding tetrapyrrole biosynthetic enzymes or treatment of cells with enzyme inhibitors frequently results in accumulation of high levels of tetrapyrrole intermediates (4), probably leading to increased formation of reactive oxygen species. PPO-deficient mutants commonly accumulate earlier heme intermediates: uroporphyrin, Copro, and also Proto (30). Accumulation of oxidized forms is caused by nonspecific oxidation of Coprogen and Protogen in the cell or during isolation (3, 20) (Fig. 1). Repression of HemJ expression in the P(*petJ*)::*hemJ* strain also led to Copro and Proto accumulation (Fig. 6). The complemented Δ*hemJ/hemG* strain expressing HemG accumulated less Copro and Proto when grown on glucose compared with the WT (not shown), indicating that the pathway is functional and provides enough Proto for normal chlorophyll accumulation and almost normal growth (Figs. S4, *C* and *D*, and S5). After transfer to medium without glucose, the cells of the Δ*hemJ/hemG* strain stopped growing. Chlorophyll levels also quickly decreased, suggesting that not enough Proto accessible to magnesium-chelatase is made (Fig. S4*C*). Interestingly, at the same moment, the cells started to accumulate an unusual porphyrin identified as harderoporphyrin (Figs. 7 and 8), a probable auto-oxidation product of harderoporphyrinogen, which is a tricarboxylic intermediate in a two-step decarboxylation of the heme precursor Coprogen (31), catalyzed by CPO (Fig. 1). This indicates problems with the Δ*hemJ/hemG* mutant at this stage of tetrapyrrole biosynthesis. Even though there are two CPO enzymes (HemN and HemF) in *Synechocystis* 6803, HemF is expected to serve as the sole CPO under prevailing oxic conditions (15). We speculate that HemF is functionally coupled with HemJ and that this coupling is disturbed in the Δ*hemJ/hemG* strain. Surprisingly, the improper coupling was not demonstrated by accumulation of

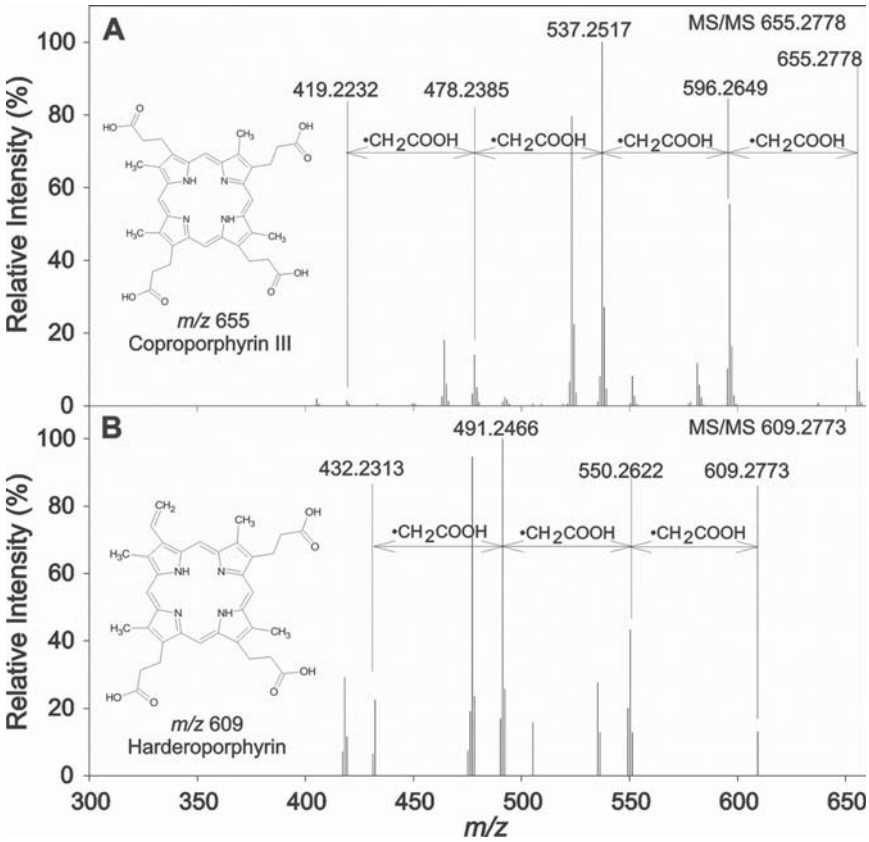

Figure 8. HRMS/MS fragmentation of the Copro (*A*) and harderoporphyrin (*B*). *A*, analytical standard of Copro was subjected to HPLC–HRMS/MS analysis to provide background data for identification of the unknown tetrapyrrole found in Δ*hemJ*/*hemG* cells. It provided molecular ion at *m/z* 655 when subjected to HPLC–HRMS/MS, and its subsequent fragmentation led to formation of ions corresponding to four consecutive losses of propionic radical. *B*, harderoporphyrin was isolated from Δ*hemJ*/*hemG* cells grown without glucose. The HPLC–HRMS/MS analysis provided molecular ion at *m/z* 609 with only three consecutive losses detected in its MS/MS spectrum. The fourth propionic group is substituted by a vinyl group as inferred from differences between Copro and harderoporphyrin *m/z* values.

Protogen (Proto) but by accumulation of harderoporphyrinogen. This indicates a reduced ability of *Synechocystis* 6803 HemF to convert harderoporphyrinogen to Protogen after replacement of downstream PPO of HemJ-type by that of the HemG type. The only other examples of harderoporphyrin accumulation are for specific mutants of human CPO, which is an oxygen-dependent HemF (32). The reduced ability to convert harderoporphyrinogen to Protogen in the abnormal CPO was explained by reduced affinity for harderoporphyrinogen, which may leave the enzyme more easily (33). This would suggest that replacement of HemJ by HemG also destabilizes the active site of HemF, implying that a physical contact between HemJ and HemF leads to conformational changes of the HemF active site. Because both Coprogen and harderoporphyrinogen are substrates for CPO, the release of harderoporphyrinogen could also occur when an excess of Coprogen is accumulated in the cell (34). However, Coprogen also accumulated in the P(*petJ*)::*hemJ* strain (Fig. 6) without concomitant accumulation of harderoporphyrin. We do not know exactly why we see harderoporphyrin accumulation particularly under autotrophic growth. It is possible that glucose, similarly to oxygen, regulates the accumulation of both CPO forms HemF and HemN. The red microalga *Galdieria partita*, also containing both forms of CPO, excretes Copro in the medium when growing mixotrophically on glucose (35). This was explained by inactivation of the oxygen-dependent CPO in microoxic conditions when grown on glucose (36). In *Synechocystis* 6803, the two-component regulatory histidine kinase Hik31 is involved in the response to glucose and in switching between photoautotrophic and photoheterotrophic growth (37). At the same time, Hik31 has an additional role in the transition between oxic and microoxic growth (38).

Substrate channeling and the presence of stable or transient multienzyme complexes is expected to be an advantageous mechanism for pathways with reactive intermediates to protect the cell from oxidative damage. In tetrapyrrole biosynthesis, most information supporting the presence of multienzyme complexes for at least some enzymes comes from immunoprecipitation followed by immunoblotting and/or MS (12, 13). In developing erythroid cells, the presence of a mitochondrial heme metabolism complex minimally consisting of FeCH, PPO, and aminolevulinic acid synthase was documented (12). In bacteria, co-immunoprecipitation and immunogold labeling supported a complex involving HemY type of PPO and FeCH in

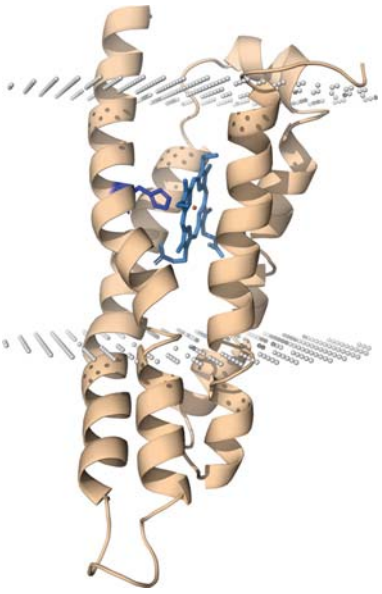

Figure 9. Model structure of *R. sphaeroides* HemJ monomer. The HemJ model was predicted by automatic structure prediction server RaptorX (53). The His-16 proposed to bind heme is shown in *blue*. For prediction of heme-binding site, the server COFACTOR was used (55). PPM server (56) was used to predict position of the protein structure model within membrane. Both the N and C termini of the protein are on the periplasmic/lumenal side of the membrane.

the thermophilic cyanobacterium *Thermosynechococcus elongatus* (13).

In pulldown experiments we aimed to co-purify HemJ with its partners in tetrapyrrole biosynthesis. The most prominent protein co-purified with HemJ was Sll1106 (Fig. 5*A*), a protein with unknown function containing an extended glycine zipper motif, which can be found in a number of channel forming proteins (39). However, it is unlikely that Sll1106 is required for PPO function, because in a set of 40 cyanobacterial genomes, HemJ was coded in 32 genomes, whereas Sll1106 homologs were present in only 20 (data not shown). A Sll1106 homolog was found also in some cyanobacteria coding for HemY-type of PPO. Thus, we do not expect Sll1106 to be directly involved in HemJ activity, and its function remains to be elucidated. Interestingly, all four FtsH protease homologs encoded in *Synechocystis* 6803 were present in significant quantities in the HemJ.f eluate (Fig. 5*A*). FtsHs are universally conserved transmembrane metalloproteases responsible for quality control of membrane and membrane-associated proteins. They form heterooligomeric complexes with distinct functions (40–42). For example, the FtsH2/3 heterooligomeric complex responsible for PSII repair and biogenesis was the most abundant in the eluate. This may reflect a functional connection to PSII or may just reflect the membrane region in the cell where the PPO reaction is performed.

Experimental procedures

Construction of Synechocystis 6803 strains

The strains used in this study were derived from nonmotile, glucose-tolerant *Synechocystis* 6803 strain obtained from the laboratory of Peter J. Nixon (Imperial College, London, UK). To prepare a strain expressing HemJ (WP_020861394.1) with a 3× FLAG tag at the C terminus (HemJ.f), the *hemJ* gene (*slr1790*) was cloned into the pPD-*C*FLAG plasmid containing the *Synechocystis 6803 psbAII* promoter, a sequence encoding the tag, kanamycin resistance cassette, and flanking sequences for homologous recombination that allow insertion of *hemJ* tagged on its C terminus into the *Synechocystis* 6803 genome in place of the *psbAII* gene (43). Because pPD-*C*FLAG plasmid containing *hemJ.f* (pPD-*hemJ.f*) isolated from *E. coli* frequently contained frameshift mutations within *hemJ*, the fragment for transformation was obtained by PCR using pPD-*hemJ.f* ligation mixture as a template. The resultant PCR fragment was used for transformation of WT and ΔPSI strains (44). The vector used for disruption of *hemJ* by a chloramphenicol resistance cassette was constructed using the megaprimer PCR method (45). First, upstream and downstream regions of *hemJ* were amplified from WT genomic DNA with flanking sequences of chloramphenicol resistance cassette from pACYC184 vector. Then the chloramphenicol resistance cassette and regions upstream and downstream of *hemJ* were mixed in one PCR with the primer annealing temperature at 50 °C. 5 μl of PCR mixture was used for transformation into the *hemJ.f Synechocystis* 6803 strain. To construct the P(*petJ*)::*hemJ* strain expressing HemJ under the control of copper-repressed promoter, p*PsbAIpetJ*-FLAG plasmid (46) was used with the *hemJ* gene inserted into specific restriction sites, leaving out the 3× FLAG tag. The resulting plasmid was used for WT transformation, and the WT copy of *hemJ* was deleted afterward. To prepare *Synechocystis* 6803 strain expressing HemG from *E. coli* under the *Synechocystis 6803 psbAII* promoter, the *hemG* gene (47) was again cloned into the pPD-*C*FLAG plasmid, leaving out the 3× FLAG tag. The WT strain was transformed with the resultant plasmid, and the WT copy was subsequently deleted. In all cases, *Synechocystis* 6803 transformants were selected on BG11 agar plates with increasing levels of corresponding antibiotic. Full segregation was confirmed by PCR.

Growth conditions

Synechocystis 6803 strains were grown photoautotrophically in BG11 medium in shaken conical flasks at 29 °C and irradiance of 40 μmol photons m^{-2} s^{-1}. The Δ*hemJ*/*hemG* strain was grown in the medium supplemented with 5 mM glucose. P(*petJ*)::*hemJ* strain was grown in the medium without copper, and the addition of 1 μM $CuSO_4$ was used for repression of *hemJ* expression. For the purification of HemJ.f protein, 4 liters of cells were grown mixotrophically to an OD_{730} of 0.5–0.7 in the medium supplemented with 5 mM glucose.

Analysis of cellular tetrapyrroles

Whole-cell absorption spectra were measured with Shimadzu UV-3000 spectrophotometer. Heme/chlorophyll precursors were measured from 2 ml of culture OD_{730} of ~0.4 using HPLC according to procedure described by Pilný *et al.* (48). For the detection of porphyrins accumulated in the Δ*hemJ/hemG* strain, 50 ml of cells were grown without glucose for 3 days and harvested at an OD_{730} of ~0.4. Pigments were extracted by an excess of 70% methanol and separated by a

HPLC method described in Pilný *et al.* (48), and their absorbance was detected by a diode-array detector.

Preparation of thylakoid membranes and protein complex purification

Harvested cells were washed and resuspended in thylakoid buffer containing 25 mM MES/NaOH, pH 6.5, 25% glycerol, 10 mM $MgCl_2$, 10 mM $CaCl_2$ and then broken in a Mini-Beadbeater-16 (Biospec). For protein purification, EDTA-free protease inhibitor (Roche) was added into the buffer prior to breaking the cells. The membranes were pelleted by centrifugation (55,000 × *g*, 20 min, 4 °C) and resuspended in excess of the thylakoid buffer, and the centrifugation step was repeated.

For the isolation of HemJ.f protein, the membrane fraction was resuspended in the thylakoid buffer and solubilized for 1 h at 10 °C with 1.5% *n*-dodecyl-β-D-maltoside (DDM; Enzo Life Sciences). After centrifugation (55,000 × *g*, 20 min, 4 °C), the solubilized proteins were purified using anti-FLAG-M2 agarose resin (Sigma–Aldrich). The resin was intensively washed with 20 resin volumes of the thylakoid buffer containing 0.04% DDM, and the HemJ.f was finally eluted with two resin volumes of the same buffer containing in addition 300 μg/ml of 3× FLAG peptide (Sigma–Aldrich).

Electrophoresis and size-exclusion chromatography

The protein composition of purified complexes was analyzed by SDS–PAGE in a denaturing 12–20% polyacrylamide gel containing 7 M urea (49). For native electrophoresis, solubilized membrane proteins or isolated complexes were separated on 4–14% CN–PAGE (50). To resolve individual components of protein complexes, the gel strip from the CN–PAGE was first incubated in 2% SDS and 1% DTT for 30 min at room temperature, and then proteins were separated along the second dimension by SDS–PAGE in a denaturing 12–20% polyacrylamide gel containing 7 M urea (49). Proteins separated by SDS–PAGE were stained with Coomassie Brilliant Blue (CBB) or SYPRO Orange afterward. Mass spectrometry analysis of CBB-stained protein bands/spots from the SDS–PAGE gels was accomplished essentially as described by Bučinská *et al.* (18).

For size-exclusion chromatography, the HemJ.f eluate prepared from ΔPSI genetic background was injected onto an Agilent-1200 HPLC and separated on a Yarra 3000 column (Phenomenex) using 25 mM HEPES buffer, pH 7.5, containing 0.25% DDM at a flow rate of 0.2 ml min^{-1} at 10 °C. Fractions corresponding to HemJ.f were pooled and concentrated on a 100-kDa cutoff microconcentrator (Millipore).

Identification and quantification of the HemJ.f-bound heme

For the analysis of heme, the HemJ.f protein was isolated by the affinity chromatography and subsequently further purified by size-exclusion chromatography (see previous paragraph). Heme was extracted from the isolated and concentrated protein by 90% of acetone, 2% HCl; passed through a 0.22-μm filter; and separated by HPLC on Nova-Pak C18 column (Waters) using a 25–100% linear gradient with H_2O (A)/acetonitrile (B) both containing 0.1% TFA as a mobile phase at a flow rate of 1 ml min^{-1} at 40 °C. Protoheme was detected using a diode-array detector (Agilent-1200). The protein concentration was estimated in two fractions from the size-exclusion chromatography by sample absorbance at 280 nm using the ProtParam tool (http://web.expasy.org/protparam) and a calculated extinction coefficient for the HemJ.f protein of 41,000 M^{-1} cm^{-1}. Full reduction of heme in HemJ.f eluate from the ΔPSI strain was achieved by adding a few grains of sodium dithionite. UV-visible spectra were measured at room temperature with a Shimadzu UV-3000 spectrophotometer.

PPO assay

PPO activity was monitored using a continuous fluorometric assay as previously described (51). Production of the fluorescent Proto, from nonfluorescent Protogen was detected using a fluorescence plate leader at 25 °C. Reaction mixtures consisted of 50 mM MOPS, pH 8.0, 2 mM GSH, 20 μM Protogen, 200 nM HemJ.f, and 1 mM menadione or benzoquinone. Protogen oxidation by Human HemY was used as a positive control.

Isolation of harderoporphyrin and HPLC–HRMS/MS analysis

The unknown tetrapyrrole (peak, 13.4 min; see Fig. 7*A*) was prepurified from 600 ml of Δ*hemJ*/*hemG* cells grown without glucose for 3 days. Harvested cells were extracted by 50 ml of 70% methanol, the solvent was evaporated on a rotary evaporator, and the dried pigments were dissolved in 2 ml of methanol. This solution was separated on Agilent-1200 using the same solvents as described for the analysis of cellular tetrapyrroles but employing a semipreparative C8 column (Luna 5 μm, 250 × 10 mm, Phenomenex). The peak corresponding to the unknown tetrapyrrole was collected and dried in a vacuum concentrator. For HPLC–HRMS/MS analysis, the sample was analyzed on Thermo Scientific Dionex UltiMate 3000 UHPLC+ (Sunnyvale, CA) equipped with a diode-array detector. Separation of compounds was performed on reversed-phase Phenomenex Kinetex C18 column (150 × 4.6 mm, 2.6 μm; Torrance, CA) using H_2O (A)/acetonitrile (B) both containing 0.1% HCOOH as a mobile phase with the flow rate of 0.5 ml min^{-1}. For the separation, the following gradient was used: A/B 85/15 (0 min), 85/15 (in 1 min), 0/100 (in 25 min), 0/100 (in 30 min), and 85/15 (in 35 min). Analysis of mass spectra was performed on a Bruker Impact HD high resolution mass spectrometer (Billerica, MA) with electrospray ionization. The following settings were used: dry temperature, 200 °C; drying gas flow, 12 liters min^{-1}; nebulizer, 3 bars; capillary voltage, 3800 V; and endplate offset, 500. The spectra were collected in the range 20–2000 *m*/*z* with precursor ion selection set to 550–700 and automatic exclusion after five spectra. The analysis was calibrated using sodium formate at the beginning of the analysis. Collision energy for fragmentation was set to 60 eV.

Protein modeling

For modeling we have used HemJ polypeptide from *R. sphaeroides* (WP_023003745) with four transmembrane helices. The modeling was performed using several automatic structure prediction servers: Robetta (52), RaptorX (53), and RaptorX-Contact (54). The server COFACTOR was used for prediction of heme-binding site (55), and PPM server (56) was used to predict the position of the protein structure model within

membrane. The protein models were aligned and visualized using PyMOL software (57).

Author contributions—P. S., R. S., and M. T. conceptualization; P. S., R. S., P. H., and M. T. formal analysis; P. S. validation; P. S., J. H., and M. T. investigation; P. S., R. S., J. H., P. H., and M. T. visualization; P. S., R. S., M. S., and M. T. methodology; P. S. and M. T. writing-original draft; P. S., R. S., M. S., P. H., and M. T. writing-review and editing; M. T. supervision; M. T. project administration.

Acknowledgments—We are grateful to the laboratory of Prof. Harry Dailey (University of Georgia) for supplying us with expression plasmid for HemY. We thank Eva Prachová and Jan Pilný for technical assistance and Peter Koník for performing the mass spectrometric analyses.

References

1. Czarnecki, O., and Grimm, B. (2012) Post-translational control of tetrapyrrole biosynthesis in plants, algae, and cyanobacteria. *J. Exp. Bot.* **63,** 1675–1687 CrossRef Medline
2. Dailey, H. A., Dailey, T. A., Gerdes, S., Jahn, D., Jahn, M., O'Brian, M. R., and Warren, M. J. (2017) Prokaryotic heme biosynthesis: multiple pathways to a common essential product. *Microbiol. Mol. Biol. Rev.* **81,** e00048-16 Medline
3. Kato, K., Tanaka, R., Sano, S., Tanaka, A., and Hosaka, H. (2010) Identification of a gene essential for protoporphyrinogen IX oxidase activity in the cyanobacterium *Synechocystis* sp. PCC6803. *Proc. Natl. Acad. Sci. U.S.A.* **107,** 16649–16654 CrossRef Medline
4. Nishimura, K., Nakayashiki, T., and Inokuchi, H. (1995) Cloning and identification of the *hemG* gene encoding protoporphyrinogen oxidase (PPO) of *Escherichia coli* K-12. *DNA Res.* **2,** 1–8 CrossRef Medline
5. Narita, S., Tanaka, R., Ito, T., Okada, K., Taketani, S., and Inokuchi, H. (1996) Molecular cloning and characterization of a cDNA that encodes protoporphyrinogen oxidase of *Arabidopsis thaliana*. *Gene* **182,** 169–175 CrossRef Medline
6. Dailey, H. A., and Dailey, T. A. (1996) Protoporphyrinogen oxidase of *Myxococcus xanthus*: expression, purification, and characterization of the cloned enzyme. *J. Biol. Chem.* **271,** 8714–8718 CrossRef Medline
7. Kobayashi, K., Masuda, T., Tajima, N., Wada, H., and Sato, N. (2014) Molecular phylogeny and intricate evolutionary history of the three isofunctional enzymes involved in the oxidation of protoporphyrinogen IX. *Genome Biol. Evol.* **6,** 2141–2155 CrossRef Medline
8. Möbius, K., Arias-Cartin, R., Breckau, D., Hännig, A. L., Riedmann, K., Biedendieck, R., Schröder, S., Becher, D., Magalon, A., Moser, J., Jahn, M., and Jahn, D. (2010) Heme biosynthesis is coupled to electron transport chains for energy generation. *Proc. Natl. Acad. Sci. U.S.A.* **107,** 10436–10441 CrossRef Medline
9. Boynton, T. O., Daugherty, L. E., Dailey, T. A., and Dailey, H. A. (2009) Identification of *Escherichia coli* HemG as a novel, menadione-dependent flavodoxin with protoporphyrinogen oxidase activity. *Biochemistry* **48,** 6705–6711 CrossRef Medline
10. Boynton, T. O., Gerdes, S., Craven, S. H., Neidle, E. L., Phillips, J. D., and Dailey, H. A. (2011) Discovery of a gene involved in a third bacterial protoporphyrinogen oxidase activity through comparative genomic analysis and functional complementation. *Appl. Environ. Microbiol.* **77,** 4795–4801 CrossRef Medline
11. Ferreira, G. C., Andrew, T. L., Karr, S. W., and Dailey, H. A. (1988) Organization of the terminal two enzymes of the heme biosynthetic pathway: orientation of protoporphyrinogen oxidase and evidence for a membrane complex. *J. Biol. Chem.* **263,** 3835–3839 Medline
12. Medlock, A. E., Shiferaw, M. T., Marcero, J. R., Vashisht, A. A., Wohlschlegel, J. A., Phillips, J. D., and Dailey, H. A. (2015) Identification of the mitochondrial heme metabolism complex. *PLoS One* **10,** e0135896 CrossRef Medline
13. Masoumi, A., Heinemann, I. U., Rohde, M., Koch, M., Jahn, M., and Jahn, D. (2008) Complex formation between protoporphyrinogen IX oxidase and ferrochelatase during haem biosynthesis in *Thermosynechococcus elongatus*. *Microbiology* **154,** 3707–3714 CrossRef Medline
14. Brzezowski, P., Richter, A. S., and Grimm, B. (2015) Regulation and function of tetrapyrrole biosynthesis in plants and algae. *Biochim. Biophys. Acta* **1847,** 968–985 CrossRef Medline
15. Goto, T., Aoki, R., Minamizaki, K., and Fujita, Y. (2010) Functional differentiation of two analogous coproporphyrinogen III oxidases for heme and chlorophyll biosynthesis pathways in the cyanobacterium *Synechocystis* sp. PCC 6803. *Plant Cell Physiol.* **51,** 650–663 CrossRef Medline
16. Sofia, H. J., Chen, G., Hetzler, B. G., Reyes-Spindola, J. F., and Miller, N. E. (2001) Radical SAM, a novel protein superfamily linking unresolved steps in familiar biosynthetic pathways with radical mechanisms: functional characterization using new analysis and information visualization methods. *Nucleic Acids Res.* **29,** 1097–1106 CrossRef Medline
17. Phillips, J. D., Whitby, F. G., Warby, C. A., Labbe, P., Yang, C., Pflugrath, J. W., Ferrara, J. D., Robinson, H., Kushner, J. P., and Hill, C. P. (2004) Crystal structure of the oxygen-dependant coproporphyrinogen oxidase (Hem13p) of *Saccharomyces cerevisiae*. *J. Biol. Chem.* **279,** 38960–38968 CrossRef Medline
18. Bučinská, L., Kiss, E., Koník, P., Knoppová, J., Komenda, J., and Sobotka, R. (2018) The ribosome-bound protein Pam68 promotes insertion of chlorophyll into the CP47 subunit of Photosystem II. *Plant Physiol.* **176,** 2931–2942 Medline
19. Hobbs, C., Dailey, H. A., and Shepherd, M. (2016) The HemQ coprohaem decarboxylase generates reactive oxygen species: implications for the evolution of classical haem biosynthesis. *Biochem. J.* **473,** 3997–4009 CrossRef Medline
20. Lermontova, I., and Grimm, B. (2006) Reduced activity of plastid protoporphyrinogen oxidase causes attenuated photodynamic damage during high-light compared to low-light exposure. *Plant J.* **48,** 499–510 CrossRef Medline
21. Kopečná, J., Pilný, J., Krynická, V., Tomčala, A., Kis, M., Gombos, Z., Komenda, J., and Sobotka, R. (2015) Lack of phosphatidylglycerol inhibits chlorophyll biosynthesis at multiple sites and limits chlorophyllide reutilization in the cyanobacterium *Synechocystis* 6803. *Plant Physiol.* **169,** 1307–1317 CrossRef Medline
22. Lim, C. K. (2010) *High-performance Liquid Chromatography and Mass Spectrometry of Porphyrins, Chlorophylls and Bilins*, World Scientific Publishing, Singapore
23. Kennedy, G. Y. (1970) Harderoporphyrin: a new porphyrin from the Harderian glands of the rat. *Comp. Biochem. Physiol.* **36,** 21–36 CrossRef Medline
24. Miller, M. J., Hermodson, M., and Gennis, R. B. (1988) The active form of the cytochrome *d* terminal oxidase complex of *Escherichia coli* is a heterodimer containing one copy of each of the two subunits. *J. Biol. Chem.* **263,** 5235–5240 Medline
25. Lu, P., Ma, D., Yan, C., Gong, X., Du, M., and Shi, Y. (2014) Structure and mechanism of a eukaryotic transmembrane ascorbate-dependent oxidoreductase. *Proc. Natl. Acad. Sci. U.S.A.* **111,** 1813–1818 CrossRef Medline
26. Gomelsky, M., and Kaplan, S. (1996) The *Rhodobacter sphaeroides* 2.4.1 rho gene: expression and genetic analysis of structure and function. *J. Bacteriol.* **178,** 1946–1954 CrossRef Medline
27. Ma, J., Peng, J., Wang, S., and Xu, J. (2012) A conditional neural fields model for protein threading. *Bioinformatics* **28,** i59–i66 CrossRef Medline
28. Li, T., Bonkovsky, H. L., and Guo, J.-T. (2011) Structural analysis of heme proteins: implications for design and prediction. *BMC Struct. Biol.* **11,** 13 CrossRef Medline
29. Jacobs, N. J., and Jacobs, J. M. (1981) Protoporphyrinogen oxidation in *Rhodopseudomonas spheroides*, a step in heme and bacteriochlorophyll synthesis. *Arch. Biochem. Biophys.* **211,** 305–311 CrossRef Medline
30. Sasarman, A., Chartrand, P., Lavoie, M., Tardif, D., Proschek, R., and Lapointe, C. (1979) Mapping of a new hem gene in *Escherichia coli* K12. *J. Gen. Microbiol.* **113,** 297–303 CrossRef Medline

31. Rand, K., Noll, C., Schiebel, H. M., Kemken, D., Dülcks, T., Kalesse, M., Heinz, D. W., and Layer, G. (2010) The oxygen-independent coproporphyrinogen III oxidase HemN utilizes harderoporphyrinogen as a reaction intermediate during conversion of coproporphyrinogen III to protoporphyrinogen IX. *Biol. Chem.* **391,** 55–63 Medline
32. Schmitt, C., Gouya, L., Malonova, E., Lamoril, J., Camadro, J. M., Flamme, M., Rose, C., Lyoumi, S., Da Silva, V., Boileau, C., Grandchamp, B., Beaumont, C., Deybach, J. C., and Puy, H. (2005) Mutations in human CPO gene predict clinical expression of either hepatic hereditary coproporphyria or erythropoietic harderoporphyria. *Hum. Mol. Genet.* **14,** 3089–3098 CrossRef Medline
33. Nordmann, Y., Grandchamp, B., de Verneuil, H., Phung, L., Cartigny, B., and Fontaine, G. (1983) Harderoporphyria: a variant hereditary coproporphyria. *J. Clin. Invest.* **72,** 1139–1149 CrossRef Medline
34. Elder, G. H., Evans, J. O., Jackson, J. R., and Jackson, A. H. (1978) Factors determining the sequence of oxidative decarboxylation of the 2- and 4-propionate substituents of coproporphyrinogen III by coproporphyrinogen oxidase in rat liver. *Biochem. J.* **169,** 215–223 CrossRef Medline
35. Stadnichuk, I., Rakhimberdieva, M. G., Bolychevtseva, Y. V., Yurina, N. P., Karapetyan, N. V., and Selyakh, I. O. (1998) Inhibition by glucose of chlorophyll a and phycocyanobilin biosynthesis in the unicellular red alga *Galdieria partita* at the stage of coproporphyrinogen III formation. *Plant Sci.* **136,** 11–23 CrossRef
36. Sarian, F. D., Rahman, D. Y., Schepers, O., and van der Maarel, M. (2016) Effects of oxygen limitation on the biosynthesis of photo pigments in the red microalgae *Galdieria sulphuraria* strain 074G. *PLoS One* **11,** e0148358 CrossRef Medline
37. Kahlon, S., Beeri, K., Ohkawa, H., Hihara, Y., Murik, O., Suzuki, I., Ogawa, T., and Kaplan, A. (2006) A putative sensor kinase, Hik31, is involved in the response of *Synechocystis* sp. strain PCC 6803 to the presence of glucose. *Microbiology* **152,** 647–655 CrossRef Medline
38. Summerfield, T. C., Nagarajan, S., and Sherman, L. A. (2011) Gene expression under low-oxygen conditions in the cyanobacterium *Synechocystis* sp. PCC 6803 demonstrates Hik31-dependent and -independent responses. *Microbiology* **157,** 301–312 CrossRef Medline
39. Kim, S., Jeon, T. J., Oberai, A., Yang, D., Schmidt, J. J., and Bowie, J. U. (2005) Transmembrane glycine zippers: physiological and pathological roles in membrane proteins. *Proc. Natl. Acad. Sci. U.S.A.* **102,** 14278–14283 CrossRef Medline
40. Mann, N. H., Novac, N., Mullineaux, C. W., Newman, J., Bailey, S., and Robinson, C. (2000) Involvement of an FtsH homologue in the assembly of functional photosystem I in the cyanobacterium *Synechocystis* sp. PCC 6803. *FEBS Lett.* **479,** 72–77 CrossRef Medline
41. Krynická, V., Tichý, M., Krafl, J., Yu, J., Kaňa, R., Boehm, M., Nixon, P. J., and Komenda, J. (2014) Two essential FtsH proteases control the level of the Fur repressor during iron deficiency in the cyanobacterium *Synechocystis* sp. PCC 6803. *Mol. Microbiol.* **94,** 609–624 CrossRef Medline
42. Komenda, J., Knoppová, J., Krynická, V., Nixon, P. J., and Tichý, M. (2010) Role of FtsH2 in the repair of Photosystem II in mutants of the cyanobacterium *Synechocystis* PCC 6803 with impaired assembly or stability of the CaMn4 cluster. *Biochim. Biophys. Acta* **1797,** 566–575 CrossRef Medline
43. Chidgey, J. W., Linhartová, M., Komenda, J., Jackson, P. J., Dickman, M. J., Canniffe, D. P., Koník, P., Pilný, J., Hunter, C. N., and Sobotka, R. (2014) A cyanobacterial chlorophyll synthase-HliD complex associates with the Ycf39 protein and the YidC/Alb3 insertase. *Plant Cell* **26,** 1267–1279 CrossRef Medline
44. Shen, G., Boussiba, S., and Vermaas, W. F. (1993) *Synechocystis* sp. PCC-6803 strains lacking Photosystem-I and phycobilisome function. *Plant Cell* **5,** 1853–1863 CrossRef Medline
45. Lee, J., Lee, H. J., Shin, M. K., and Ryu, W. S. (2004) Versatile PCR-mediated insertion or deletion mutagenesis. *BioTechniques* **36,** 398–400 CrossRef Medline
46. Knoppová, J., Sobotka, R., Tichý, M., Yu, J., Konik, P., Halada, P., Nixon, P. J., and Komenda, J. (2014) Discovery of a chlorophyll binding protein complex involved in the early steps of photosystem II assembly in *Synechocystis*. *Plant Cell* **26,** 1200–1212 CrossRef Medline
47. Sasarman, A., Letowski, J., Czaika, G., Ramirez, V., Nead, M. A., Jacobs, J. M., and Morais, R. (1993) Nucleotide sequence of the *hemG* gene involved in the protoporphyrinogen oxidase activity of *Escherichia coli* K12. *Can. J. Microbiol.* **39,** 1155–1161 CrossRef Medline
48. Pilný, J., Kopečná, J., Noda, J., and Sobotka, R. (2015) Detection and quantification of heme and chlorophyll precursors using a High Performance Liquid Chromatography (HPLC) system equipped with two fluorescence detectors. *Bio-protocol* **5,** e1390
49. Dobáková, M., Sobotka, R., Tichý, M., and Komenda, J. (2009) Psb28 protein is involved in the biogenesis of the photosystem II inner antenna CP47 (PsbB) in the cyanobacterium *Synechocystis* sp. PCC 6803. *Plant Physiol.* **149,** 1076–1086 Medline
50. Wittig, I., Karas, M., and Schägger, H. (2007) High resolution clear native electrophoresis for in-gel functional assays and fluorescence studies of membrane protein complexes. *Mol. Cell Proteomics* **6,** 1215–1225 CrossRef Medline
51. Shepherd, M., and Dailey, H. A. (2005) A continuous fluorimetric assay for protoporphyrinogen oxidase by monitoring porphyrin accumulation. *Anal. Biochem.* **344,** 115–121 CrossRef Medline
52. Kim, D. E., Chivian, D., and Baker, D. (2004) Protein structure prediction and analysis using the Robetta server. *Nucleic Acids Res.* **32,** W526–W531 CrossRef Medline
53. Källberg, M., Wang, H., Wang, S., Peng, J., Wang, Z., Lu, H., and Xu, J. (2012) Template-based protein structure modeling using the RaptorX web server. *Nat. Protoc.* **7,** 1511–1522 CrossRef Medline
54. Wang, S., Sun, S., Li, Z., Zhang, R., and Xu, J. (2017) Accurate *de novo* prediction of protein contact map by ultra-deep learning model. *PLoS Comput. Biol.* **13,** e1005324 CrossRef Medline
55. Zhang, C., Freddolino, P. L., and Zhang, Y. (2017) COFACTOR: improved protein function prediction by combining structure, sequence and protein-protein interaction information. *Nucleic Acids Res.* **45,** W291–W299 CrossRef Medline
56. Lomize, M. A., Pogozheva, I. D., Joo, H., Mosberg, H. I., and Lomize, A. L. (2012) OPM database and PPM web server: resources for positioning of proteins in membranes. *Nucleic Acids Res.* **40,** D370–D376 CrossRef Medline
57. DeLano, W. L. (2012) *The PyMOL Molecular Graphics System*, version 2.0, Schroedinger, LLC, New York

for non-published parts

Petra Skotnicová
petraskotnicova@seznam.cz
Proteins involved in the tetrapyrrole pathway in *Synechocystis* sp. PCC 6803 and their localization in the proximity of PSII biogenesis, Ph.D. Thesis, 2019

University of South Bohemia in České Budějovice
Faculty of Science
Branišovská 1760
CZ-37005 České Budějovice, Czech Republic
Phone: +420 387 776 201
www.prf.jcu.cz, e-mail: sekret-fpr@prf.jcu.cz